THE IMPACT OF GENOMIC INSTABILITY ON GERMLINE DEVELOPMENT AND MUTATION ACCUMULATION IN MICE

A Dissertation

Presented to the Faculty of the Graduate School

of Cornell University

In Partial Fulfillment of the Requirements for the Degree of

Doctor of Philosophy

by

Jordana Corinne Bloom

August 2020

THE IMPACT OF GENOMIC INSTABILITY ON GERMLINE DEVELOPMENT AND MUTATION ACCUMULATION IN MICE

Jordana Corinne Bloom, Ph.D.

Cornell University 2020

The ability of organisms to pass their genetic information onwards to subsequent generations is crucial for survival and propagation of a species. In mice, embryonic germ cells are set aside very early in development to become the germline lineage. During development, these germ cells rapidly migrate and proliferate to the location of the future gonads over the course of only a few days. Importantly, while DNA replication associated with rapid cell proliferation is often subject to spontaneous errors, the germline has been shown to be highly refractory to mutation accumulation in comparison to somatic cells. To begin understanding the extent to which primordial germ cells (PGCs) are similar, or dissimilar, to other well-studied cell types in their response to altered genomic integrity, I developed a transgenic mouse strain which expresses a DNA double strand break (DSB) sensor specifically in PGCs. This strain provided me with a tool to monitor DNA DSB repair dynamics *in vivo*. Using this strain, I assessed the impact of ionizing radiation-induced DNA damage on PGCs and examined the impact of this damage on the downstream post-natal germ cell reserve (Chapter 2).

Additionally, to better understand the DNA damage response (DDR)

in these cells, I exposed pregnant mice to ionizing radiation (IR) at specific gestational time points and assessed the DDR. Our results show that PGCs prior to sex determination lack a G1 cell cycle checkpoint. Subsequent to sex determination, the response to IR-induced DNA damage differs between female and male PGCs. IR of female PGCs caused uncoupling of germ cell differentiation and meiotic initiation, while male PGCs exhibited repression of piRNA metabolism and transposon de-repression (Chapter 3).

I also used whole genome single-cell DNA sequencing to assess whether genetic rescue of DNA repair-deficient germ cells leads to increased mutation incidence and biases. I generated *Fancm* and *p21* null mutations on an isogenic strain background and observed that loss of *p21* in *Fancm* null mutants leads to a partial, but significant rescue of germ cells in males. With this $Fancm^{-/-}$ PGC-proliferation defective mutant, I examined how mutation burden is impacted when DNA damage checkpoints are abrogated. Importantly, I observed an increase in the incidence of complex mutations in double mutants, highlighting that rescuing germ cell quantity through checkpoint bypass leads to a decrease in germline genome quality.

Lastly, in Chapter 4, I examined how genome integrity is maintained in mouse meiocytes which either have unrepaired meiotic DSBs ($Trip13^{Gt/Gt}$) or unsynapsed chromosomes ($Spo11^{-/-}$). I show that signaling through p53 and TAp63, is responsible for elimination of oocytes with asynapsis or unrepaired DSBs. I also show that checkpoint kinase I (CHK1) becomes activated by

persistent DSBs in oocytes and to an increased degree when CHK2 is absent. Taken together, the work described uncovers novel insights into how germ cells with DNA damage can become developmentally defective, leaving only those genetically fit cells to establish the adult germline.

BIOGRAPHICAL SKETCH

Jordana Corinne Bloom was born in New York, New York in 1991 to loving parents, Leslie Weiss-Bloom and Michael Bloom. She grew up in Tenafly, New Jersey and graduated from Tenafly High School in 2010. She obtained her undergraduate degree from Haverford College in Haverford, Pennsylvania where she majored in Biology and minored in Psychology. In 2014, she was awarded the school's Marian Koshland Prize in Biology for "demonstrating outstanding contributions to the Department in the areas of academics, research and service." Also, during her time at Haverford, she played for the school's Division III Varsity Tennis Team.

Jordana moved to Ithaca, New York in the summer of 2014 to begin graduate school at Cornell University in the Biochemistry, Molecular and Cell Biology (BMCB) PhD program housed in the Department of Molecular Biology and Genetics. She joined the lab of Dr. John C. Schimenti in the Spring of 2015 to conduct her thesis research.

Dedicated to all those individuals who supported and encouraged me along the way.

ACKNOWLEDGMENTS

I would like to first thank my thesis advisor, Dr. John Schimenti. John's mentorship over the years has been crucial to my development as a creative, independent scientist. He gave me a lot of freedom to pursue ideas and experiments that I thought were interesting and was always available to provide crucial guidance when I needed it. While, John once jokingly described his mentorship style in a lab meeting as "survival of the fittest," I think a better analogy is more to one of a "lifeguard/guardian angel," who, while allowing you to grow from the disappointments and successes of graduate school, science and life, is always watching out for your well-being. Thank you for being part of my scientific journey.

Next, I would like to thank my thesis committee members, Dr. Robert Weiss and Dr. Tudorita Tumbar. Their feedback and guidance over the years always helped to improve my research and scientific scholarship. In addition to my committee members, I would also like to thank Drs. Paula Cohen, Jen Grenier, and Rebecca Williams who have all been scientific mentors and friends.

Additionally, I would like to acknowledge all the members of the Schimenti lab (past and present) who I overlapped with during my time at Cornell; I learned something from each and every one of you. Notably, I want to especially thank Dr. Vera Rinaldi and Dr. Adrian McNairn who were both always willing to discuss projects and share their experimental protocols. Also, a special thanks to Regina Chase who befriended both me and my mice.

Lastly, I want to thank my family and close friends. My parents and brother have always been my unwavering supporters and their love has been

incredibly valuable throughout my PhD. I am also thankful for the friends I met here in Ithaca, including: Catalina Pereira, Adam Bisogni, Alexandra Hinck, and Aaron Joiner. Thank you for all the laughs and memories (including some serious discussions about how we hope to improve academia some day!)

And finally, a special acknowledgement to my fiercest champion, best friend and better half, Robert Battaglia. I am incredibly grateful that our paths crossed here at Cornell and I am looking forward to continuing our life together as a married couple.

TABLE OF CONTENTS

CHAPTER 1

INTRODUCTION

1. Germ Cell Development

The Embryonic Origins of Germ Cells

Zoologists realized over a century ago that cells during embryogenesis segregate into germline and somatic lineages (McLaren 2003). In mammals, this dichotomy is first evident during gastrulation, when primordial germ cells (PGCs), the embryonic precursors of both male and female gametes, are specified (Lawson et al. 1999; Ohinata et al. 2009). Mouse PGCs begin as a group of ~45 cells in the epiblast 6-6.5 days post fertilization (E6-6.5) (Saitou et al. 2002). Interestingly, induction of germ cell precursors during this period of development has been shown to be position-dependent based on cell transplantation experiments where cells relocated from distal areas of the epiblast to the appropriate proximal-posterior region are also capable of germ cell specification (Tam and Zhou 1996). Once specified, expression of pluripotency-associated genes *Oct4, Sox2,* and *Nanog* become increasingly restricted to PGCs and by E8.0 expression of these genes become PGC-specific in the embryo (Yamaguchi et al. 2005; Yabuta et al. 2006; Rosner et al. 1990). After specification, PGCs simultaneously migrate and proliferate to the location of the future gonads where they undergo roughly 9 population doublings over the course of 7 days to reach a peak population of ~25,000 cells (Nikolic et al. 2016). These PGCs located in the genital ridge/fetal gonad,

form the founding germ cell population from which the entire adult germline in both females and males is established (Tam and Snow 1981).

The Sexually Dimorphic Developmental Trajectory of Embryonic Germ Cells

Once PGCs begin to reach the developing gonad around E10.5 (Tam and Snow 1981), they exit their pluripotent, migratory state and become capable of initiating sexual differentiation and meiosis. During this licensing period, which takes ~2 days, expression of the RNA-binding protein, *Dazl* is required. Mutants lacking *Dazl* expression fail to express markers of female or male differentiation and are not capable of meiotic entry (Lin et al. 2008; Gill et al. 2011). Under normal conditions, sex determination begins once licensing is complete and it is during this time that female and male gonads begin to appear morphologically distinct from one another (Koubova et al. 2006). In males, PGCs are located within primitive testis cords, while in females, PGCs are spread throughout the fetal gonad (Ewen and Koopman 2010).

At E13.5, the cellular fates between male and female PGCs begin to differ. Female germ cells begin to undergo meiotic initiation, while male germ cells continue on a mitotic cell cycle program before undergoing quiescence ~2 days later (Western et al. 2008; Soh et al. 2015). Meiotic entry in both sexes requires the protein stimulated by retinoic acid gene 8 (STRA8) (Anderson et al. 2008). Expression of this protein is induced by an anterior to posterior wave of retinoic acid (RA) signaling in the fetal gonad (Koubova et al. 2006). Both male and female fetal gonads encounter RA signaling, but male embryos

express the cytochrome P450 enzyme CYP26B1, which degrades RA and inhibits meiotic induction (Bowles et al. 2006). Importantly, this mechanism of meiotic initiation, rather than requiring activating signals to begin meiosis in the female germline, requires inhibition of meiotic signaling in the male germline.

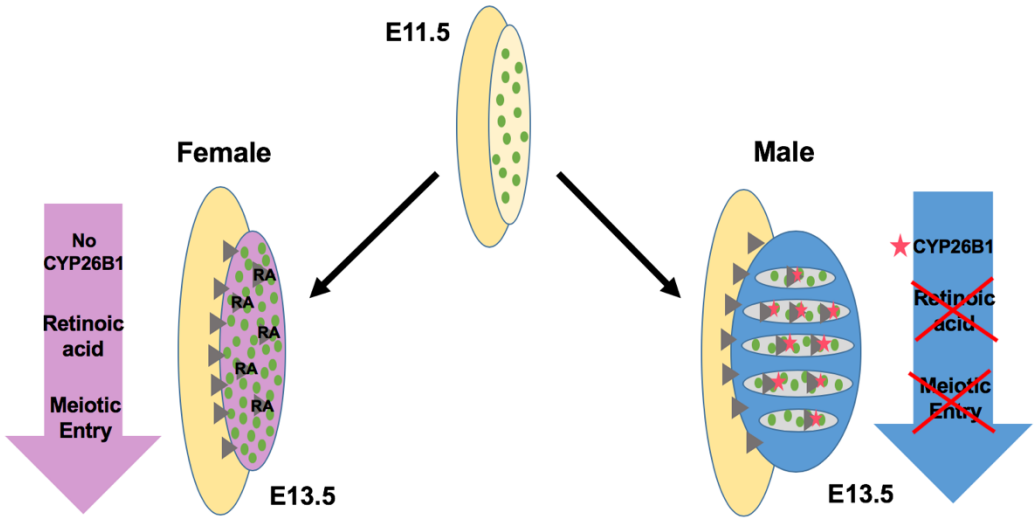

Figure 1.1. Diagram summarizing the sexually dimorphic developmental trajectory of embryonic germ cells. In response to retinoic acid signaling, E13.5 female germ cells begin meiotic entry in an anterior to posterior wave (left). Expression of CYP26B1 leads to retinoic acid degradation and the suppression of meiotic entry in E13.5 male germ cells (right).

Meiotic initiation in male gonads begins postnatally through repression of *Cyp26b1* (Bowles et al. 2006; Koubova et al. 2006; Anderson et al. 2008). Once *Cyp26b1* is no longer expressed, spermatogenic precursors gain the

ability to respond to RA, express *Stra8,* and initiate meiosis in regularly interspersed waves throughout the lifetime of the male (Endo et al. 2017). Recently, in male germ cells, STRA8 was shown to bind to promoters and induce the expression of thousands of genes, including those related to meiotic prophase I, G1/S cell cycle transition and inhibitors of the mitotic cell cycle (Kojima et al. 2019). A comparison of gene expression in wild-type, *Stra8*-deficient and *Dazl*-deficient fetal ovaries also showed that induction of many genes associated with meiosis directly depend on STRA8 activity (Soh et al. 2015).

Female Meiosis

The female germline is comprised of a finite number of oocytes which arise during embryonic development (as described above). These germ cells begin meiotic prophase I in a semi-synchronous manner based on when they are exposed to RA signaling (Bowles and Koopman 2007). These cells arrest prior to birth only to resume meiosis I upon ovulation, and progress to meiosis II only if fertilized (Zhang et al. 2014).

After the initiation of meiosis, meiotic prophase I begins. Prophase I, the longest stage of meiosis, is divided into five sub-stages based on the morphological appearance of the chromosomes (Cobb and Handel 1998). Importantly, the progression through meiotic prophase I sub-stages under normal conditions correlates with meiotic DNA double strand break (DSB) repair dynamics (Handel and Schimenti 2010). Once pre-meiotic DNA

replication is complete, entry into the first sub-stage of prophase I, leptonema, is marked by the presence of ~200-300 endogenously programmed DSBs. In the next stage, called zygonema, pairing between homologous chromosomes initiates through synaptonemal complex assembly (Lesch and Page 2012). In pachynema, homologous chromosomes are fully synapsed and DSBs get repaired through homologous recombination (crossing over) (Mézard et al. 2015). In the diplotene stage, the synaptonemal complex breaks down and homologous chromosomes are only held together at sites of recombination. And lastly, in diakinesis, the meiotic spindle begins to form and chromosomes condense further in preparation for the first meiotic division (Gray and Cohen 2016).

The first meiotic arrest, often referred to as dictyate arrest, occurs in diplonema. In the first few days following birth, the oocytes undergo folliculogenesis where they become surrounded by characteristic flattened granulosa cells (Peters 1969). Oocytes in these follicles are termed “primordial” and it is these primordial follicles which constitute the finite oocyte pool, often referred to as the “ovarian reserve,” present in females of reproductive age (Findlay et al. 2015). Poor ovarian reserve is a crucial limiting factor in any treatment aimed to improve fertility (Jirge 2016). Sensitive mechanisms have evolved to eliminate oocytes which have sustained DNA damage (Heyer et al. 2000; Suh et al. 2006; Bolcun-Filas et al. 2014). Under normal conditions, this system works well to ensure effective elimination of defective oocytes, but because the pool of oocytes is limited, loss of too many

primordial follicles can lead to primary ovarian insufficiency (POI), sterility and ovarian failure (Welt 2008; Oktay 2006). Approximately 40% of all female breast cancer survivors experience POI/premature ovarian failure and the health ramifications of this condition can be quite severe including, but not limited to, menopause-like symptoms, bone loss, and increased risk of heart disease (Jankowska 2017; Woodruff 2015; Oktay 2006).

Mechanistic insights into how oocytes detect DNA damage (and, by extension, how to prevent loss of the ovarian reserve) have made significant progress in recent years (Suh et al. 2006; Bolcun-Filas et al. 2014; Rinaldi, Hsieh, et al. 2017; Winship et al. 2018; Livera et al. 2008). In Chapter 4, the lab's most recent contribution to this field is described. Using two mouse models of oocyte loss, we show that the removal of both *p53* and *TAp63* rescues oocytes to wild-type levels. The two mouse models used in the study include a homozygous null mutant of *Spo11* and a homozygous gene-trap mutant of *Trip13*.

SPO11 is a widely conserved meiosis-specific topoisomerase type II-like protein which catalyzes DSB formation in leptonema through transient, covalent protein-DNA intermediates (Keeney and Kleckner 1995; Liu et al. 1995; Keeney et al. 1997). Meiotic DSB formation in mouse also requires additional accessory proteins such as MEI4 (Kumar et al. 2015), MEI1 (Libby et al. 2002), and IHO1 (Stanzione et al. 2016), but once DSBs are formed, SPO11 is removed from DNA and 5' strands are resected to yield 3' single-stranded tails (Keeney 2008). These 3' single-stranded tails can then invade

homologous DNA duplexes and give rise to recombination products (Keeney 2001). SPO11-induced DSBs are repaired to form either crossovers or non-crossovers. Tight regulation of crossovers ensures that only ~10% of these DSBs are resolved as crossovers (Gray and Cohen 2016). SPO11 is also required for efficient homolog pairing. When SPO11 is absent, meiotic DSBs do not form and there is a failure of homologous chromosomes to synapse (Romanienko and Camerini-Otero 2000; Baudat et al. 2000; Boateng et al. 2013). Due to the widespread asynapsis, *Spo11*$^{-/-}$ females are born with a severely reduced oocyte pool which becomes exhausted within a few weeks after puberty (Di Giacomo et al. 2005).

The second mutant we examined in Chapter 4 was *Trip13*$^{Gt/Gt}$. *Trip13* is the mouse ortholog of pachytene checkpoint 2 *(PCH2)* present in *Saccharomyces cerevisiae* and *Caenorhabditis elegans*. In *S. cerevisiae* and *C. elegans*, the "pachytene checkpoint" monitors two features of meiotic chromosome biology: 1) DSB repair and 2) chromosome synapsis (Bhalla and Dernburg 2005; Wu and Burgess 2006). In mice, *Trip13*$^{Gt/Gt}$ mutants were shown to undergo synapsis normally, but exhibited extensive unrepaired DNA damage due to failed recombination (Li and Schimenti 2007). Often phenotypic analysis of meiotic mutants (such as *Dmc1*$^{-/-}$ and *Msh5*$^{-/-}$) reveal defects in both synapsis and DSB repair (Di Giacomo et al. 2005). Therefore, the identification of a mutant defective in meiotic DNA repair, but capable of synapsis is useful for distinguishing the cellular responses toward these two defects. Oocytes defective for either DSB repair alone (as in *Trip13*$^{Gt/Gt}$) or in

both synapsis and DSB repair are almost all eliminated by late gestation and prior to puberty (Di Giacomo et al. 2005; Li and Schimenti 2007), yet genetic removal of meiotic DSB formation in DSB repair mutants manifests in an oocyte loss phenotype more similar to that of *Spo11* mutants (Di Giacomo et al. 2005; Reinholdt and Schimenti 2005; McNairn et al. 2017; Li and Schimenti 2007).

Previous work from the Schimenti lab has revealed that CHK2 (checkpoint kinase 2) signaling to TRP53/TAp63 is important for eliminating the majority of *Trip13*$^{Gt/Gt}$ mutant oocytes (Bolcun-Filas et al. 2014), but deletion of *Chk2* only rescued *Spo11*$^{-/-}$ to ~25% of wild type levels (Rinaldi, Bolcun-Filas, et al. 2017). Therefore, the experiments described in Chapter 4 aimed to test whether there is a another pathway either complementary to or distinct from CHK2, but which also signals to TRP53 and TAp63, is present in *Spo11*$^{-/-}$ oocytes.

2. DNA Damage

Types of DNA Damage

Each cell within a multicellular organism is estimated to experience tens of thousands of DNA lesions per day (Lindahl and Barnes 2000). These lesions, if not repaired, can block genome replication and transcription (Jackson and Bartek 2009). DNA damage primarily arises from three sources, including environmental agents, reactive oxygen species (ROS) generated by oxidative phosphorylation, and spontaneous hydrolysis of nucleotide residues

(Lindahl 1993; Friedberg et al. 2005). Approximately 75% of lesions encountered by cells under normal conditions are single-strand DNA (ssDNA) breaks arising from either oxidative damage during metabolism or base hydrolysis (Giglia-Mari et al. 2011). Notably, when two single-strand breaks (SSBs) arise in close proximity or when the DNA replication machinery encounters a SSB, DSBs are formed. DSBs, while not nearly as common as SSBs, have the potential to be extremely cytotoxic because an undamaged complement is not available to repair the DNA break (Jackson and Bartek 2009).

Environmental agents that can cause DNA damage include ultraviolet light (UV), ionizing radiation (IR) and chemotherapeutics (Barnes and Lindahl 2004). The research presented in Chapters 2-4 of this dissertation focuses on the effect of IR-induced DNA damage on germ cells. IR-induced DNA damage has been studied in many contexts and is known to cause primarily DSBs in DNA (Ciccia and Elledge 2010; Featherstone and Jackson 1999). The following section will describe various approaches cells use to respond to DNA damage and will include a particular focus on how cells respond to DNA DSB lesions.

Responses to DNA DSBs

Cell Cycle Checkpoint Activation

Cell cycle checkpoints are surveillance mechanisms that monitor cell growth, DNA replication, chromosome integrity and chromosome segregation.

In eukaryotes, the cell cycle is divided into four phases. DNA replication occurs in “Synthesis” or S-phase and chromosome segregation occurs at “Mitosis” or M-phase. Two “Gap” phases, G1 and G2, separate S-phase and M-phase, respectively (Barnum and O’Connell 2014). The proteins that drive cell cycle progression are called cyclin-dependent kinases (CDKs). These serine/threonine kinases are only able to promote S-phase and M-phase when bound by their appropriate cyclin partner. In contrast to CDKs, cyclins are tightly controlled at the level of translation and ubiquitin-dependent proteolysis (Lim and Kaldis 2013).

Many of the mechanisms regulating cell cycle checkpoint response are highly conserved from yeast to mammals. Some of the first studies in eukaryotes examining cell cycle arrest induced by DNA damage were performed in *S. cerevisiae.* In these studies, IR was shown to induce a cell cycle delay proportional to the severity of the DNA damage exposure (Weinert and Hartwell 1988; Hartwell and Weinert 1989). Subsequent studies have shown that the cell cycle can be arrested at the G1/S transition, within S-phase or at the G2/M transition depending on which stage of the cell cycle the DNA damage-induced lesion is detected (Zhou and Elledge 2000). Activation of these checkpoints allows time for DNA repair pathways to operate before entry into the next phase of the cell cycle (Khanna and Jackson 2001).

While there are many different lesion-specific responses for DNA repair, the common goal of DNA damage-induced cell cycle checkpoint responses is to maintain CDKs in an inactive state until the damage is fixed (Ciccia and

Elledge 2010). The checkpoints can broadly be defined as those involving the transcription factor and tumor suppressor *p53* and those involving checkpoint kinase *Chk1* (Barnum and O'Connell 2014). G1 checkpoint activation is mediated by post-translational modifications on P53. P53's N-terminal serine-15 site can be phosphorylated by a number of DNA damage sensing kinases including ATM (Ataxia Telangiectasia Mutated), ATR (Ataxia Telangiectasia and Rad3-related) and DNA-PKcs (Kitagawa and Kastan 2005). Once activated via ATM and CHK2, P53 becomes stabilized, forms a tetramer and acts as a transcription factor for many genes, including the cyclin-dependent kinase inhibitor, *Cdkn1a* (which encodes P21) (Karimian et al. 2016). P21 induces a G1 arrest by inhibiting the CDKs present at this cell cycle stage until the DNA damage is repaired. Additionally, P53 is involved in inducing a prolonged G2 arrest in response to the presence of persistent DNA damage (Giono and Manfredi 2006).

Recruitment of CHK1 to sites of DNA damage during S- and G2-phase leads to arrest at these stages of the cell cycle. Complexes of checkpoint proteins, including ATR, assemble on exposed single-stranded DNA coated by Replication Protein A (RPA) (Maréchal and Zou 2013). Once activated, ATR can phosphorylate CHK1. CHK1 then, in turn, phosphorylates proteins which inhibit the formation of cell cycle phase-specific cyclin/CDK complexes (Shiotani and Zou 2009). Importantly, there are instances throughout the cell cycle where CHK1 and CHK2 act redundantly (Bartek and Lukas 2003). In Chapter 4 of this dissertation, we show evidence of this phenomenon in the

oocyte DNA damage response (DDR) where loss of CHK2 signaling leads to a subsequent increase in CHK1 phosphorylation. As highlighted throughout this section, the purpose of DNA damage-induced cell cycle checkpoint activation is to give cells time to repair DNA lesions. The section immediately following this one goes on to describe what is known about DNA repair with a specific focus on repair of DNA DSBs.

DNA DSB Repair

DSB repair can be completed by a number of different pathways. Pathway choice depends on the extent of DNA end processing and when during the cell cycle the lesion is identified. Broadly speaking, DNA repair pathways can be divided into two categories: non-homologous end-joining (NHEJ) and homologous recombination (HR). While HR is often referred to as an “error-free” repair mechanism, NHEJ is error-prone (Jackson and Bartek 2009). Classical NHEJ does not require DNA end resection and involves the ligation of broken DNA ends without the use of a homologous template (Davis and Chen 2013). HR, in contrast, requires a homologous sister chromatid, but is limited to acting in S- and G2-phases of the cell cycle (Ciccia and Elledge 2010).

Post-mitotic cells and G1-phase cycling cells repair DSBs through NHEJ. During classical NHEJ, the ends of DNA breaks are quickly recognized by the Ku70/Ku80 heterodimer. The dimer loads onto DNA and activates the catalytic subunit of DNA-PK (DNA-PKc) (Mahaney et al. 2009). DNA-PKc

stabilizes DSB ends and prevents end resection through a series of phosphorylation reactions. Once DNA-PKc is loaded, re-ligation of the broken ends is performed by XRCC4/LIG4 (Meek et al. 2008). The balance between end stabilization and end processing is regulated by many factors, but DNA breaks that contain ends incapable of ligation are regulated in an ATM kinase-dependent manner (Macrae et al. 2008; Matsuoka et al. 2007).

More recently, an alternative NHEJ pathway has been identified which occurs when there is limited DSB end resection (on the scale of 5-25 nucleotides) (Sfeir and Symington 2015). This alternative NHEJ pathway (also known as microhomology-mediated end joining/MMEJ) functions as a backup to the classical NHEJ pathway described in the previous paragraph. In this pathway, PARP1 competes with Ku binding to promote HR (Wang et al. 2006). Interestingly, both PARP1 and ATM recruit factors needed for HR but lesions where only a small amount of resection occurs undergo MMEJ. During MMEJ repair, micro-homologous sequences align internal to the broken end leading to deletions of sequence flanking the DSB prior to ligation (Mateos-Gomez et al. 2015; Sfeir and Symington 2015).

DSBs can also be recognized by the MRE11-RAD50-NBS1 (MRN) complex. This complex promotes ATM activation and preparation for HR repair. Like KU and PARP1, the MRN complex also associates with DNA ends. In addition to end stabilization, MRE11 has endo- and exo-nuclease activity that catalyze the initial steps for HR DSB end resection. NBS1, the “N” of the MRN complex, associates with the C-terminal region of ATM to recruit

the kinase to DSBs. End resection is regulated by ATM through CtIP and 3' ssDNA ends formed via resection are coated by RPA. As described in the Cell Cycle Checkpoint Activation section earlier, RPA-coated ssDNA plays a critical role in activating the ATR kinase. However, if RAD51 filaments replace RPA on ssDNA then strand invasion into homologous sequences of the sister chromatid can occur resulting in HR events.

The regulation of DSB repair pathway choice has important ramifications with regards to genome fidelity and stability. One protein involved in pathway choice is the tumor suppressor P53-binding protein, 53BP1. 53BP1 is continuously expressed in the nucleus and forms foci at sites of DNA damage (Schultz et al. 2000). The protein binds exposed histone H4 lysine 20 dimethylated (H4K20me2) sites on chromatin via its Tudor domain (Botuyan et al. 2006). DSB resection by ATM-CtIP is inhibited by 53BP1 and 53BP1 has been shown to promote NHEJ by increasing the stability and mobility of DSB ends to find each other and ligate (Dimitrova et al. 2008; Difilippantonio et al. 2008). Famously, 53BP1 and BRCA1 have been shown to be antagonistic to one another in mediating repair pathway choice (Daley and Sung 2014). Hypomorphic alleles of *Brca1* skew repair pathway choice towards 53BP1-mediated NHEJ repair. In mouse, *Brca1* single mutants are embryonic lethal but if repair pathway balance is restored with co-deletion of *53bp1,* then BRCA1 deficiency becomes compatible with viability (Cao et al. 2009).

In Chapter 2 of this dissertation, the generation and validation of a transgenic mouse model to detect DNA damage in PGCs is described. This

mouse model combines a PGC-specific promoter with a fluorescently tagged fragment of 53BP1's Tudor binding domain generated by Titia de Lange's lab (Dimitrova et al. 2008). Even though the reporter generates foci at sites of DNA DSBs, Chapters 2 and 5 expand on the idea of repair pathway choice and the caveats of a 53BP1-based reporter.

A portion of Chapter 3 describes research performed examining germline mutation accumulation in a DNA repair deficient mouse model. The model we used contained a frameshift mutation in the gene, *Fancm. Fancm* is the largest subunit of the Fanconi Anemia Core Complex, which consists of a number of proteins that, when mutated, cause the disease Fanconi Anemia (FA). FA is a chromosomal instability syndrome which leads to cancer predisposition, bone marrow failure, congenital abnormalities and infertility (Joenje and Patel 2001). Studies in cell culture systems have shown that *Fancm* facilitates cell cycle checkpoint activation at sites of arrested DNA replication forks, particularly in the contexts of interstrand crosslinks (ICL) (Deans and West 2009). Additionally, *Fancm* has also been reported to mediate fork reversal when the lagging strand template is partially single-stranded and bound by RPA (Gari et al. 2008).

FANCM initiates repair pathway activation by forming a heterodimeric complex with FAAP24 (FA associated protein 24 kDa). Together, the dimer recognizes DNA lesions and recruits the FA core complex (Xue et al. 2015). Eight of the FA proteins (FANCA/B/C/E/F/G/L/M) form a multi-subunit ubiquitin E3 ligase core complex, which mono-ubiquitinates FANCD2 and FANCI in

response to genotoxic stress (Moldovan and D'Andrea 2009; Deans and West 2009). During pathway activation, multiple FA proteins undergo phosphorylation by ATR-CHK1 signaling kinases (Grompe and D'Andrea 2001), which demonstrates the interconnection between the FA and ATR pathways. FA pathway associated DNA lesions must be excised and repaired prior to the reactivation of DNA replication. Lesion bypass often requires the creation of a DSB followed by translesion synthesis (TLS) to repair the damage. TLS DNA polymerases can be highly error-prone, leading to the generation of mutations during DNA repair (Harfe and Jinks-Robertson 2000; Stone et al. 2012). Additionally, formation of a DSB during this process can lead to stimulation of the ATM kinase, thereby adding another layer of connectivity and crosstalk between DDR pathways (Lukas et al. 2004).

The reduction of germ cells in *Fancm* male mutants has been previously shown to be partially rescued by co-deletion of the cell cycle checkpoint associated cyclin-dependent kinase inhibitor, *p21* (Luo et al. 2014). In Chapter 3, we used this genetic system to test the hypothesis that germ cells rescued due to DNA damage checkpoint bypass may have a higher germline mutational burden than their counterparts with intact checkpoints. By examining this relationship, we sought to increase our understanding of the connection between cell cycle checkpoint activation and DNA damage repair.

What happens if, after a prolonged period of time, the DNA damage present in the cell cannot be repaired? Or, what happens if the extent of damage is too overwhelming to be repaired effectively? The next, and final,

section of “Responses to DNA DSBs” discusses the mechanisms employed by cells in these situations.

Senescence, Differentiation and Cell Death

The response to DNA damage often depends on the cell type and the severity of damage. Mild DNA damage can be repaired during a transient cell cycle arrest, but more severe and irreparable injury can lead to senescence or cell death (Surova and Zhivotovsky 2013).

Cellular senescence is a condition in which cells exit the cell cycle, remain viable and metabolically active, but become permanently arrested. Senescence was first described in fibroblast cell lines where a state of permanent cell cycle arrest occurred after serial passaging in culture (Hayflick and Moorhead 1961). The limited proliferative lifespan of non-transformed cell lines is known specifically as “replicative senescence.” Every time a normal cell proliferates, telomeres at the ends of chromosomes shorten (Harley et al. 1990; Kim et al. 1994). These telomere ends are capped by proteins which protect them from activating the DDR (Denchi and de Lange 2007; Wu et al. 2006). During replicative senescence, telomeres reach a critically short length and stimulate DDR activity (d’Adda di Fagagna 2008). Notably, the DDR plays an essential role in both senescence initiation and maintenance. Studies have shown that inactivation of CHK2, P53 and P21 extends the proliferative capacity of cells grown under normal culture conditions (Gire et al. 2004; Brown et al. 1997; Bond et al. 1994).

More pertinent to this dissertation, is the observation that senescence can also occur in the absence of critically short telomeres and in response to DNA damage of either a persistent or extensive nature (Di Leonardo et al. 1994; Robles and Adami 1998; Chen et al. 2004). This “premature senescence,” although induced by different stressors than replicative senescence, shares an underlying induction of the DDR. While cellular senescence permanently arrests the cell cycle of damages cells and therefore blocks proliferation, cell death leads to destruction and removal of the damaged cell (Matt and Hofmann 2016). Senescent cells also actively secrete pro-inflammatory cytokines (Burton and Faragher 2015) thus, in some cases, cell death may be a better alternative.

Cells can trigger both apoptosis and necroptosis in response to DNA damage. A hallmark feature of apoptotic signaling is the activation of caspases. Caspases are aspartate-specific cysteine proteases that function to process and activate pro-inflammatory cytokines as well as cleave numerous proteins during the apoptotic response (McIlwain et al. 2013). Caspases involved in apoptosis can be divided into initiator caspases and effector caspases. Both classes are present in the cell at all times, but as inactive zymogens. In response to cellular stress, the caspases get activated via proteolytic cleavage (Li and Yuan 2008). Mitochondria also play a role in apoptosis and key initiators of this pathway belong to the B cell lymphoma-2 (BCL-2) family of proteins which includes PUMA, NOXA and BAX (in addition to many others). Members of the BCL-2 family which contain BH (BCL-2

homology) domains regulate the release of mitochondrial cytochrome c and serve an anti-apoptotic function (Youle and Strasser 2008).

BAX and members of the BAX-like subfamily of proteins promote apoptosis by poking holes in the mitochondrial outer membrane. NOXA and PUMA are members of the pro-apoptotic BH3-only subfamily which become transcriptionally upregulated by P53 following DNA damage. Exposure to significant levels of DNA damage induces expression of BH3-only subfamily members which then bind and inhibit the activity of pro-survival proteins leading to apoptosis (Czabotar et al. 2014; Youle and Strasser 2008).

Necroptosis is a form of regulated necrosis that can also be stimulated in response to DNA damage (Vandenabeele et al. 2010). Morphologically, necroptosis resembles necrosis in terms of loss of membrane integrity and release of cellular components into the extracellular space, but importantly the response is regulated rather than uncontrolled (Vanden Berghe et al. 2014). Necroptotic cell death is characterized by lack of caspase activation and the involvement of cell death receptor ligands, like TNF-α (Surova and Zhivotovsky 2013). Notably, there are still gaps in our understanding about how distinct cell fates are determined in response to genotoxic stresses. While it is generally appreciated that the extent of DNA damage has a large influence on cell fate choices, there is also evidence that cell fate decisions are influenced by the type of lesion present and type of cell exposed.

In addition to senescence and cell death, DNA damage can induce some non-terminally differentiated cell types to differentiate (Sherman et al.

2011). One important example of this outside the immune system includes neuronal stem and progenitor cells (NSPCs). In these stem cells, IR-induced p53-mediated DNA damage promotes axon regeneration *in vivo* and loss of *p53* leads to impaired glial lineage differentiation (Di Giovanni et al. 2006; Zheng et al. 2008). DNA damage-induced cellular differentiation is relevant to the research described in Chapter 3 where the DDR in developing germ cells is examined. In this chapter, IR-induced DNA damage leads to an increase in RA signaling in both female and male PGCs. The connection between RA and differentiation has a long history that includes the establishment of retinoid-based "differentiation therapy" as a treatment for Acute Promyelocytic Leukemia (APL) (Fenaux and Degos 1997; Weiss and Ito 2015). RA treatment has also been used to induce differentiation in ESC culture systems and evidence for RA pathway stimulation in response to DNA damage has been reported in mESCs (Kim et al. 2009; Serio et al. 2019).

Sensitivity of Stem Cells and Germ Cells to DNA Damage

Most studies examining the impact of exogenous genotoxic stressors on germ cells have focused on post-natal germ cell development (Russell et al. 1981; Favor 1999; Rinaldi, Hsieh, et al. 2017; Enguita-Marruedo et al. 2019; Singh et al. 2018). Yet, there have been some studies which showed that mutations in several DNA repair genes impact PGC development, but have subtle effects on other embryonic- and post-natal cell types (Agoulnik et al. 2002; Luo et al. 2014; Luo and Schimenti 2015; Nadler and Braun 2000;

Hamer and de Rooij 2018). Additionally, germ cells in gastrulating mouse embryos were shown to readily undergo apoptosis in response to low doses of IR, leading to a depletion of the PGC pool, however the underlying mechanisms were not delineated (Heyer et al. 2000). Taken together, these studies indicated that PGCs are hypersensitive to DNA damage, but also revealed gaps in our understanding about the DNA damage response and repair mechanisms active in the mammalian fetal germline.

PGCs have several properties resembling mESCs, including rapid proliferation, low mutation rate, and similar transcriptomes (Hong et al. 2007; Cervantes et al. 2002; Grskovic et al. 2007). Using proper culture conditions, mESCs can even be differentiated into PGC-like cells (PGCLCs) in only a few days (Hayashi et al. 2011). mESCs also have a highly sensitive DDR when compared to other cultured cell types such as mouse embryonic fibroblasts (MEFs) (Hong and Stambrook 2004; Chuykin et al. 2008; Suvorova et al. 2016; Tichy and Stambrook 2008). As described in the “Cell Cycle Checkpoint Activation” section, the canonical DDR in most cell types involves the activation of a G1 cell cycle arrest, but induction of this checkpoint in response to DNA damage is absent in mouse and primate ESCs in response to IR (Hong and Stambrook 2004; Hong et al. 2007; Fluckiger et al. 2006). Although the lack of a G1 cell cycle arrest response would appear to be in conflict with a highly effective DDR, the speculated reason for this strategy is that rather than attempting to repair damage otherwise sufficient to arrest the cell cycle at G1, ESCs sustaining this level of damage would simply get culled from the

population. Interestingly, NSPCs also do not activate a G1 cell cycle block in response to DNA damage (Roque et al. 2012).

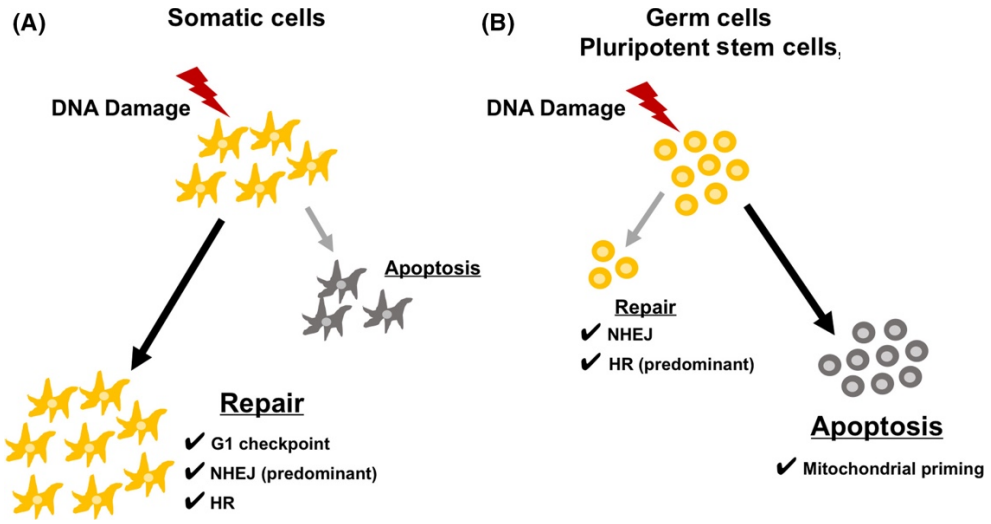

Figure 1.2. Comparison of responses to DNA damage in differentiated somatic cells vs. germ cells, pluripotent stem cells. (A) In response to DNA damage, somatic cells are more likely than germ cells/ES cells to undergo cell cycle arrest and attempt DNA repair, including utilization of error-prone repair mechanisms such as non-homologous end joining. (B) Germ cells and pluripotent stem cells are predisposed to apoptosis in response to DNA damage and when DNA repair mechanisms are activated in these cells, error-free mechanisms such as homologous recombination are favored. (Figure adapted from Bloom et al. 2019).

Taken together, the similarities between PGCs and mESCs led us to explore what, if any, features of the DDR observed in cultured stem cells might be active in the fetal germline with the overarching goal being to gain a better understanding of DDR mechanisms in PGCs (see Chapter 3 for the results related to this work).

3. Mutation Accumulation and the Germline

Ramifications

Germline mutations are the source of all heritable diseases and evolutionary adaptations. Perturbations to PGC development, and the accumulation of mutations, would have the potential to profoundly impact the function and quality of the germline at all subsequent stages of development. In particular, early mutational events in PGCs would be expanded clonally, thus pervading the adult germ cell population. Importantly, the spontaneous mutation rate of ESCs and the germline is remarkably low, further suggesting that PGCs, and subsequent stages of gametogenesis, have a highly effective DDR.

In order to assess how germline mutational burden is impacted when DNA damage checkpoints are abrogated, we examined mutation incidence in a PGC proliferation-defective mouse model. Using whole genome single cell DNA sequencing of germ cells, we were able to highlight the potential ramifications of manipulating DNA damage checkpoints to facilitate increased germ cell survival (Chapter 3). The following two sections of the Introduction

describe differences between germline and somatic cell mutation accumulation and discuss factors known to impact mutation rate in the germline.

Comparison of Germline and Somatic Cell Mutation Rates

Even prior to the next-generation sequencing (NGS) genomics era, researchers were able to observe that the mutation frequency differed between ESCs and fibroblast cell lines. These studies utilized selectable loci and compared the frequency of resistant clones arising between different cell types. The mutation rate of ESCs at the time was considered a proxy for germline mutation rate because of their totipotency. What they observed was that mutation frequencies are approximately two orders of magnitude lower in ESCs than MEFs and tail-tip fibroblasts (Cervantes et al. 2002; Hong et al. 2007). More recently, however, comparisons between germline and somatic mutation rates have also supported these earlier studies (Milholland et al. 2017). For mice, the germline mutation frequency is estimated to be between 4.6-6.5 x 10^{-9} mutations per base pair per generation (Uchimura et al. 2015; Ohno et al. 2014) and whole genome sequencing of parent-offspring trios in humans has estimated an average rate of 1.2 x 10^{-8} (Conrad et al. 2011; Besenbacher et al. 2015).

In addition to the unique features of germ cell DNA damage sensitivity which may help explain how the germline mutation rate is lower than that of somatic cells, transcriptome analyses have revealed that testicular tissue

expresses the most genes of any mammalian organ (~90% of all genes are expressed) (Soumillon et al. 2013; Melé et al. 2015). A possible explanation to account for this finding eluded scientists for a while, but recently it has been suggested that this widespread transcription evolved as a mechanism to keep the germline mutation rate low. In a groundbreaking study, researchers found that genes on transcribed DNA strands during spermatogenesis have lower mutation rates than those on un-transcribed strands, supporting this possibility as a broad-based mechanism to reduce mutation accumulation in germ cells (Xia et al. 2020).

Factors Effecting Germline Mutation Rate

More than three-fourths of *de novo* point mutations are inherited from the paternal allele (Rahbari et al. 2016). This bias towards paternally originating mutations arises from differences between oogenesis and spermatogenesis. After puberty, spermatogonial stem cells (SSCs) divide mitotically every few weeks to both maintain the SSC pool and generate differentiated spermatogonial cells to produce sperm throughout the lifetime of males. In contrast, oocytes only undergo one round of DNA replication prior to maturation and remain arrested until ovulation. Therefore, the opportunity to accumulate mutations due to DNA replication errors in the male germline is significantly higher than in the female germline and is reflected in the biased inheritance of paternal originating mutations (Goldmann et al. 2016; Conrad et al. 2011). Further indication supporting DNA replication associated errors on

the male germline comes from observations correlating an increase in the number of inherited *de novo* mutations in offspring with advanced paternal age (Kong et al. 2012).

Studies examining factors influencing germline mutation rate have not been limited to examining paternal age though. Maternal age is also a contributing factor. A study of sequenced Icelanders and their parents, determined that the number of maternally inherited *de novo* point mutations increases by ~0.37 per year of maternal age, whereas mutations of paternal origin increase by ~1.5 per year (Jónsson et al. 2017). An explanation for an increase in maternal age-related mutations has been attributed to the accumulation of DNA lesions or damage-induced mutations during prolonged meiotic arrest (Goriely 2016; Ségurel et al. 2014; Gao et al. 2016). However, a less appreciated explanation for maternal age effect may be related to the reliance of zygotes on oocyte-derived protein and transcript reserves until the four-cell stage (Braude et al. 1988). The first few post-zygotic cell divisions have been found to be relatively mutagenic (Huang et al. 2014; Acuna-Hidalgo et al. 2015) and if replication or repair machinery deteriorates with maternal age, then this could lead to *de novo* mutations of non-parental origin trending with maternal age (Gao et al. 2019).

Interestingly, while the average number of *de novo* mutations found in an offspring's genome increases with both paternal and maternal age, the rate of mutation accumulation was found to vary significantly across different families of similar ancestry, ranging from 0.19 to 3.24 *de novo* mutations per year. In

some families, an increase in parental age of one year was associated with extra mutations, while in other family lineages the number of new mutations barely increased at all with age (Sasani et al. 2019). While the factors accounting for this variability are not yet understood, a recent article found that the germline mutation rate in young adults is predictive of both reproductive lifespan and longevity (Cawthon et al. 2020).

4. Research Focus and Goals of this Dissertation

The ability of organisms to transmit their genetic information to subsequent generations is crucial for the survival and propagation of a species. In this dissertation, I examined genome maintenance mechanisms present in the developing mammalian germline with the aim to systematically explore how these cells respond to DNA damage using both environmental and genetic perturbations.

During my PhD research, I developed an embryonic germ cell-specific DNA DSB-sensing transgenic reporter mouse and validated that it can be used as a tool to visualize PGC DSB dynamics in an antibody-independent manner (Chapter 2). I observed that rapidly proliferating PGCs prior to sex determination have a cell cycle checkpoint response similar to mESCs, that the DDR between female and male PGCs is dimorphic post-sex determination, and that genetically ablating germline checkpoint responses during PGC proliferation leads to germ cells with a higher mutational incidence (Chapter 3). And lastly, I showed that checkpoint proteins CHK2 and CHK1 work

redundantly to remove post-natal oocytes with unrepaired DSBs (Chapter 4). In the final chapter of the dissertation (Chapter 5), I will describe some limitations of the work described and suggest potential avenues for future related studies.

References

Acuna-Hidalgo R, Bo T, Kwint MP, van de Vorst M, Pinelli M, Veltman JA, Hoischen A, Vissers LELM, Gilissen C. 2015. Post-zygotic Point Mutations Are an Underrecognized Source of De Novo Genomic Variation. *Am J Hum Genet* **97**: 67–74.

Agoulnik AI, Lu B, Zhu Q, Truong C, Ty MT, Arango N, Chada KK, Bishop CE. 2002. A novel gene, Pog, is necessary for primordial germ cell proliferation in the mouse and underlies the germ cell deficient mutation, gcd. *Hum Mol Genet* **11**: 3047–3053.

Anderson EL, Baltus AE, Roepers-Gajadien HL, Hassold TJ, de Rooij DG, van Pelt AMM, Page DC. 2008. Stra8 and its inducer, retinoic acid, regulate meiotic initiation in both spermatogenesis and oogenesis in mice. *Proc Natl Acad Sci USA* **105**: 14976–14980.

Barnes DE, Lindahl T. 2004. Repair and genetic consequences of endogenous DNA base damage in mammalian cells. *Annu Rev Genet* **38**: 445–476.

Barnum KJ, O'Connell MJ. 2014. Cell cycle regulation by checkpoints.

Methods Mol Biol **1170**: 29–40.

Bartek J, Lukas J. 2003. Chk1 and Chk2 kinases in checkpoint control and cancer. *Cancer Cell* **3**: 421–429.

Baudat F, Manova K, Yuen JP, Jasin M, Keeney S. 2000. Chromosome synapsis defects and sexually dimorphic meiotic progression in mice lacking *Spo11*. *Mol Cell* **6**: 989–998.

Besenbacher S, Liu S, Izarzugaza JMG, Grove J, Belling K, Bork-Jensen J, Huang S, Als TD, Li S, Yadav R, et al. 2015. Novel variation and de novo mutation rates in population-wide de novo assembled Danish trios. *Nat Commun* **6**: 5969.

Bhalla N, Dernburg AF. 2005. A conserved checkpoint monitors meiotic chromosome synapsis in Caenorhabditis elegans. *Science* **310**: 1683–1686.

Bloom JC, Loehr AR, Schimenti JC, Weiss R. 2019. Germline Genome Protection: Implicaions for Gamete Quality and Germ Cell Tumorigenesis. *Andrology* **7:** 516-526.

Boateng KA, Bellani MA, Gregoretti IV, Pratto F, Camerini-Otero RD. 2013. Homologous pairing preceding SPO11-mediated double-strand breaks in mice. *Dev Cell* **24**: 196–205.

Bolcun-Filas E, Rinaldi VD, White ME, Schimenti JC. 2014. Reversal of female infertility by Chk2 ablation reveals the oocyte DNA damage checkpoint pathway. *Science* **343**: 533–536.

Bond JA, Wyllie FS, Wynford-Thomas D. 1994. Escape from senescence in

human diploid fibroblasts induced directly by mutant p53. *Oncogene* **9**: 1885–1889.

Botuyan MV, Lee J, Ward IM, Kim J-E, Thompson JR, Chen J, Mer G. 2006. Structural basis for the methylation state-specific recognition of histone H4-K20 by 53BP1 and Crb2 in DNA repair. *Cell* **127**: 1361–1373.

Bowles J, Knight D, Smith C, Wilhelm D, Richman J, Mamiya S, Yashiro K, Chawengsaksophak K, Wilson MJ, Rossant J, et al. 2006. Retinoid signaling determines germ cell fate in mice. *Science* **312**: 596–600.

Bowles J, Koopman P. 2007. Retinoic acid, meiosis and germ cell fate in mammals. *Development* **134**: 3401–3411.

Braude P, Bolton V, Moore S. 1988. Human gene expression first occurs between the four- and eight-cell stages of preimplantation development. *Nature* **332**: 459–461.

Brown JP, Wei W, Sedivy JM. 1997. Bypass of senescence after disruption of p21CIP1/WAF1 gene in normal diploid human fibroblasts. *Science* **277**: 831–834.

Burton DGA, Faragher RGA. 2015. Cellular senescence: from growth arrest to immunogenic conversion. *Age (Omaha)* **37**: 27.

Cao L, Xu X, Bunting SF, Liu J, Wang R-H, Cao LL, Wu JJ, Peng T-N, Chen J, Nussenzweig A, et al. 2009. A selective requirement for 53BP1 in the biological response to genomic instability induced by Brca1 deficiency. *Mol Cell* **35**: 534–541.

Cawthon RM, Meeks HD, Sasani TA, Smith KR, Kerber RA, O'Brien E, Baird

L, Dixon MM, Peiffer AP, Leppert MF, Quinlan AR, Jorde LB. 2020. Germline mutation rates in young adults predict longevity and reproductive lifespan. *Scientific Reports*.

Cervantes RB, Stringer JR, Shao C, Tischfield JA, Stambrook PJ. 2002. Embryonic stem cells and somatic cells differ in mutation frequency and type. *Proc Natl Acad Sci USA* **99**: 3586–3590.

Chen J-H, Stoeber K, Kingsbury S, Ozanne SE, Williams GH, Hales CN. 2004. Loss of proliferative capacity and induction of senescence in oxidatively stressed human fibroblasts. *J Biol Chem* **279**: 49439–49446.

Chuykin IA, Lianguzova MS, Pospelova TV, Pospelov VA. 2008. Activation of DNA damage response signaling in mouse embryonic stem cells. *Cell Cycle* **7**: 2922–2928.

Ciccia A, Elledge SJ. 2010. The DNA damage response: making it safe to play with knives. *Mol Cell* **40**: 179–204.

Cobb J, Handel MA. 1998. Dynamics of meiotic prophase I during spermatogenesis: from pairing to division. *Semin Cell Dev Biol* **9**: 445–450.

Conrad DF, Keebler JEM, DePristo MA, Lindsay SJ, Zhang Y, Casals F, Idaghdour Y, Hartl CL, Torroja C, Garimella KV, et al. 2011. Variation in genome-wide mutation rates within and between human families. *Nat Genet* **43**: 712–714.

Czabotar PE, Lessene G, Strasser A, Adams JM. 2014. Control of apoptosis by the BCL-2 protein family: implications for physiology and therapy.

Nat Rev Mol Cell Biol **15**: 49–63.

d'Adda di Fagagna F. 2008. Living on a break: cellular senescence as a DNA-damage response. *Nat Rev Cancer* **8**: 512–522.

Daley JM, Sung P. 2014. 53BP1, BRCA1, and the choice between recombination and end joining at DNA double-strand breaks. *Mol Cell Biol* **34**: 1380–1388.

Davis AJ, Chen DJ. 2013. DNA double strand break repair via non-homologous end-joining. *Transl Cancer Res* **2**: 130–143.

Deans AJ, West SC. 2009. FANCM connects the genome instability disorders Bloom's Syndrome and Fanconi Anemia. *Mol Cell* **36**: 943–953.

Denchi EL, de Lange T. 2007. Protection of telomeres through independent control of ATM and ATR by TRF2 and POT1. *Nature* **448**: 1068–1071.

Di Giacomo M, Barchi M, Baudat F, Edelmann W, Keeney S, Jasin M. 2005. Distinct DNA-damage-dependent and -independent responses drive the loss of oocytes in recombination-defective mouse mutants. *Proc Natl Acad Sci USA* **102**: 737–742.

Di Giovanni S, Knights CD, Rao M, Yakovlev A, Beers J, Catania J, Avantaggiati ML, Faden AI. 2006. The tumor suppressor protein p53 is required for neurite outgrowth and axon regeneration. *EMBO J* **25**: 4084–4096.

Di Leonardo A, Linke SP, Clarkin K, Wahl GM. 1994. DNA damage triggers a prolonged p53-dependent G1 arrest and long-term induction of Cip1 in normal human fibroblasts. *Genes Dev* **8**: 2540–2551.

Difilippantonio S, Gapud E, Wong N, Huang C-Y, Mahowald G, Chen HT, Kruhlak MJ, Callen E, Livak F, Nussenzweig MC, et al. 2008. 53BP1 facilitates long-range DNA end-joining during V(D)J recombination. *Nature* **456**: 529–533.

Dimitrova N, Chen Y-CM, Spector DL, de Lange T. 2008. 53BP1 promotes non-homologous end joining of telomeres by increasing chromatin mobility. *Nature* **456**: 524–528.

Endo T, Freinkman E, de Rooij DG, Page DC. 2017. Periodic production of retinoic acid by meiotic and somatic cells coordinates four transitions in mouse spermatogenesis. *Proc Natl Acad Sci USA* **114**: E10132–E10141.

Enguita-Marruedo A, Martín-Ruiz M, García E, Gil-Fernández A, Parra MT, Viera A, Rufas JS, Page J. 2019. Transition from a meiotic to a somatic-like DNA damage response during the pachytene stage in mouse meiosis. *PLoS Genet* **15**: e1007439.

Ewen KA, Koopman P. 2010. Mouse germ cell development: from specification to sex determination. *Mol Cell Endocrinol* **323**: 76–93.

Favor J. 1999. Mechanisms of mutation induction in germ cells of the mouse as assessed by the specific locus test. *Mutat Res* **428**: 227–236.

Featherstone C, Jackson SP. 1999. DNA double-strand break repair. *Curr Biol* **9**: R759-61.

Fenaux P, Degos L. 1997. Differentiation therapy for acute promyelocytic leukemia. *N Engl J Med* **337**: 1076–1077.

Findlay JK, Hutt KJ, Hickey M, Anderson RA. 2015. How is the number of primordial follicles in the ovarian reserve established? *Biol Reprod* **93**: 111.

Fluckiger A-C, Marcy G, Marchand M, Négre D, Cosset F-L, Mitalipov S, Wolf D, Savatier P, Dehay C. 2006. Cell cycle features of primate embryonic stem cells. *Stem Cells* **24**: 547–556.

Friedberg EC, Walker GC, Siede W, Wood RD, eds. 2005. *DNA Repair and Mutagenesis*. illustrated. American Society for Microbiology Press.

Gao Z, Moorjani P, Sasani TA, Pedersen BS, Quinlan AR, Jorde LB, Amster G, Przeworski M. 2019. Overlooked roles of DNA damage and maternal age in generating human germline mutations. *Proc Natl Acad Sci USA* **116**: 9491–9500.

Gao Z, Wyman MJ, Sella G, Przeworski M. 2016. Interpreting the dependence of mutation rates on age and time. *PLoS Biol* **14**: e1002355.

Gari K, Décaillet C, Delannoy M, Wu L, Constantinou A. 2008. Remodeling of DNA replication structures by the branch point translocase FANCM. *Proc Natl Acad Sci USA* **105**: 16107–16112.

Giglia-Mari G, Zotter A, Vermeulen W. 2011. DNA damage response. *Cold Spring Harb Perspect Biol* **3**: a000745.

Gill ME, Hu Y-C, Lin Y, Page DC. 2011. Licensing of gametogenesis, dependent on RNA binding protein DAZL, as a gateway to sexual differentiation of fetal germ cells. *Proc Natl Acad Sci USA* **108**: 7443–7448.

Giono LE, Manfredi JJ. 2006. The p53 tumor suppressor participates in multiple cell cycle checkpoints. *J Cell Physiol* **209**: 13–20.

Gire V, Roux P, Wynford-Thomas D, Brondello J-M, Dulic V. 2004. DNA damage checkpoint kinase Chk2 triggers replicative senescence. *EMBO J* **23**: 2554–2563.

Goldmann JM, Wong WSW, Pinelli M, Farrah T, Bodian D, Stittrich AB, Glusman G, Vissers LELM, Hoischen A, Roach JC, et al. 2016. Parent-of-origin-specific signatures of de novo mutations. *Nat Genet* **48**: 935–939.

Goriely A. 2016. Decoding germline de novo point mutations. *Nat Genet* **48**: 823–824.

Gray S, Cohen PE. 2016. Control of meiotic crossovers: from double-strand break formation to designation. *Annu Rev Genet* **50**: 175–210.

Grompe M, D'Andrea A. 2001. Fanconi anemia and DNA repair. *Hum Mol Genet* **10**: 2253–2259.

Grskovic M, Chaivorapol C, Gaspar-Maia A, Li H, Ramalho-Santos M. 2007. Systematic identification of cis-regulatory sequences active in mouse and human embryonic stem cells. *PLoS Genet* **3**: e145.

Hamer G, de Rooij DG. 2018. Mutations causing specific arrests in the development of mouse primordial germ cells and gonocytes. *Biol Reprod* **99**: 75–86.

Handel MA, Schimenti JC. 2010. Genetics of mammalian meiosis: regulation, dynamics and impact on fertility. *Nat Rev Genet* **11**: 124–136.

Harfe BD, Jinks-Robertson S. 2000. DNA polymerase zeta introduces multiple mutations when bypassing spontaneous DNA damage in Saccharomyces cerevisiae. *Mol Cell* **6**: 1491–1499.

Harley CB, Futcher AB, Greider CW. 1990. Telomeres shorten during ageing of human fibroblasts. *Nature* **345**: 458–460.

Hartwell LH, Weinert TA. 1989. Checkpoints: controls that ensure the order of cell cycle events. *Science* **246**: 629–634.

Hayashi K, Ohta H, Kurimoto K, Aramaki S, Saitou M. 2011. Reconstitution of the mouse germ cell specification pathway in culture by pluripotent stem cells. *Cell* **146**: 519–532.

Hayflick L, Moorhead PS. 1961. The serial cultivation of human diploid cell strains. *Exp Cell Res* **25**: 585–621.

Heyer BS, MacAuley A, Behrendtsen O, Werb Z. 2000. Hypersensitivity to DNA damage leads to increased apoptosis during early mouse development. *Genes Dev* **14**: 2072–2084.

Hong Y, Cervantes RB, Tichy E, Tischfield JA, Stambrook PJ. 2007. Protecting genomic integrity in somatic cells and embryonic stem cells. *Mutat Res* **614**: 48–55.

Hong Y, Stambrook PJ. 2004. Restoration of an absent G1 arrest and protection from apoptosis in embryonic stem cells after ionizing radiation. *Proc Natl Acad Sci USA* **101**: 14443–14448.

Huang AY, Xu X, Ye AY, Wu Q, Yan L, Zhao B, Yang X, He Y, Wang S, Zhang Z, et al. 2014. Postzygotic single-nucleotide mosaicisms in

whole-genome sequences of clinically unremarkable individuals. *Cell Res* **24**: 1311–1327.

Jackson SP, Bartek J. 2009. The DNA-damage response in human biology and disease. *Nature* **461**: 1071–1078.

Jankowska K. 2017. Premature ovarian failure. *Prz Menopauzalny* **16**: 51–56.

Jirge PR. 2016. Poor ovarian reserve. *J Hum Reprod Sci* **9**: 63–69.

Joenje H, Patel KJ. 2001. The emerging genetic and molecular basis of Fanconi anaemia. *Nat Rev Genet* **2**: 446–457.

Jónsson H, Sulem P, Kehr B, Kristmundsdottir S, Zink F, Hjartarson E, Hardarson MT, Hjorleifsson KE, Eggertsson HP, Gudjonsson SA, et al. 2017. Parental influence on human germline de novo mutations in 1,548 trios from Iceland. *Nature* **549**: 519–522.

Karimian A, Ahmadi Y, Yousefi B. 2016. Multiple functions of p21 in cell cycle, apoptosis and transcriptional regulation after DNA damage. *DNA Repair (Amst)* **42**: 63–71.

Keeney S. 2001. Mechanism and control of meiotic recombination initiation. *Curr Top Dev Biol* **52**: 1–53.

Keeney S. 2008. Spo11 and the Formation of DNA Double-Strand Breaks in Meiosis. *Genome Dyn Stab* **2**: 81–123.

Keeney S, Giroux CN, Kleckner N. 1997. Meiosis-specific DNA double-strand breaks are catalyzed by Spo11, a member of a widely conserved protein family. *Cell* **88**: 375–384.

Keeney S, Kleckner N. 1995. Covalent protein-DNA complexes at the 5’ strand

termini of meiosis-specific double-strand breaks in yeast. *Proc Natl Acad Sci USA* **92**: 11274–11278.

Khanna KK, Jackson SP. 2001. DNA double-strand breaks: signaling, repair and the cancer connection. *Nat Genet* **27**: 247–254.

Kim M, Habiba A, Doherty JM, Mills JC, Mercer RW, Huettner JE. 2009. Regulation of mouse embryonic stem cell neural differentiation by retinoic acid. *Dev Biol* **328**: 456–471.

Kim NW, Piatyszek MA, Prowse KR, Harley CB, West MD, Ho PL, Coviello GM, Wright WE, Weinrich SL, Shay JW. 1994. Specific association of human telomerase activity with immortal cells and cancer. *Science* **266**: 2011–2015.

Kitagawa R, Kastan MB. 2005. The ATM-dependent DNA damage signaling pathway. *Cold Spring Harb Symp Quant Biol* **70**: 99–109.

Kojima ML, de Rooij DG, Page DC. 2019. Amplification of a broad transcriptional program by a common factor triggers the meiotic cell cycle in mice. *Elife* **8**.

Kong A, Frigge ML, Masson G, Besenbacher S, Sulem P, Magnusson G, Gudjonsson SA, Sigurdsson A, Jonasdottir A, Jonasdottir A, et al. 2012. Rate of de novo mutations and the importance of father's age to disease risk. *Nature* **488**: 471–475.

Koubova J, Menke DB, Zhou Q, Capel B, Griswold MD, Page DC. 2006. Retinoic acid regulates sex-specific timing of meiotic initiation in mice. *Proc Natl Acad Sci USA* **103**: 2474–2479.

Kumar R, Ghyselinck N, Ishiguro K, Watanabe Y, Kouznetsova A, Höög C, Strong E, Schimenti J, Daniel K, Toth A, et al. 2015. MEI4 – a central player in the regulation of meiotic DNA double-strand break formation in the mouse. *J Cell Sci* **128**: 1800–1811.

Lawson KA, Dunn NR, Roelen BA, Zeinstra LM, Davis AM, Wright CV, Korving JP, Hogan BL. 1999. Bmp4 is required for the generation of primordial germ cells in the mouse embryo. *Genes Dev* **13**: 424–436.

Lesch BJ, Page DC. 2012. Genetics of germ cell development. *Nat Rev Genet* **13**: 781–794.

Li J, Yuan J. 2008. Caspases in apoptosis and beyond. *Oncogene* **27**: 6194–6206.

Li XC, Schimenti JC. 2007. Mouse pachytene checkpoint 2 (*Trip13*) is required for completing meiotic recombination but not synapsis. *PLoS Genet* **3**: e130.

Libby BJ, De La Fuente R, O'Brien MJ, Wigglesworth K, Cobb J, Inselman A, Eaker S, Handel MA, Eppig JJ, Schimenti JC. 2002. The mouse meiotic mutation mei1 disrupts chromosome synapsis with sexually dimorphic consequences for meiotic progression. *Dev Biol* **242**: 174–187.

Lim S, Kaldis P. 2013. Cdks, cyclins and CKIs: roles beyond cell cycle regulation. *Development* **140**: 3079–3093.

Lin Y, Gill ME, Koubova J, Page DC. 2008. Germ cell-intrinsic and -extrinsic factors govern meiotic initiation in mouse embryos. *Science* **322**: 1685–1687.

Lindahl T. 1993. Instability and decay of the primary structure of DNA. *Nature* **362**: 709–715.

Lindahl T, Barnes DE. 2000. Repair of endogenous DNA damage. *Cold Spring Harb Symp Quant Biol* **65**: 127–133.

Liu J, Wu TC, Lichten M. 1995. The location and structure of double-strand DNA breaks induced during yeast meiosis: evidence for a covalently linked DNA-protein intermediate. *EMBO J* **14**: 4599–4608.

Livera G, Petre-Lazar B, Guerquin M-J, Trautmann E, Coffigny H, Habert R. 2008. p63 null mutation protects mouse oocytes from radio-induced apoptosis. *Reproduction* **135**: 3–12.

Lukas J, Lukas C, Bartek J. 2004. Mammalian cell cycle checkpoints: signalling pathways and their organization in space and time. *DNA Repair (Amst)* **3**: 997–1007.

Luo Y, Hartford SA, Zeng R, Southard TL, Shima N, Schimenti JC. 2014. Hypersensitivity of primordial germ cells to compromised replication-associated DNA repair involves ATM-p53-p21 signaling. *PLoS Genet* **10**: e1004471.

Luo Y, Schimenti JC. 2015. MCM9 deficiency delays primordial germ cell proliferation independent of the ATM pathway. *Genesis* **53**: 678–684.

Macrae CJ, McCulloch RD, Ylanko J, Durocher D, Koch CA. 2008. APLF (C2orf13) facilitates nonhomologous end-joining and undergoes ATM-dependent hyperphosphorylation following ionizing radiation. *DNA Repair (Amst)* **7**: 292–302.

Mahaney BL, Meek K, Lees-Miller SP. 2009. Repair of ionizing radiation-induced DNA double-strand breaks by non-homologous end-joining. *Biochem J* **417**: 639–650.

Maréchal A, Zou L. 2013. DNA damage sensing by the ATM and ATR kinases. *Cold Spring Harb Perspect Biol* **5**.

Mateos-Gomez PA, Gong F, Nair N, Miller KM, Lazzerini-Denchi E, Sfeir A. 2015. Mammalian polymerase θ promotes alternative NHEJ and suppresses recombination. *Nature* **518**: 254–257.

Matsuoka S, Ballif BA, Smogorzewska A, McDonald ER, Hurov KE, Luo J, Bakalarski CE, Zhao Z, Solimini N, Lerenthal Y, et al. 2007. ATM and ATR substrate analysis reveals extensive protein networks responsive to DNA damage. *Science* **316**: 1160–1166.

Matt S, Hofmann TG. 2016. The DNA damage-induced cell death response: a roadmap to kill cancer cells. *Cell Mol Life Sci* **73**: 2829–2850.

McIlwain DR, Berger T, Mak TW. 2013. Caspase functions in cell death and disease. *Cold Spring Harb Perspect Biol* **5**: a008656.

McLaren A. 2003. Primordial germ cells in the mouse. *Dev Biol* **262**: 1–15.

McNairn AJ, Rinaldi VD, Schimenti JC. 2017. Repair of meiotic DNA breaks and homolog pairing in mouse meiosis requires a minichromosome maintenance (MCM) paralog. *Genetics* **205**: 529–537.

Meek K, Dang V, Lees-Miller SP. 2008. DNA-PK: the means to justify the ends? *Adv Immunol* **99**: 33–58.

Melé M, Ferreira PG, Reverter F, DeLuca DS, Monlong J, Sammeth M, Young

TR, Goldmann JM, Pervouchine DD, Sullivan TJ, et al. 2015. The human transcriptome across tissues and individuals. *Science* **348**: 660–665.

Mézard C, Jahns MT, Grelon M. 2015. Where to cross? New insights into the location of meiotic crossovers. *Trends Genet* **31**: 393–401.

Milholland B, Dong X, Zhang L, Hao X, Suh Y, Vijg J. 2017. Differences between germline and somatic mutation rates in humans and mice. *Nat Commun* **8**: 15183.

Moldovan G-L, D'Andrea AD. 2009. How the fanconi anemia pathway guards the genome. *Annu Rev Genet* **43**: 223–249.

Nadler JJ, Braun RE. 2000. Fanconi anemia complementation group C is required for proliferation of murine primordial germ cells. *Genesis* **27**: 117–123.

Nikolic A, Volarevic V, Armstrong L, Lako M, Stojkovic M. 2016. Primordial germ cells: current knowledge and perspectives. *Stem Cells Int* **2016**: 1741072.

Ohinata Y, Ohta H, Shigeta M, Yamanaka K, Wakayama T, Saitou M. 2009. A signaling principle for the specification of the germ cell lineage in mice. *Cell* **137**: 571–584.

Ohno M, Sakumi K, Fukumura R, Furuichi M, Iwasaki Y, Hokama M, Ikemura T, Tsuzuki T, Gondo Y, Nakabeppu Y. 2014. 8-oxoguanine causes spontaneous de novo germline mutations in mice. *Sci Rep* **4**: 4689.

Oktay K. 2006. Measuring the Impact of Chemotherapy on Fertility in Women

With Breast Cancer. *J Clin Oncol* **24**: 4044–4046.

Peters H. 1969. The development of the mouse ovary from birth to maturity. *Acta Endocrinol (Copenh)* **62**: 98–116.

Rahbari R, Wuster A, Lindsay SJ, Hardwick RJ, Alexandrov LB, Turki SA, Dominiczak A, Morris A, Porteous D, Smith B, et al. 2016. Timing, rates and spectra of human germline mutation. *Nat Genet* **48**: 126–133.

Reinholdt LG, Schimenti JC. 2005. Mei1 is epistatic to Dmc1 during mouse meiosis. *Chromosoma* **114**: 127–134.

Rinaldi VD, Bloom JC, Schimenti JC. 2020. Oocyte Elimination Through DNA Damage Signaling from CHK1/CHK2 to p53 and p63. *Genetics*.

Rinaldi VD, Bolcun-Filas E, Kogo H, Kurahashi H, Schimenti JC. 2017a. The DNA damage checkpoint eliminates mouse oocytes with chromosome synapsis failure. *Mol Cell* **67**: 1026–1036.e2.

Rinaldi VD, Hsieh K, Munroe R, Bolcun-Filas E, Schimenti JC. 2017b. Pharmacological Inhibition of the DNA Damage Checkpoint Prevents Radiation-Induced Oocyte Death. *Genetics* **206**: 1823–1828.

Robles SJ, Adami GR. 1998. Agents that cause DNA double strand breaks lead to p16INK4a enrichment and the premature senescence of normal fibroblasts. *Oncogene* **16**: 1113–1123.

Romanienko PJ, Camerini-Otero RD. 2000. The mouse *Spo11* gene is required for meiotic chromosome synapsis. *Mol Cell* **6**: 975–987.

Roque T, Haton C, Etienne O, Chicheportiche A, Rousseau L, Martin L, Mouthon M-A, Boussin FD. 2012. Lack of a p21waf1/cip -dependent

G1/S checkpoint in neural stem and progenitor cells after DNA damage in vivo. *Stem Cells* **30**: 537–547.

Rosner MH, Vigano MA, Ozato K, Timmons PM, Poirier F, Rigby PW, Staudt LM. 1990. A POU-domain transcription factor in early stem cells and germ cells of the mammalian embryo. *Nature* **345**: 686–692.

Russell LB, Selby PB, von Halle E, Sheridan W, Valcovic L. 1981. The mouse specific-locus test with agents other than radiations: interpretation of data and recommendations for future work. *Mutat Res* **86**: 329–354.

Saitou M, Barton SC, Surani MA. 2002. A molecular programme for the specification of germ cell fate in mice. *Nature* **418**: 293–300.

Sasani TA, Pedersen BS, Gao Z, Baird L, Przeworski M, Jorde LB, Quinlan AR. 2019. Large, three-generation human families reveal post-zygotic mosaicism and variability in germline mutation accumulation. *Elife* **8**.

Schultz LB, Chehab NH, Malikzay A, Halazonetis TD. 2000. p53 binding protein 1 (53BP1) is an early participant in the cellular response to DNA double-strand breaks. *J Cell Biol* **151**: 1381–1390.

Ségurel L, Wyman MJ, Przeworski M. 2014. Determinants of mutation rate variation in the human germline. *Annu Rev Genomics Hum Genet* **15**: 47–70.

Serio RN, Laursen KB, Urvalek AM, Gross SS, Gudas LJ. 2019. Ethanol promotes differentiation of embryonic stem cells through retinoic acid receptor-γ. *J Biol Chem* **294**: 5536–5548.

Sfeir A, Symington LS. 2015. Microhomology-Mediated End Joining: A Back-

up Survival Mechanism or Dedicated Pathway? *Trends Biochem Sci* **40**: 701–714.

Sherman MH, Bassing CH, Teitell MA. 2011. Regulation of cell differentiation by the DNA damage response. *Trends Cell Biol* **21**: 312–319.

Shiotani B, Zou L. 2009. ATR signaling at a glance. *J Cell Sci* **122**: 301–304.

Singh P, Aggarwal LM, Parry SA, Raman MJ. 2018. Radiation dosimetry and repair kinetics of DNA damage foci in mouse pachytene spermatocyte and round spermatid stages. *Mutagenesis* **33**: 231–239.

Soh YQS, Junker JP, Gill ME, Mueller JL, van Oudenaarden A, Page DC. 2015. A gene regulatory program for meiotic prophase in the fetal ovary. *PLoS Genet* **11**: e1005531.

Soumillon M, Necsulea A, Weier M, Brawand D, Zhang X, Gu H, Barthès P, Kokkinaki M, Nef S, Gnirke A, et al. 2013. Cellular source and mechanisms of high transcriptome complexity in the mammalian testis. *Cell Rep* **3**: 2179–2190.

Stanzione M, Baumann M, Papanikos F, Dereli I, Lange J, Ramlal A, Tränkner D, Shibuya H, de Massy B, Watanabe Y, et al. 2016. Meiotic DNA break formation requires the unsynapsed chromosome axis-binding protein IHO1 (CCDC36) in mice. *Nat Cell Biol* **18**: 1208–1220.

Stone JE, Lujan SA, Kunkel TA, Kunkel TA. 2012. DNA polymerase zeta generates clustered mutations during bypass of endogenous DNA lesions in Saccharomyces cerevisiae. *Environ Mol Mutagen* **53**: 777–786.

Suh E-K, Yang A, Kettenbach A, Bamberger C, Michaelis AH, Zhu Z, Elvin JA, Bronson RT, Crum CP, McKeon F. 2006. p63 protects the female germ line during meiotic arrest. *Nature* **444**: 624–628.

Surova O, Zhivotovsky B. 2013. Various modes of cell death induced by DNA damage. *Oncogene* **32**: 3789–3797.

Suvorova II, Grigorash BB, Chuykin IA, Pospelova TV, Pospelov VA. 2016. G1 checkpoint is compromised in mouse ESCs due to functional uncoupling of p53-p21Waf1 signaling. *Cell Cycle* **15**: 52–63.

Tam PP, Snow MH. 1981. Proliferation and migration of primordial germ cells during compensatory growth in mouse embryos. *J Embryol Exp Morphol* **64**: 133–147.

Tam PP, Zhou SX. 1996. The allocation of epiblast cells to ectodermal and germ-line lineages is influenced by the position of the cells in the gastrulating mouse embryo. *Dev Biol* **178**: 124–132.

Tichy ED, Stambrook PJ. 2008. DNA repair in murine embryonic stem cells and differentiated cells. *Exp Cell Res* **314**: 1929–1936.

Uchimura A, Higuchi M, Minakuchi Y, Ohno M, Toyoda A, Fujiyama A, Miura I, Wakana S, Nishino J, Yagi T. 2015. Germline mutation rates and the long-term phenotypic effects of mutation accumulation in wild-type laboratory mice and mutator mice. *Genome Res* **25**: 1125–1134.

Vanden Berghe T, Linkermann A, Jouan-Lanhouet S, Walczak H, Vandenabeele P. 2014. Regulated necrosis: the expanding network of non-apoptotic cell death pathways. *Nat Rev Mol Cell Biol* **15**: 135–147.

Vandenabeele P, Galluzzi L, Vanden Berghe T, Kroemer G. 2010. Molecular mechanisms of necroptosis: an ordered cellular explosion. *Nat Rev Mol Cell Biol* **11**: 700–714.

Wang M, Wu W, Wu W, Rosidi B, Zhang L, Wang H, Iliakis G. 2006. PARP-1 and Ku compete for repair of DNA double strand breaks by distinct NHEJ pathways. *Nucleic Acids Res* **34**: 6170–6182.

Weinert TA, Hartwell LH. 1988. The RAD9 gene controls the cell cycle response to DNA damage in Saccharomyces cerevisiae. *Science* **241**: 317–322.

Weiss CN, Ito K. 2015. DNA damage: a sensible mediator of the differentiation decision in hematopoietic stem cells and in leukemia. *Int J Mol Sci* **16**: 6183–6201.

Welt CK. 2008. Primary ovarian insufficiency: a more accurate term for premature ovarian failure. *Clin Endocrinol (Oxf)* **68**: 499–509.

Western PS, Miles DC, van den Bergen JA, Burton M, Sinclair AH. 2008. Dynamic regulation of mitotic arrest in fetal male germ cells. *Stem Cells* **26**: 339–347.

Winship AL, Stringer JM, Liew SH, Hutt KJ. 2018. The importance of DNA repair for maintaining oocyte quality in response to anti-cancer treatments, environmental toxins and maternal ageing. *Hum Reprod Update* **24**: 119–134.

Woodruff TK. 2015. Oncofertility: a grand collaboration between reproductive medicine and oncology. *Reproduction* **150**: S1-10.

Wu H-Y, Burgess SM. 2006. Two distinct surveillance mechanisms monitor meiotic chromosome metabolism in budding yeast. *Curr Biol* **16**: 2473–2479.

Wu L, Multani AS, He H, Cosme-Blanco W, Deng Y, Deng JM, Bachilo O, Pathak S, Tahara H, Bailey SM, et al. 2006. Pot1 deficiency initiates DNA damage checkpoint activation and aberrant homologous recombination at telomeres. *Cell* **126**: 49–62.

Xia B, Yan Y, Baron M, Wagner F, Barkley D, Chiodin M, Kim SY, Keefe DL, Alukal JP, Boeke JD, et al. 2020. Widespread transcriptional scanning in the testis modulates gene evolution rates. *Cell* **180**: 248–262.e21.

Xue X, Sung P, Zhao X. 2015. Functions and regulation of the multitasking FANCM family of DNA motor proteins. *Genes Dev* **29**: 1777–1788.

Yabuta Y, Kurimoto K, Ohinata Y, Seki Y, Saitou M. 2006. Gene expression dynamics during germline specification in mice identified by quantitative single-cell gene expression profiling. *Biol Reprod* **75**: 705–716.

Yamaguchi S, Kimura H, Tada M, Nakatsuji N, Tada T. 2005. Nanog expression in mouse germ cell development. *Gene Expr Patterns* **5**: 639–646.

Youle RJ, Strasser A. 2008. The BCL-2 protein family: opposing activities that mediate cell death. *Nat Rev Mol Cell Biol* **9**: 47–59.

Zhang H, Liu L, Li X, Busayavalasa K, Shen Y, Hovatta O, Gustafsson J-Å, Liu K. 2014. Life-long in vivo cell-lineage tracing shows that no oogenesis originates from putative germline stem cells in adult mice. *Proc Natl*

Acad Sci USA **111**: 17983–17988.

Zheng H, Ying H, Yan H, Kimmelman AC, Hiller DJ, Chen A-J, Perry SR, Tonon G, Chu GC, Ding Z, et al. 2008. p53 and Pten control neural and glioma stem/progenitor cell renewal and differentiation. *Nature* **455**: 1129–1133.

Zhou BB, Elledge SJ. 2000. The DNA damage response: putting checkpoints in perspective. *Nature* **408**: 433–439.

CHAPTER 2

A REPORTER MOUSE FOR *IN VIVO* DETECTION OF DNA DAMAGE IN EMBRYONIC GERM CELLS

*This chapter is a reprint with minor reformatting of the manuscript: Bloom, J.C. and Schimenti, J.C. A Reporter Mouse for *In Vivo* Detection of DNA Damage in Embryonic Germ Cells. *genesis.* 2020;e23368. https://doi.org/10.1002/dvg.23368

1- Abstract

Maintaining genome integrity in the germline is essential for survival and propagation of a species. In both mouse and human, germ cells originate during fetal development and are hypersensitive to both endogenous and exogenous DNA damaging agents. Currently, mechanistic understanding of how primordial germ cells respond to DNA damage is limited in part by the tools available to study these cells. We developed a mouse transgenic reporter strain expressing a 53BP1-mCherry fusion protein under the control of the Oct4ΔPE embryonic germ cell-specific promoter. This reporter binds sites of DNA double strand breaks (DSBs) on chromatin, forming foci. Using

ionizing radiation as a DNA double strand break-inducing agent, we show that the transgenic reporter expresses specifically in the embryonic germ cells of both sexes and forms DNA damage induced foci in both a dose- and time-dependent manner. The dynamic time-sensitive and dose-sensitive DNA damage detection ability of this transgenic reporter, in combination with its specific expression in embryonic germ cells, makes it a versatile and valuable tool for increasing our understanding of DNA damage responses in these unique cells.

KEYWORDS: primordial germ cells, DNA damage, DNA repair, fertility, double strand breaks

2- Introduction

In most contexts, DNA double strand breaks (DSBs) are damage-induced lesions which can arise as a by-product of normal cellular processes or from exogenous damaging agents (Featherstone and Jackson 1999). If not repaired correctly, DSBs can be mutagenic and lead to deletions, translocations, and other chromosomal rearrangements. If left unrepaired, they can trigger cell death (Cannan and Pederson 2016). The most common method of detecting DSBs is by immunolabeling with an antibody against different markers of DNA damage, such as γH2AX (Podhorecka et al. 2010). While frequently used, this method requires cell fixation and depends on

antibody specificity and sensitivity. More recently, a number of labs have begun to use fluorescent reporters of p53 binding protein 1 (53BP1) to quantify DSBs in individual living cultured cells (Karanam et al. 2012; Miwa et al. 2013). A major advantage of this method is that fixation and subsequent immunohistochemistry are not required for DSB visualization. Forgoing fixation enables visualization of DNA repair dynamics over time.

Preserving genome integrity in germ cells is essential for successful transmission of hereditary information to future generations and survival of a species. In many organisms, including mice and humans, germ cells are first specified during embryonic development (Tam and Snow 1981; Ginsburg et al. 1990; Gomperts et al. 1994). These primordial germ cells (PGCs), arising from a small progenitor pool, migrate and proliferate to subsequently form the entire adult germline (Tam and Snow 1981; Gomperts et al. 1994). Perturbations to PGC development and growth, including those affecting genomic integrity of PGCs, can lead to a severe reduction or complete loss of germ cells in sexually mature adults (Hamer and de Rooij 2018). Notably, mutations in a number of genes involved in DNA repair cause depletion of PGCs and consequently a reduction of germ cells post-natally, while having very subtle effects in the soma (Nadler and Braun 2000; Agoulnik et al. 2002; Luo et al. 2014; Luo and Schimenti 2015). Furthermore, mouse PGCs are particularly hypersensitive to ionizing radiation (IR)-induced DSBs, but the basis for this sensitivity remains unknown (Heyer et al. 2000), in part due to the limited accessibility and numbers of fetal germ cells. Improvement to our current

understanding of the mechanisms responsible for hypersensitivity of these cells to exogenous and endogenous DNA damage would benefit substantially from new research-enabling experimental tools. Here, we describe a transgenic mouse model for *in vivo* DSB detection specifically in fetal germ cells, alleviating technical barriers for studying DNA damage and repair in this difficult-to-access embryonic cell population.

3- Materials and Methods

All graphing and statistical analyses in the study were performed using GraphPad Prism8.

Vector construction and generation of Tg(Oct4ΔPE-53BP1mCherry)1Jcs mice

The Oct4ΔPE-53BP1mCherry construct was produced by replacing the GFP portion of the Oct4ΔPE-GFP plasmid (Addgene plasmid #52382) with a 53BP1-mCherry fragment (Dimitrova et al. 2008) (Addgene plasmid #19835). The GFP fragment was removed via *Afe*I and *Fse*I restriction enzyme digestion of the Oct4ΔPE-GFP plasmid. Re-introduction of an ~200bp conserved portion of the *Oct4* promoter adjacent to the excised GFP sequence was performed via PCR amplification (see Table 1 for a list of primers used). During this step, a *Pac*I restriction site was also added. Next, the 53BP1-mCherry reporter was PCR amplified with primers designed to add *Pac*I and *Fse*I restriction sites to the 5' and 3' ends, then ligated into the

recipient Oct4ΔPE plasmid lacking GFP to make the final construct for pronuclear injection.

Prior to pronuclear injection, the construct was linearized and gel purified to remove plasmid backbone. Following gel purification, the linearized Oct4ΔPE-53BP1mCherry reporter was injected at a concentration of 1.5 ng/ul into FVBxB62J F1 hybrid embryos and transgene positive animals were genotype as described below. The use of mice in this study was approved by Cornell's Institutional Animal Care and Use Committee.

Genotyping strategy

Crude lysates for PCR were prepared as described (Truett et al. 2000). Genotyping primers are provided in Table 1. PCR conditions were as follows: initial denaturation at 95°C for 4 minutes, then 30 cycles of 95°C for 30 seconds, 62.5°C for 50 seconds, 72°C for 40 seconds, and a final elongation at 72°C for 5 minutes. For identification of transgene positive animals, the presence of a 131 bp PCR product was assessed on an agarose gel.

Table 1. Oligonucleotides used in this study

Name	Sequence 5' to 3'	Purpose
Oct4consF	gatcagcgctcgcctcagtt	Re-introduction of conserved portion of Oct4deltaPE-GFP plasmid
Oct4consR	atataGGCCGGCCcagctTTAATTAAtgcccaccttccccatga	Re-introduction of conserved portion of Oct4deltaPE-GFP plasmid+addition of PacI restriction site

DSB-Oct4 F	tacttaattaaCCACCATGGTGAGCAAG	53BP1-mCherry reporter amplification
DSB-Oct4 R	atatggccggccCTCATTCACCGGTGTTG	53BP1-mCherry reporter amplification
DSBgenoF	catcaaggagttcatgcg	Genotyping primer
DSBgenoR	ccttggtcaccttcagc	Genotyping primer

Fertility assessments

Transgene positive and negative mice (at 8 weeks old) were housed with C57BL/6J wild type animals of the opposite sex. Litter sizes were determined by counting pups on the day of birth.

To quantify sperm, cauda epididymides from 8 week old mice were minced in 2 mL of 1X PBS and then incubated for 15 minutes at 37°C to allow spermatozoa to swim out. Sperm were then diluted 1:5 in 1X PBS and counted with a hemocytometer.

Histology

Testes were collected from 8 week old males, fixed in Bouin's overnight, washed with 70% ethanol for 24 hours and then embedded in paraffin. Testes were sectioned at 6 μm and stained with hematoxylin and eosin (H&E).

Irradiation exposure

Mice were placed in a ^{137}cesium irradiator with a rotating turntable and exposed to the doses of radiation specified.

Whole mount staining

Whole mount staining was conducted as described (Rinaldi et al. 2018). Genital ridges were stained using primary antibody rabbit anti-DDX4/MVH (1:500, ab13840; Abcam) and anti-rabbit Alexa Fluor 488 secondary antibody (1:1000). P0 ovaries and testes were labeled with rat anti-Tra98/GCNA (1:500, ab82527; Abcam) and anti-rat Alexa Fluor 488 secondary antibody (1:1000). Samples were imaged on an upright Zeiss LSM880 confocal microscope using an either 10X NA 0.45 water immersion C-Apochromat objective (for the P0 ovaries and testes) or a 40X NA 1.1 water immersion C-Apochromat objective (for the genital ridges).

Foci quantification

Foci quantification was performed using Arivis Vision4D 3.1.1 analysis software. The following parameters were used and applied to all images: puncta diameter=3 μm (threshold=5), nuclei diameter 14 μm (threshold=10; split sensitivity 63%), volume without holes 200 μm^3 to 10000 μm^3.

Germ cell quantification

Germ cells from the 3 medial optical sections of each P0 ovary and testis collected were quantified as described in Rinaldi *et al.* 2018.

Resource Availability

The Tg(Oct4ΔPE-53BP1mCherry)1Jcs mouse-line is available upon request.

4- Results

Functional Validation of the Oct4ΔPE-53BP1mCherry Reporter Transgene

To better understand DSB response dynamics in embryonic germ cells, and to eliminate the need for dual antibody labeling with both a germ cell and DNA damage response marker, we a built a reporter construct in which the Oct4ΔPE embryonic germ cell promoter (Yoshimizu et al. 1999) drives an established DSB-sensing reporter (Figure 2.1A) (Dimitrova et al. 2008). This promoter fragment (which lacks a proximal enhancer element) has been well characterized for its ability to drive specific expression in primordial germ cells, later stage fetal germ cells, and in the germ cells of juvenile postnatal testes (Sabour et al. 2011; Yeom et al. 1996; Szabó et al. 2002; Yoshimizu et al. 1999). The reporter is composed of mCherry fused to the Tudor binding domain of the 53BP1 protein and functions by binding to the H4K20me2 chromatin mark which becomes exposed adjacent to DNA DSBs (Dimitrova et al. 2008). In the absence of DSBs, the reporter is expressed in the nucleus in a diffuse pattern, but once DSBs are induced, the reporter forms foci at the sites of damage.

The Oct4ΔPE-53BP1mCherry reporter construct (Figure 2.1A) was microinjected into single cell mouse zygotes, and founder transgenics were identified via PCR with transgene-specific primers. Following germline transmission of the transgene, sexually mature transgene positive males and females were paired for timed matings. Gonads from male and female transgene positive embryos were collected at embryonic day 13.5 (E13.5), fixed, and co-labeled with the germ cell marker MVH (mouse vasa homolog; formally, DDX4) to assess if transgene expression was specific to germ cells in both sexes (Figure 2.1B). After confirming PGC-specific expression of the transgene, we validated that its expression does not have a detrimental impact on the fertility of transgene-positive adult female and male animals (Figure 2.2A-E).

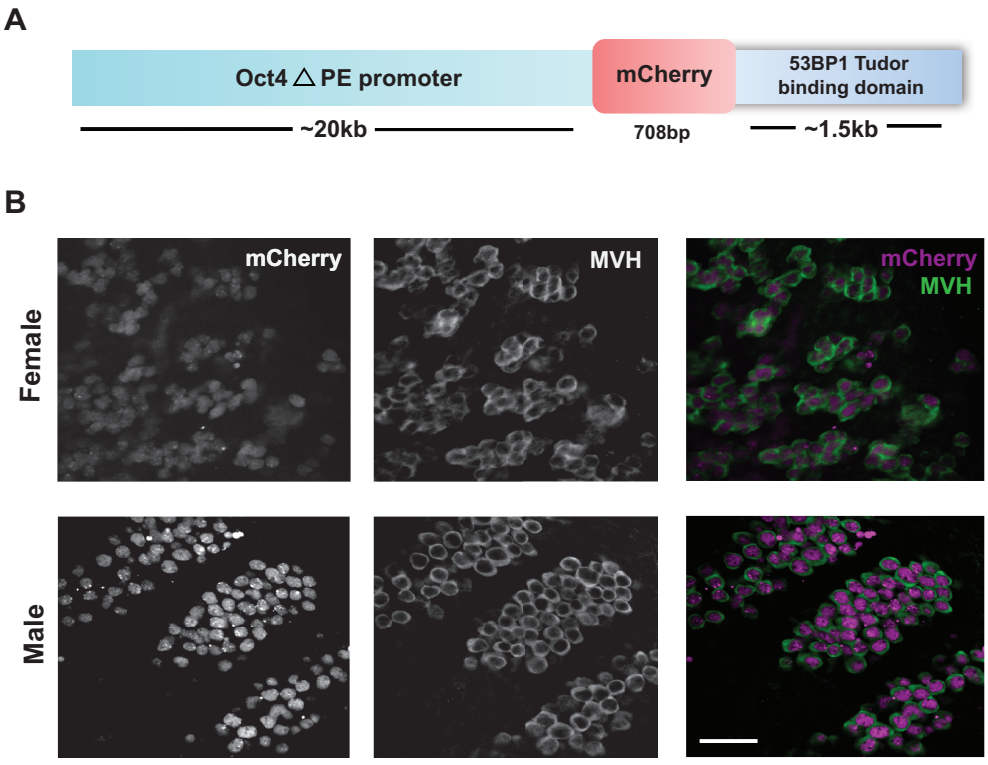

Figure 2.1. Creation of a mouse line expressing an Oct4ΔPE-53BP1-mCherry transgene specifically in male and female embryonic germ cells. (A) Schematic diagram of transgene construct with the Oct4ΔPE embryonic germ cell specific promoter and the 53BP1-mCherry DNA double strand break sensing reporter. (B) Whole mount immunofluorescence images of E13.5 transgenic male and female genital ridges with panels on the left showing endogenous mCherry reporter localization, middle panels showing antibody labeling of the cytoplasmic germ cell marker MVH (DDX4), and panels on the right showing the corresponding merged image. Scale bar= 50 μm

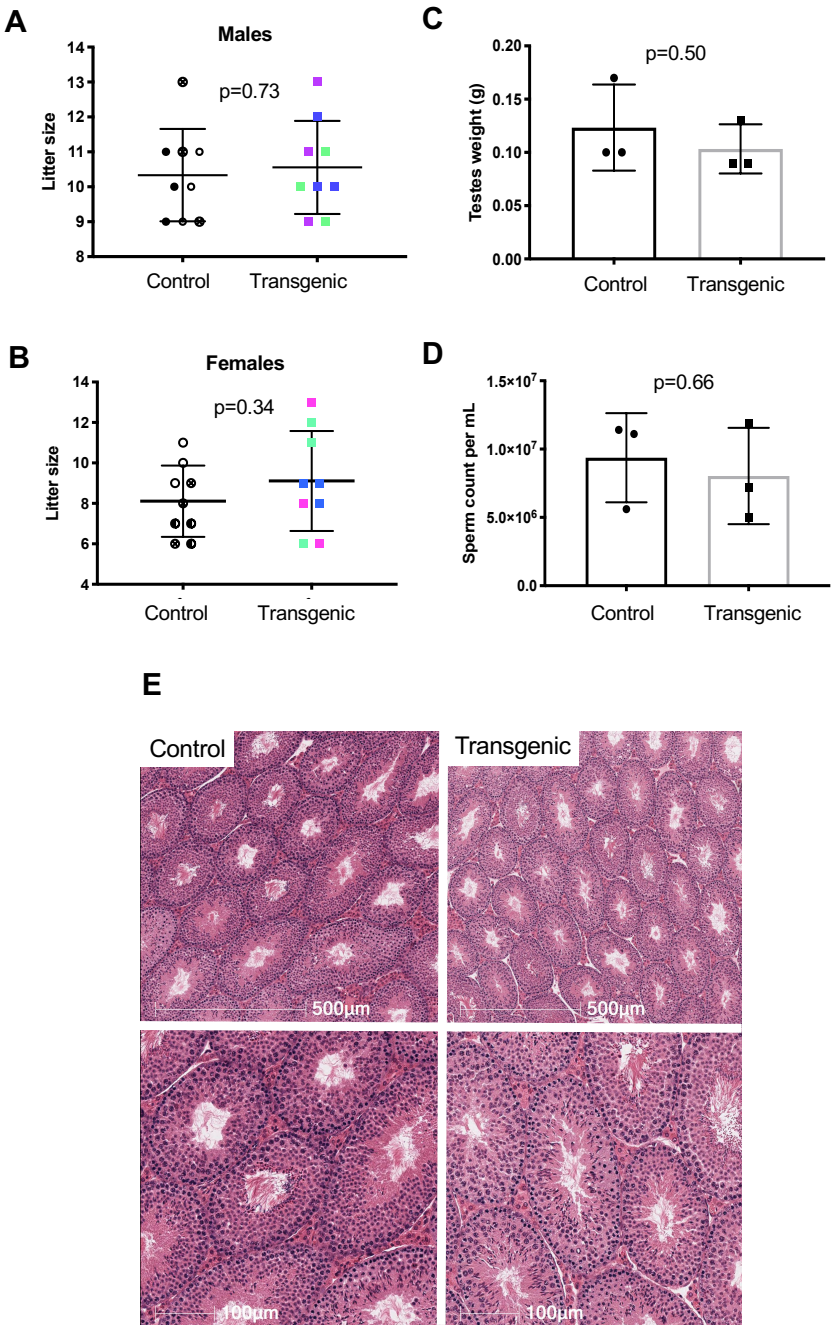

Figure 2.2. Expression of the Oct4ΔPE 53BP1-mCherry transgene does not alter fertility. (A) Litter sizes from transgenic and transgene-negative males mated to wild type females. Average litter sizes (± SD) produced by

transgene-negative and –positive males were 10.3±1.3 and 10.6±1.3 respectively. (B) Litter sizes from transgenic and transgene-negative females mated to wild type males. Average litter sizes (± SD) produced by transgene-negative and –positive females were 8.1±1.8 and 9.1±2.5 respectively. (C) Testes weights of transgenic and transgene-negative males. Average testes weights (± SD) of transgene-negative and –positive males were 0.12g±0.04 g and 0.1g±0.02 g respectively. (D) Caudal epididymis sperm counts of transgenic and transgene-negative males. Average sperm counts (± SD) of transgene-negative and –positive males were $9.37x10^6 \pm 3.27x10^6$ and $8.03x10^6 \pm 3.52x10^6$ respectively. (E) Hematoxylin and eosin (H&E) staining of testis cross-sections from 8 week old males. Top row: scale bar=500 μm; bottom row: scale bar=100 μm.

We next sought to determine whether the DSB sensing reporter portion of the transgene was functional. To examine this, we exposed pregnant mice at 13.5dpc to a single low dose of IR (1Gy) and quantified focus formation 1 hour later compared to unirradiated transgene-positive counterparts (Figure 2.3A). Quantification of foci revealed that the reporter functions in both a dose-dependent (Figure 2.3B, C) and time-dependent manner with damage-induced foci being undetectable 24 hours after IR (Figure 2.4). While tissue fixation was performed here, the fluorescent reporter is also amenable to live cell

imaging applications, which should provide even greater signal (Joosen et al. 2014).

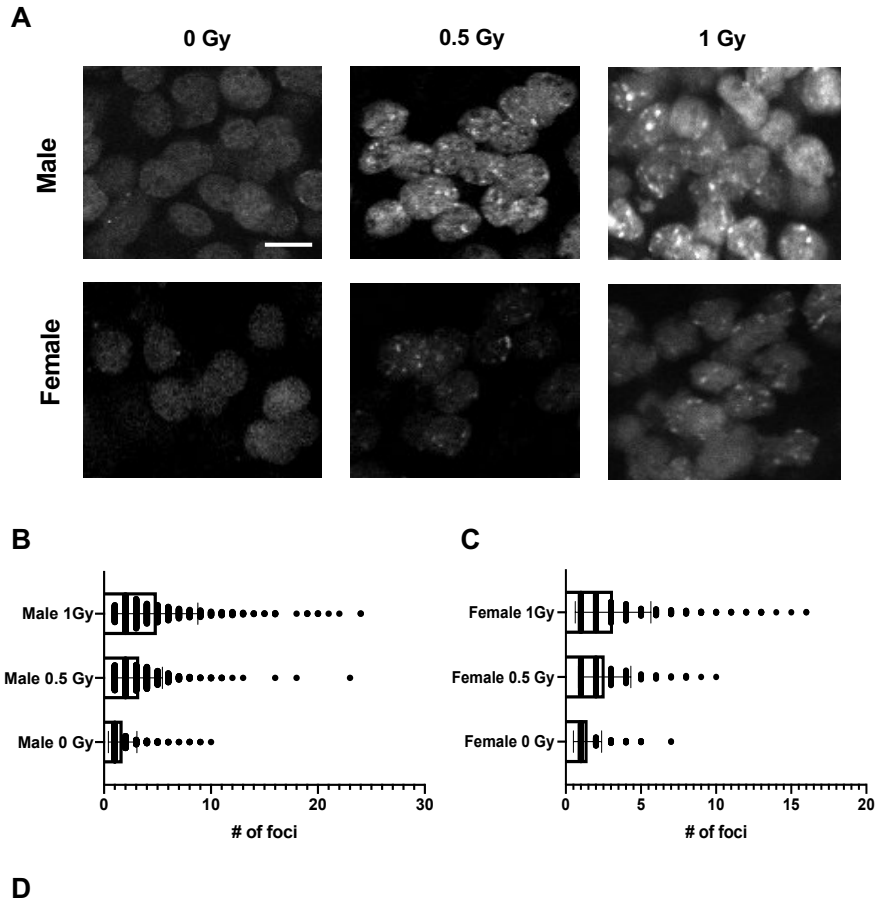

D

		Foci Metrics				
	Dose (Gy)	Mean	Standard Dev.	Mode	# of nuclei quantified	% nuclei with >1 focus
Male	0	1.7	1.3	1	686	15
	0.5	3.3	2.2	2	882	27
	1	4.9	3.8	2	634	46
Female	0	1.4	0.9	1	385	11
	0.5	2.6	1.7	2	216	19
	1	3.1	2.5	1	672	17

Figure 2.3. Primordial germ cells of Oct4ΔPE 53BP1-mCherry transgenic mice form radiation-induced foci in a dose-dependent manner. (A) Whole mount immunofluorescence images of E13.5 transgenic male and female genital ridges 1 hour after exposure to 0, 0.5, or 1 Gy of radiation. Scale

bar=10 μM. (B) Foci quantification of transgenic male PGCs at the doses shown in A; p-values derived from a non-parametric Mann-Whitney U test where $p<0.0001$ for all comparisons shown. (C) Foci quantification of transgenic female PGCs at the doses shown in A; p-values derived from a non-parametric Mann-Whitney U test where $p=0.018$ for the 0.5 vs. 1 Gy statistical comparison and $p<0.0001$ for the 0 vs. 0.5 Gy and 0 vs. 1 Gy comparisons. (D) Table of reporter induction metrics in response to radiation including mean number of foci formed, mode, number of nuclei quantified per condition and the percentage of nuclei with more than one focus.

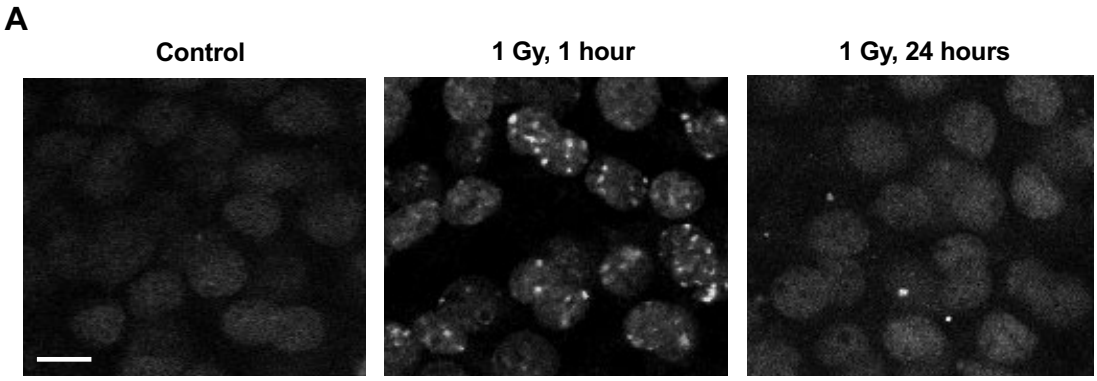

Figure 2.4. Oct4ΔPE 53BP1-mCherry transgene responds to DNA damage dynamically, in a time-dependent manner. Whole mount immunofluorescence images of E13.5 transgenic genital ridges given 1 Gy of radiation and collected 1 hour and 24 hours after exposure. Leftmost image is from an un-irradiated control. Scale bar=10 μm.

Radiation-induced Reporter Foci Dynamics Differ Between Male and Female E13.5 PGCs

While IR cause both female and male PGCs to form mCherry foci in a dose-dependent manner, the average number of induced foci differed between the sexes (Figure 2.3B, C). At E13.5, female germ cells had fewer foci than males, and the percentage of nuclei with >1 focus in response to increasing IR doses remained fairly constant. In contrast, the percentage of nuclei with >1 focus steadily increased in male germ cells with increasing IR dosages (Figure 2.3D). We speculate that these differences might be due to the different developmental trajectories of the sexes at this time point. At E13.5, female germ cells begin to enter the leptotene stage of prophase I in meiosis I (Speed 1982). Upon meiotic entry, the germ cells produce endogenously programmed DSBs that induce, and are required for, meiotic homologous recombination (HR) and pairing of homologous chromosomes (Handel and Schimenti 2010). While repair of DSBs in meiosis occurs exclusively via HR pathway components, 53BP1 is associated primarily with the non-homologous end joining (NHEJ) DSB repair pathway. Therefore, its activity as a DSB responsive element may be down-regulated during early meiosis (Enguita-Marruedo et al. 2019; Singh et al. 2018), resulting in less 53BP1-based reporter foci detection in the female germ cells at this time. Additionally, since the transgene promoter is downregulated in female germ cells upon meiotic entry (Sabour et al. 2011), this may contribute to the difference in foci dynamics.

An Acute Dose of Radiation During Fetal Development Leads to a Reduction of Germ Cells in Males and Females at Birth

In order to assess the ramifications of DNA damage on PGCs, we performed the same experimental treatment conditions as previously described, but collected female and male gonads at birth rather than at E13.5 (Figure 2.5A). Quantification of postnatal germ cells indicated that both IR doses used were sufficient to cause a reduction in germ cells at birth in both sexes (Figure 2.5B, C).

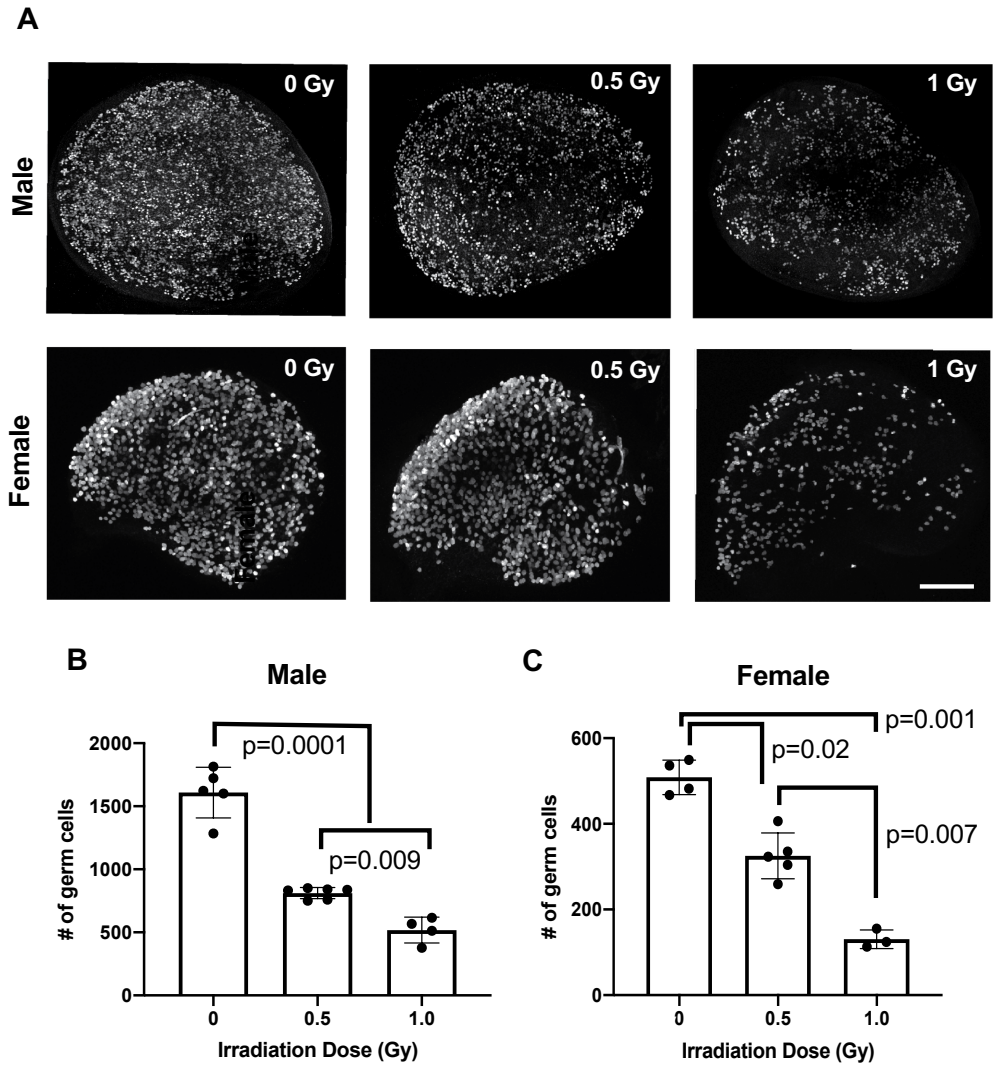

Figure 2.5. Acute radiation-induced DNA damage during fetal development leads to a reduction in germ cells at birth. (A) Whole mount maximum intensity immunofluorescence images of P0 testes and ovaries labeled with germ cell marker Tra98/GCNA in which the irradiation dose noted corresponds to the amount of radiation exposure the samples experienced *in utero* at E13.5. Scale bar=200 μM. (B) Germ cell quantification of P0 testes at the doses shown in A. Number of germ cells quantified from the 3 centermost sections of each sample is graphed; p-values derived from a non-parametric Mann-Whitney U test. (C) Germ cell quantification of P0 ovaries at the doses shown in A and quantified as in B; p-values derived from a non-parametric Mann-Whitney U test.

5- Discussion

Here, we validate and demonstrate the functionality of a mouse transgenic reporter line designed to aid the study of DNA damage induction and responses in embryonic germ cells. The reporter, like the parental vector designed for generic expression in cultured cells (Dimitrova et al. 2008), was responsive to both the dose of DNA damage and time after DNA damage exposure. While numerous techniques can provide a static read-out of DNA damage, the dynamic nature of reporter allows for the examination of DNA repair activity in real time and under various different contexts, such as during *ex vivo* culture of fetal gonads (Coveney et al. 2008). Additionally, the

sensitivity of the reporter to low doses of DNA damage is conducive to further studies aimed at understanding the unique sensitivity of primordial germ cells to DNA double strand breaks.

6- Acknowledgments

This work was supported by National Institutes of Health grants S10-OD018516 (to Cornell's Imaging Facility), R01HD082568 to J.C.S., and an Institutional training grant T32HD057854 that supported J.C.B. The authors would like thank R. Munroe and C. Abratte of Cornell's Stem Cell and Transgenic Core Facility, and R. Williams for assistance with microscopy and image analysis training.

References

Agoulnik, A. I., Lu, B., Zhu, Q., Truong, C., Ty, M. T., Arango, N., … Bishop, C. E. (2002). A novel gene, Pog, is necessary for primordial germ cell proliferation in the mouse and underlies the germ cell deficient mutation, gcd. *Human Molecular Genetics*, *11*(24), 3047–3053. https://doi.org/10.1093/hmg/11.24.3047

Cannan, W. J., & Pederson, D. S. (2016). Mechanisms and Consequences of Double-Strand DNA Break Formation in Chromatin. *Journal of Cellular Physiology*, *231*(1), 3–14. https://doi.org/10.1002/jcp.25048

Coveney, D., Cool, J., Oliver, T., & Capel, B. (2008). Four-dimensional

analysis of vascularization during primary development of an organ, the gonad. *Proceedings of the National Academy of Sciences of the United States of America*, *105*(20), 7212–7217. https://doi.org/10.1073/pnas.0707674105

Dimitrova, N., Chen, Y.-C. M., Spector, D. L., & de Lange, T. (2008). 53BP1 promotes non-homologous end joining of telomeres by increasing chromatin mobility. *Nature*, *456*(7221), 524–528. https://doi.org/10.1038/nature07433

Enguita-Marruedo, A., Martín-Ruiz, M., García, E., Gil-Fernández, A., Parra, M. T., Viera, A., … Page, J. (2019). Transition from a meiotic to a somatic-like DNA damage response during the pachytene stage in mouse meiosis. *PLoS Genetics*, *15*(1), e1007439. https://doi.org/10.1371/journal.pgen.1007439

Featherstone, C., & Jackson, S. P. (1999). DNA double-strand break repair. *Current Biology*, *9*(20), R759-61. https://doi.org/10.1016/S0960-9822(00)80005-6

Ginsburg, M., Snow, M. H., & McLaren, A. (1990). Primordial germ cells in the mouse embryo during gastrulation. *Development*, *110*(2), 521–528.

Gomperts, M., Wylie, C., & Heasman, J. (1994). Primordial germ cell migration. *Ciba Foundation Symposium*, *182*, 121–34; discussion 134.

Hamer, G., & de Rooij, D. G. (2018). Mutations causing specific arrests in the development of mouse primordial germ cells and gonocytes. *Biology of Reproduction*, *99*(1), 75–86. https://doi.org/10.1093/biolre/ioy075

Handel, M. A., & Schimenti, J. C. (2010). Genetics of mammalian meiosis: regulation, dynamics and impact on fertility. *Nature Reviews. Genetics*, *11*(2), 124–136. https://doi.org/10.1038/nrg2723

Heyer, B. S., MacAuley, A., Behrendtsen, O., & Werb, Z. (2000). Hypersensitivity to DNA damage leads to increased apoptosis during early mouse development. *Genes & Development*, *14*(16), 2072–2084.

Joosen, L., Hink, M. A., Gadella, T. W. J., & Goedhart, J. (2014). Effect of fixation procedures on the fluorescence lifetimes of Aequorea victoria derived fluorescent proteins. *Journal of Microscopy*, *256*(3), 166–176. https://doi.org/10.1111/jmi.12168

Karanam, K., Kafri, R., Loewer, A., & Lahav, G. (2012). Quantitative live cell imaging reveals a gradual shift between DNA repair mechanisms and a maximal use of HR in mid S phase. *Molecular Cell*, *47*(2), 320–329. https://doi.org/10.1016/j.molcel.2012.05.052

Luo, Y., Hartford, S. A., Zeng, R., Southard, T. L., Shima, N., & Schimenti, J. C. (2014). Hypersensitivity of primordial germ cells to compromised replication-associated DNA repair involves ATM-p53-p21 signaling. *PLoS Genetics*, *10*(7), e1004471. https://doi.org/10.1371/journal.pgen.1004471

Luo, Y., & Schimenti, J. C. (2015). MCM9 deficiency delays primordial germ cell proliferation independent of the ATM pathway. *Genesis*, *53*(11), 678–684. https://doi.org/10.1002/dvg.22901

Miwa, S., Tome, Y., Yano, S., Hiroshima, Y., Uehara, F., Mii, S., … Hoffman,

R. M. (2013). Single cell time-lapse imaging of focus formation by the DNA damage-response protein 53BP1 after UVC irradiation of human pancreatic cancer cells. *Anticancer Research*, *33*(4), 1373–1377.

Nadler, J. J., & Braun, R. E. (2000). Fanconi anemia complementation group C is required for proliferation of murine primordial germ cells. *Genesis*, *27*(3), 117–123. https://doi.org/10.1002/1526-968X(200007)27:3<117::AID-GENE40>3.0.CO;2-7

Podhorecka, M., Skladanowski, A., & Bozko, P. (2010). H2AX Phosphorylation: Its Role in DNA Damage Response and Cancer Therapy. *Journal of Nucleic Acids*, *2010*. https://doi.org/10.4061/2010/920161

Rinaldi, V. D., Bloom, J. C., & Schimenti, J. C. (2018). Whole mount immunofluorescence and follicle quantification of cultured mouse ovaries. *Journal of Visualized Experiments*, (135). https://doi.org/10.3791/57593

Sabour, D., Araúzo-Bravo, M. J., Hübner, K., Ko, K., Greber, B., Gentile, L., … Schöler, H. R. (2011). Identification of genes specific to mouse primordial germ cells through dynamic global gene expression. *Human Molecular Genetics*, *20*(1), 115–125. https://doi.org/10.1093/hmg/ddq450

Singh, P., Aggarwal, L. M., Parry, S. A., & Raman, M. J. (2018). Radiation dosimetry and repair kinetics of DNA damage foci in mouse pachytene spermatocyte and round spermatid stages. *Mutagenesis*, *33*(3), 231–

239. https://doi.org/10.1093/mutage/gey007

Speed, R. M. (1982). Meiosis in the foetal mouse ovary. I. An analysis at the light microscope level using surface-spreading. *Chromosoma*, *85*(3), 427–437. https://doi.org/10.1007/bf00330366

Szabó, P. E., Hübner, K., Schöler, H., & Mann, J. R. (2002). Allele-specific expression of imprinted genes in mouse migratory primordial germ cells. *Mechanisms of Development*, *115*(1–2), 157–160. https://doi.org/10.1016/S0925-4773(02)00087-4

Tam, P. P., & Snow, M. H. (1981). Proliferation and migration of primordial germ cells during compensatory growth in mouse embryos. *Journal of Embryology and Experimental Morphology*, *64*, 133–147.

Truett, G. E., Heeger, P., Mynatt, R. L., Truett, A. A., Walker, J. A., & Warman, M. L. (2000). Preparation of PCR-quality mouse genomic DNA with hot sodium hydroxide and tris (HotSHOT). *Biotechniques*, *29*(1), 52–54. https://doi.org/10.2144/00291bm09

Yeom, Y. I., Fuhrmann, G., Ovitt, C. E., Brehm, A., Ohbo, K., Gross, M., … Schöler, H. R. (1996). Germline regulatory element of Oct-4 specific for the totipotent cycle of embryonal cells. *Development*, *122*(3), 881–894.

Yoshimizu, T., Sugiyama, N., De Felice, M., Yeom, Y. I., Ohbo, K., Masuko, K., … Matsui, Y. (1999). Germline-specific expression of the Oct-4/green fluorescent protein (GFP) transgene in mice. *Development, Growth & Differentiation*, *41*(6), 675–684. https://doi.org/10.1046/j.1440-169x.1999.00474.x

CHAPTER 3

SEXUALLY DIMORPHIC DNA DAMAGE RESPONSES AND MUTATION AVOIDANCE IN THE MOUSE GERMLINE

*This chapter is a reprint with minor reformatting of the manuscript: Bloom, J.C. and Schimenti, J.C. Sexually Dimorphic DNA Damage Responses and Mutation Avoidance in the Mouse Germline. (*currently under review)*

1- Abstract

Germ cells specified during fetal development form the foundation of the mammalian germline. These primordial germ cells (PGCs) undergo rapid proliferation, yet the germline is highly refractory to mutation accumulation compared to somatic cells. Importantly, while the presence of endogenous or exogenous DNA damage has the potential to impact PGCs, there is little known about how these cells respond to stressors. To better understand the DNA damage response (DDR) in these cells, we exposed pregnant mice to ionizing radiation (IR) at specific gestational time points and assessed the DDR in PGCs. Our results show that PGCs prior to sex determination lack a

G1 cell cycle checkpoint. Additionally, the response to IR-induced DNA damage differs between female and male PGCs post-sex determination. IR of female PGCs caused uncoupling of germ cell differentiation and meiotic initiation, while male PGCs exhibited repression of piRNA metabolism and transposon de-repression. We also used whole genome single-cell DNA sequencing to reveal that genetic rescue of DNA repair-deficient germ cells (*Fancm*$^{-/-}$) leads to increased mutation incidence and biases. Importantly, our work uncovers novel insights into how PGCs exposed to DNA damage can become developmentally defective, leaving only those genetically fit cells to establish the adult germline.

KEYWORDS: Primordial germ cells, DNA damage, FancM, genome maintenance, fertility, transposons, cell cycle checkpoint, single-cell DNA sequencing

2- *Introduction*

Specification of the germline in humans and mice occurs during embryonic development (Ginsburg et al. 1990), during which PGCs undergo a rapid expansion to populate the fetal gonad (Gomperts et al. 1994). Early in mouse embryogenesis, PGCs are specified as a group of ~45 cells in the epiblast of 6-6.5 post-fertilization embryos (E6-6.5) (Ewen and Koopman 2010). After specification, PGCs both proliferate and migrate to the location of

the future gonads where they undergo roughly 9 population doublings over the span of 7 days to reach a peak population of ~25,000 cells (Nikolic et al. 2016). These PGCs form the founding germ cell population from which the entire adult germline in both females and males is established (Tam and Snow 1981).

Perturbations to PGC development, especially those that cause accumulation of mutations, can profoundly impact the function and quality of the germline at all subsequent stages of development. In particular, early mutational events in PGCs would be expanded clonally, thus pervading the adult germ cell population. Remarkably, the spontaneous mutation rate in gametes is ~100 times lower than that of somatic cells (Milholland et al. 2017), suggesting that PGCs, and subsequent stages of gametogenesis, have a highly effective DDR. The ability to suppress mutation transmission in germ cells is essential for maintenance of the germline's genome integrity, and thus, genetic stability of species and avoidance of birth defects. However, how this suppression is achieved is still incompletely understood.

Studies examining the impact of exogenous genotoxic stressors on germ cells have largely focused on postnatal germ cell development (Russell et al. 1981; Favor 1999; Rinaldi, Hsieh, et al. 2017; Enguita-Marruedo et al. 2019; Singh et al. 2018). Fetal germ cells comprise a small population of cells that are difficult to access, but there are some reports in the literature indicating that PGCs are hypersensitive to DNA damage (Hamer and de Rooij 2018). These studies show that mutations in several DNA repair genes impact

PGC development, but have subtle effects on other embryonic- and post-natal cell types (Agoulnik et al. 2002; Luo et al. 2014; Luo and Schimenti 2015; Nadler and Braun 2000). Furthermore, germ cells in gastrulating mouse embryos readily undergo apoptosis in response to low dose IR, leading to depletion of the PGC pool; however the underlying mechanisms were not delineated (Heyer et al. 2000). During normal PGC development, some cells are lost through BAX-mediated apoptosis, implying that there are robust quality control mechanisms present and engaged in these germ cells even under physiological conditions (Stallock et al. 2003; Rucker et al. 2000). Exposure to environmental genotoxic agents during fetal development has the potential to impact not only the fetus, but also the future offspring of the fetus through its developing germline. In addition to genetic effects, intrinsic and extrinsic stressors may evoke epigenetic changes to fetal germ cells, possibly impacting fertility and causing adverse health outcomes in subsequent generations. However, our understanding of how PGCs respond to stressors remains under-explored.

DNA damage in the form of double strand breaks (DSBs), which can arise spontaneously (for example during DNA replication) or induced by extrinsic exposures, are particularly dangerous to the genome because they can cause gross chromosomal rearrangements and insertions/deletions (indels). Consequently, the cellular responses to DSBs, commonly induced experimentally by IR, have been studied in many contexts (Ciccia and Elledge 2010; Featherstone and Jackson 1999). While DSBs can be damaging to any

cell type in the body, the potential consequences are greater for stem cell populations that would propagate mutations to all progeny cells. Therefore, the DDR in these cells is of particular importance. A tractable system for studying stem cells in mammals are mouse embryonic stem cells (mESCs), and they are highly sensitive to IR exposure compared to other well-studied cell types such as mouse embryonic fibroblasts (MEFs) (Hong and Stambrook 2004; Chuykin et al. 2008; Suvorova et al. 2016; Tichy and Stambrook 2008). Interestingly, PGCs have several properties resembling mESCs, including rapid proliferation, low mutation rate, and similar transcriptomes (Hong et al. 2007; Cervantes et al. 2002; Grskovic et al. 2007). Under proper culture conditions, mESCs can even be differentiated into PGC-like cells (PGCLCs) in just a few days (Hayashi et al. 2011). This raises the possibility that PGCs and mESCs have similar DDRs that are distinct from terminally differentiated cells, and that ESCs, which are very easily cultured, can be used as a guide for studying DDRs of other stem cells including PGCs.

In this study, we examined the PGC response to IR-induced DNA damage at two distinct stages of development: 1) when PGCs are bipotent prior to sex determination at E11.5, and 2) subsequent to the initiation of sex determination at E13.5 (Endo et al. 2019). At E11.5, female and male fetal gonads are morphologically indistinguishable from one another, but by E13.5 the gonads are morphologically distinct (Koubova et al. 2006). Additionally, the developmental trajectories of male and female PGCs begin to diverge at this time. Female germ cells begin to undergo meiotic initiation at E13.5, while

male germ cells continue on a mitotic cell cycle program before becoming quiescent ~2 days later (Anderson et al. 2008). By examining the IR-induced DDR in PGCs both before and after sex determination, we uncovered novel developmental context-dependent responses to DNA damage. We show that before sex determination, irradiated PGCs lack a G1 cell cycle checkpoint similar to mESCs. After sex determination, we show that male PGCs re-gain G1 checkpoint activity while female PGCs do not, and instead prematurely initiate an abortive oogonial differentiation program. We also assessed mutational burden and the role of cell cycle checkpoints in mutation prevention in an intrinsic DNA damage model, *Fancm*-deficient mice, that exhibit p21-dependent PGC depletion in males (Luo et al. 2014). Overall, our studies reveal the importance of cell cycle checkpoints in preventing accumulation of complex mutations in the germline, and the differentiation of the DDR during germ cell development.

3- Results

Mouse PGCs Lack a G1 Cell Cycle Checkpoint

In a proliferating population of cells, acute DNA damage can activate cell cycle checkpoints at a number of different cell cycle stages (Shaltiel et al. 2015). These checkpoints give cells a chance to respond to the damage and can lead to a shift in the population's cell cycle distribution compared to control, undamaged cells. The canonical DDR in many cell types involves

activation of a checkpoint at the G1 stage of the cell cycle, but notably, this checkpoint is absent in mouse and primate ESCs (Hong et al. 2007; Hong and Stambrook 2004; Fluckiger et al. 2006). The speculated reason for this strategy is that rather than attempting repair of a mutational load sufficient to stop the cell cycle at G1 as do most somatic cells, ESCs sustaining substantial DNA damage of a cell-deleterious nature get culled subsequently by other mechanisms. Mouse neural stem and progenitor cells (NSPCs) and hematopoietic stem cells (HSCs) also do not activate a G1 cell cycle block in response to IR (Roque et al. 2012; Brown et al. 2015).

To determine whether PGCs lack a G1 DNA damage checkpoint, we exposed pregnant mice at E11.5 to 5 Gy IR, then 8 hours later dissected fetal gonads for flow cytometric cell cycle analysis. The mice expressed GFP in germ cells (Szabo et al. 2002), enabling us to distinguish PGCs from gonadal somatic cells. The IR treatment caused a marked shift in the PGC cell cycle distribution, indicative of an absent G1 cell cycle checkpoint (Figure 3.1A). This response was similar to that previously reported for mESCs (Hong and Stambrook 2004), an observation we confirmed here (Figure 3.2). The dramatic decrease of PGCs in G1 in turn altered the distribution of cells in S- and G2/M-stages (Figure 3.1B-D) indicating the presence of a robust G2 checkpoint arrest similarly identified in mESCs.

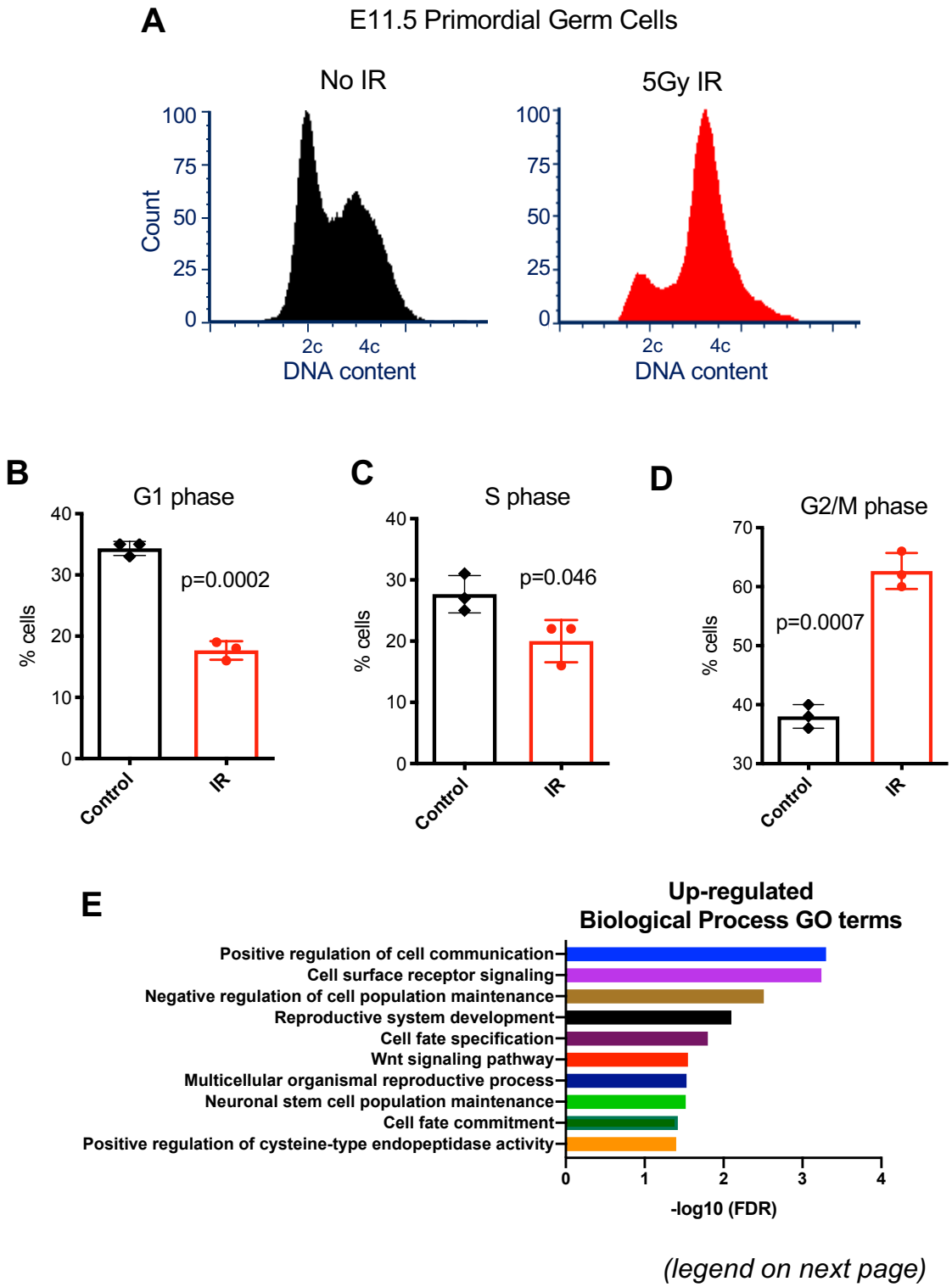

(legend on next page)

Figure 3.1. PGCs at E11.5 lack a G1 cell cycle checkpoint in response to irradiation-induced DNA damage. A. Representative cell cycle profiles of control and treated primordial germ cells. B. Percentage of G1 phase cells in both control and treated conditions. C. Percentage of S phase cells in both control and treated conditions. D. Percentage of G2/M phase cells in both control and treated conditions. E. Significantly enriched Gene Ontology terms among up-regulated genes in response to irradiation at E11.5.

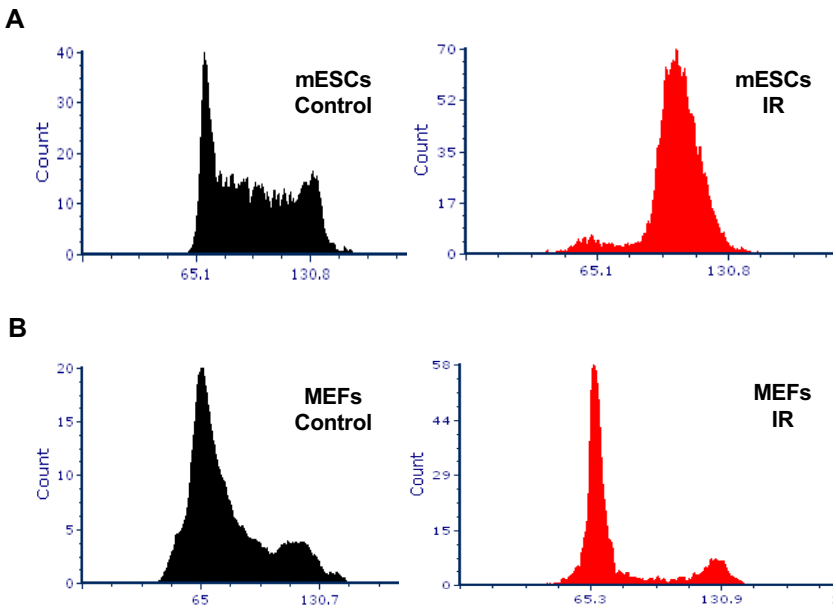

Figure 3.2. mESCs lack a G1 cell cycle checkpoint in response to IR-induced DNA damage. A. Mouse embryonic stem cells (mESCs) were treated with 10 Gy of irradiation (right panel) or untreated (left panel). Eight hours after irradiation, cells were trypsinized, stained, and subjected to flow

cytometry to assess cell-cycle distribution. B. Same as in A except with primary mouse embryonic fibroblasts (MEFs) rather than mESCs.

Irradiation Leads to Decreased piRNA Metabolism and Transposon de-repression in the Fetal Male Germline

To better understand the molecular nature of the DDR in bipotent PGCs, we performed RNA-seq on PGCs purified from irradiated embryos compared to control PGCs at the same time point in development (E11.5). Comparisons between irradiated and unirradiated samples 4 hours after treatment revealed 282 differentially expressed genes with 124 genes up-regulated two-fold or higher and 18 genes down-regulated two-fold or lower. Gene Ontology analysis (Mi et al. 2019) highlighted a number of significant terms among the genes up-regulated in response to IR (Figure 3.1E), most notably cell-to-cell communication, factors involved in stem cell population maintenance, and activation of apoptotic processes through cysteine endopeptidase activity (Earnshaw et al. 1999).

Having found that E11.5 PGCs lack a G1 cell cycle checkpoint, we next asked if and when the G1 checkpoint response is re-established in this lineage. Establishment of a G1 checkpoint response would indicate that the lineage re-gained a more canonical DDR, typical of most differentiated cells. Strikingly, irradiation of male embryonic germ cells at E13.5 induced G1 cell cycle arrest, indicating that they acquired this ability for the first time in their development (Figure 3.3A-D). To gain insight into the molecular

consequences of DNA damage in these cells, we examined the transcriptomes of irradiated E13.5 male PGCs to unirradiated controls using RNA-seq. During normal male PGC development, there is widespread demethylation of the genome (Ernst et al. 2017). This global DNA demethylation leads to de-repression of silenced transposons, but also coincides with an upregulation of piRNA signaling to repress transposon expression (Rojas-Ríos and Simonelig 2018). Activation of piRNA signaling is crucial for normal developmental progression of fetal male germ cells (Nguyen and Laird 2019). Gene Ontology (GO) analysis highlighted a number of gene categories down-regulated in response to IR, revealing perturbations to critical male germ cell-specific developmental pathways related to gene silencing, cell differentiation and piRNA signaling (Figure 3.4A).

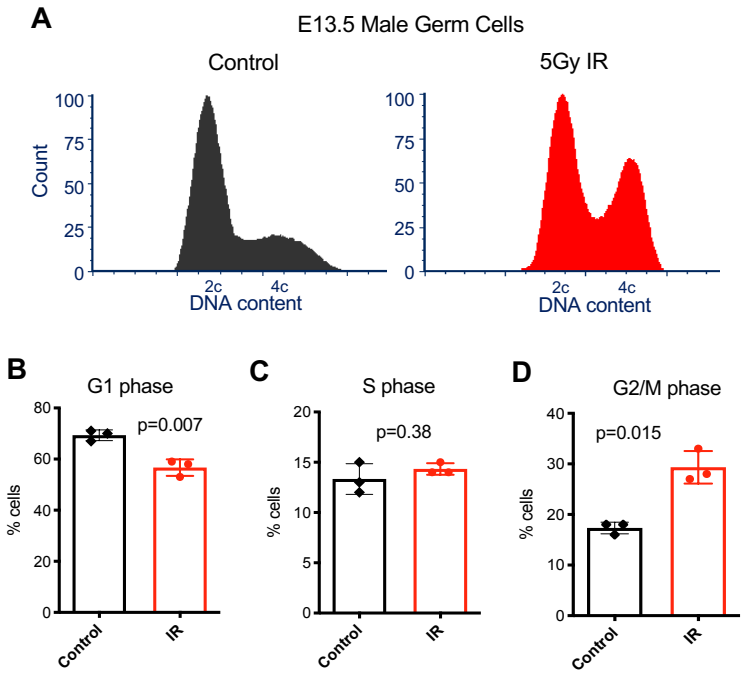

(legend on next page)

Figure 3.3. E13.5 male germ cells acquire a DNA damage responsive G1 cell cycle checkpoint. A. Representative cell cycle profiles of control and treated E13.5 male germ cells. B. Percentage of G1 phase cells in both control and treated conditions. C. Percentage of S phase cells in both control and treated conditions. D. Percentage of G2/M phase cells in both control and treated conditions.

To further understand the DDR in E13.5 male germ cells, we examined the expression of genes associated with piRNA metabolism in our dataset. The vast majority (all except one) were robustly down-regulated in response to IR (Figure 3.4B). Next, we asked whether the down-regulation of piRNA metabolism led to transposon activation in the irradiated male germ cells. We observed that the majority of expressed transposons fall into families that are capable of transposition (Figure 3.5) (Deniz et al. 2019). Additionally, when we compare the expression of all differentially expressed transposons with an adjusted p value<0.05, all but one were de-repressed in irradiated germ cells (Figure 3.4C).

Finally, we conducted small RNA sequencing to examine the expression of piRNAs and observed that the majority were down-regulated in response to IR (Figure 3.4D). Therefore, induction of DNA damage in mouse embryonic germ cells suppresses piRNA activity by downregulating both piRNA biogenesis factors and the piRNAs themselves.

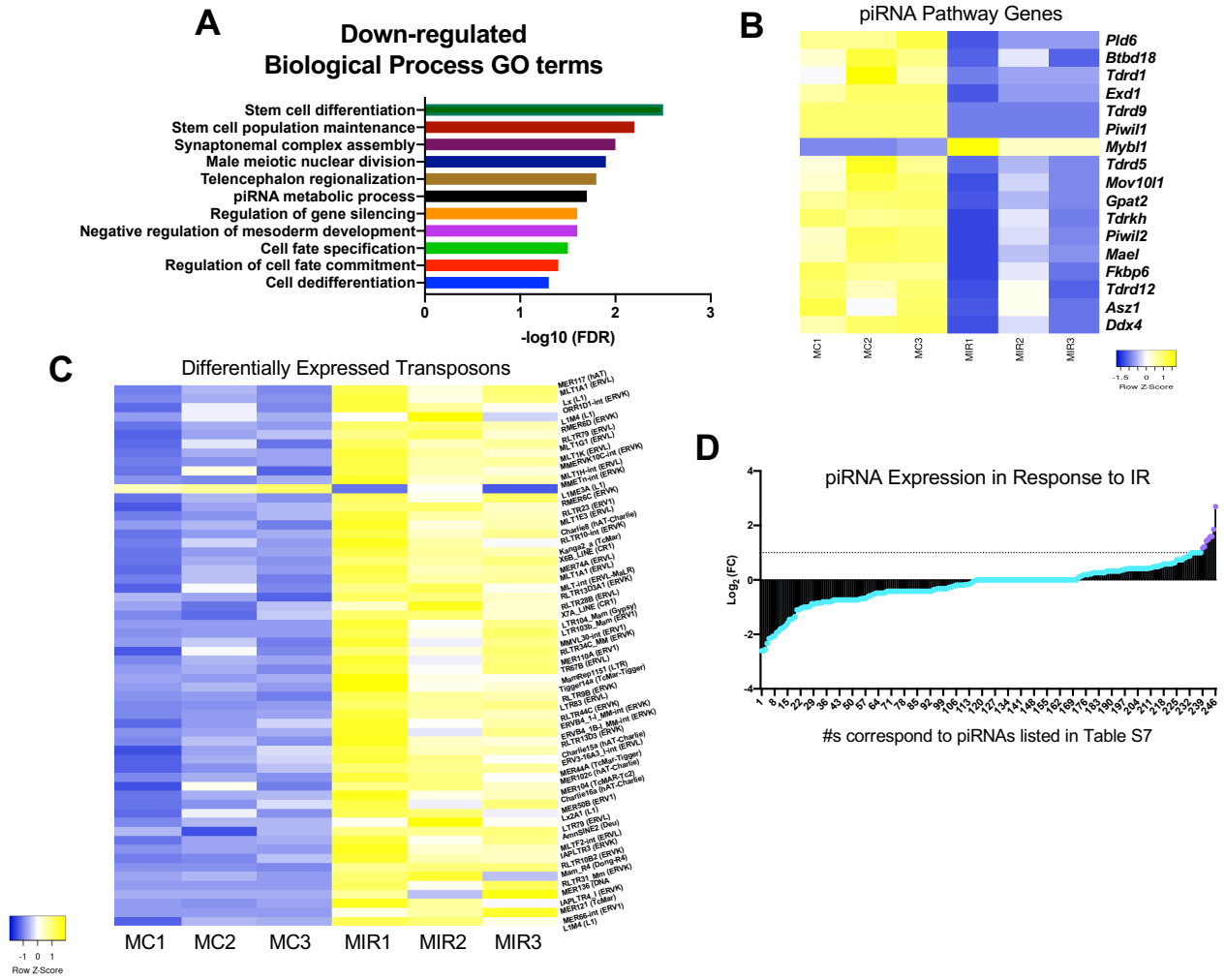

Figure 3.4. Irradiation exposure at E13.5 leads to down-regulation of piRNA metabolism and de-repression of transposons in male germ cells.

A. Significantly enriched GO terms among down-regulated genes in response to irradiation in E13.5 male germ cells. B. Expression of piRNA metabolic process genes in control and irradiated E13.5 male germ cells. C. Heatmap of differentially expressed transposons between control and irradiated samples with an adjusted p-value<0.05. D. Fold change in piRNA expression in

response to IR from small-RNA sequencing. The majority of the piRNAs (shown in blue) are not significantly up-regulated in response to IR. (abbreviations: MC=male no IR control; MIR= male IR treated)

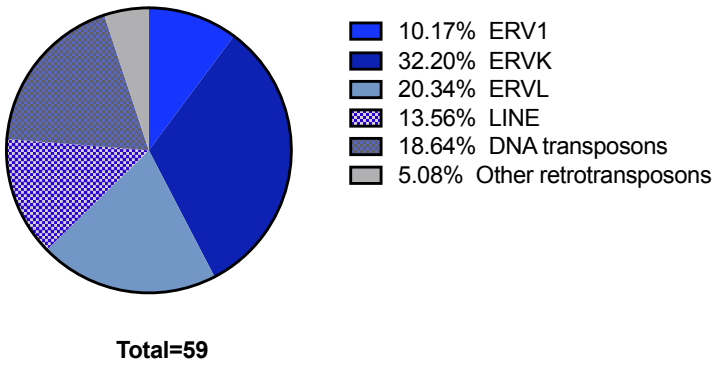

Figure 3.5. Expressed TE families in E13.5 male germ cells. (related to Figure 3.4) Distribution of transposon family classes represented among the differentially expressed transposons with adjusted p-values<0.05.

Irradiation of Female Germ Cells Leads to an Uncoupling of Oocyte Differentiation and Meiosis

As described above, post-sex determination male PGCs (E13.5) acquire a G1 checkpoint response as they come to the end of their highly proliferative phase. With respect to female PGCs, like their counterparts at E11.5, IR caused a marked shift in the number of cells with 4C DNA content, indicating that they also lacked a G1 checkpoint at this stage (Figure 3.6A-D). However, the fate of normal female germ cells differs at E13.5, as they begin transitioning into a meiotically competent cell cycle program. Interestingly, the

IR-induced cell cycle profile of E13.5 female germ cells did not differ from the profile at E11.5 (Figure 3.6A). We hypothesized that rather than representing a lack of a mitotic G1 checkpoint, these cells might actually represent prematurely-arising oocytes resulting from IR induction. Consistent with this possibility, we noted that this cell cycle profile was remarkably similar to that reported for normal E14.5 female germ cells (Miles et al. 2010).

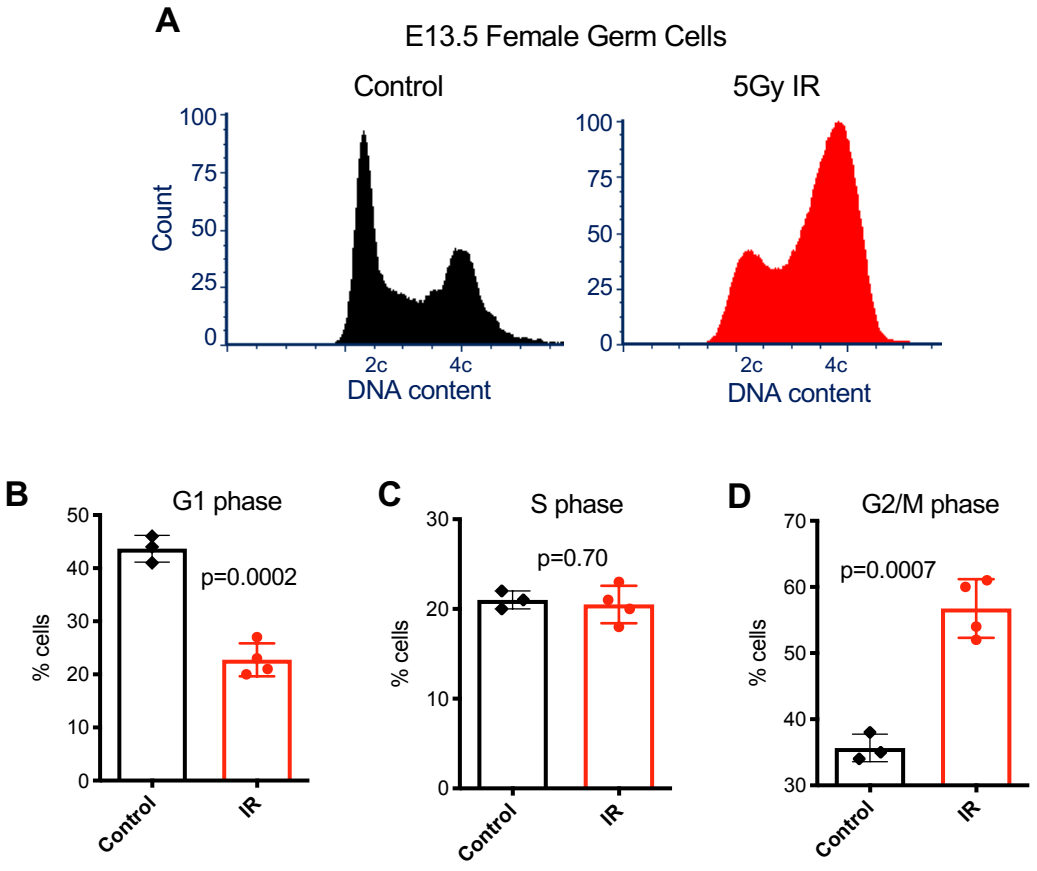

Figure 3.6. Enrichment of G2/M phase cells in IR exposed E13.5 female germ cells. A. Representative cell cycle profiles of control and treated E13.5 female germ cells. B. Percentage of G1 phase cells in both control and treated

conditions. C. Percentage of S phase cells in both control and treated conditions. D. Percentage of G2/M phase cells in both control and treated conditions.

To test this hypothesis, we performed RNA-seq of the IR-exposed E13.5 germ cells, and compared the up- and down-regulated genes to a list of pluripotency-related genes expressed in fetal germ cells (Sangrithi et al. 2017; Lesch et al. 2013). Several genes (23) associated with pluripotency were downregulated in response to IR (Figure 3.7A), consistent with IR exposure causing premature differentiation of female PGCs. Additionally, comparisons between irradiated and unirradiated E13.5 female germ cells 8 hours after treatment also revealed an increase in retinoic acid (RA) responsive genes (Figure 3.7B).

Entry into meiosis requires the completion of pre-meiotic DNA replication and an extended Prophase I stage (Speed 1982; Soh et al. 2017). Moreover, initiation of the meiotic program in female germ cells occurs in an anterior to posterior wave of RA signaling in the fetal gonad (Koubova et al. 2006). Therefore, based on the increased expression of RA responsive genes and the dramatic upsurge in G2/M phase cells (Figure 3.6D), we hypothesized that IR stimulates RA-associated gene expression, which in turn stimulates meiotic entry. To explore this possibility, we took advantage of a published dataset where the embryonic ovary was dissected into thirds and RNA-sequencing performed on the anterior and posterior portions (Soh et al. 2015).

Comparison to that dataset revealed that gene expression in irradiated fetal germ cells is more similar to the portion of the embryonic gonad which has been exposed to RA and initiated meiotic entry (Figure 3.7C).

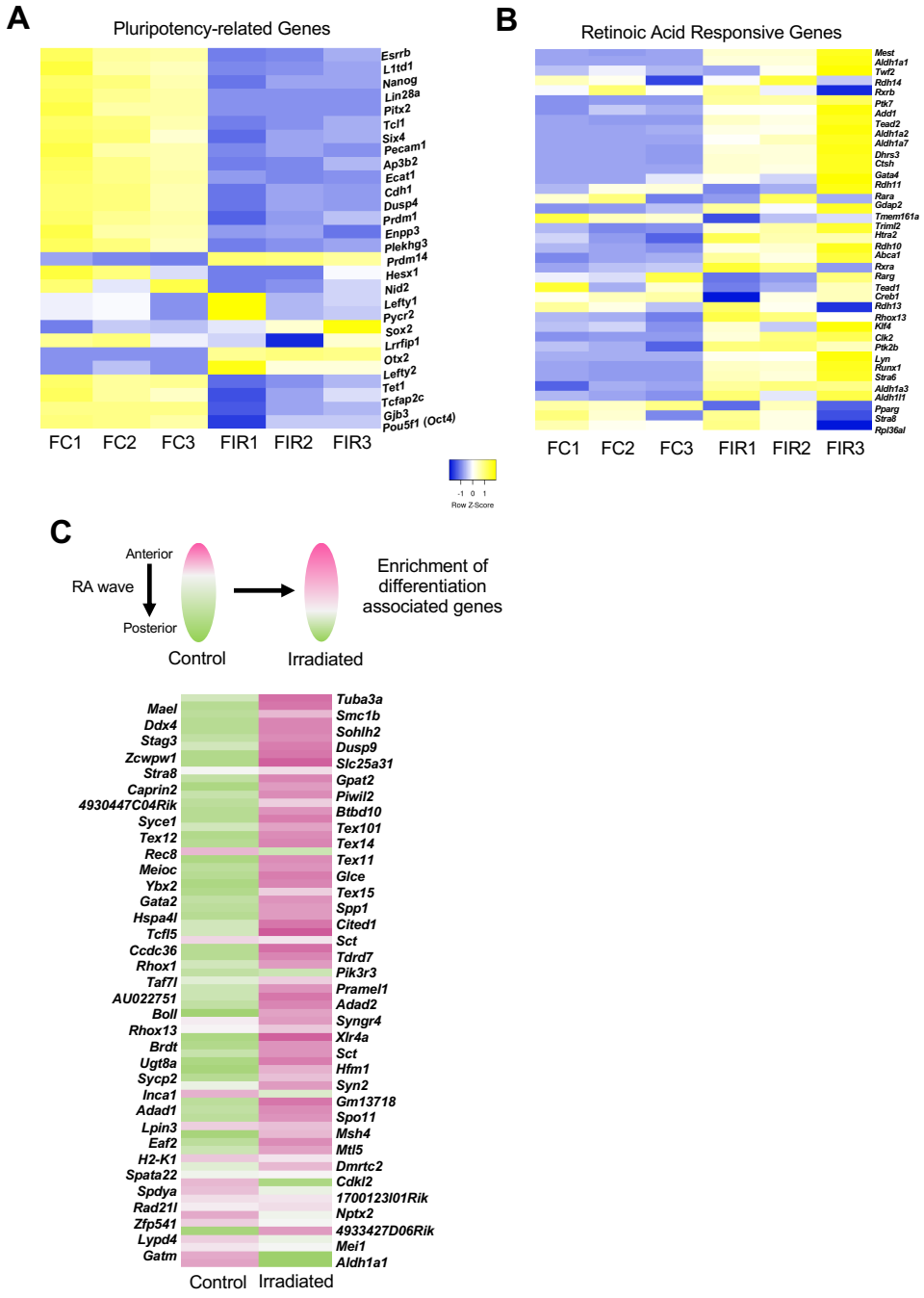

(legend on next page)

Figure 3.7. Irradiation exposure at E13.5 leads to pre-mature retinoic acid signaling and meiotic entry disruption in female germ cells. A. Expression of pluripotency-associated genes in control and irradiated E13.5 female germ cells. B. Expression of retinoic acid responsive genes in control and irradiated E13.5 female germ cells. C. Expression of genes associated with spatial development of the fetal ovary in control and irradiated samples. The heatmap is comprised of genes upregulated in response to RA exposure, pink indicates higher expression, green indicates lower expression (genes listed on the left are associated with even rows of the heatmap and genes listed on the right are associated with the odd rows; reference dataset used for comparison from (Soh et al. 2015). (abbreviations: FC=female no IR control; FIR= female IR treated)

Upon entry into meiosis, a set of primarily meiosis-specific genes become highly expressed (Sangrithi et al. 2017; Lesch et al. 2013). Surprisingly, analysis of these genes in our dataset revealed that rather than being more highly expressed in germ cells exposed to IR, they are down-regulated (Figure 3.8). This result, which seemingly conflicts with the IR-induced enrichment of gene expression associated with RA signaling, led us to conclude that IR causes an uncoupling of oogonial differentiation from meiotic entry. Previous work in mouse has demonstrated that oogonial differentiation and meiosis are dissociable from one another (Dokshin et al. 2013), but,

importantly, our work has uncovered a mechanism by which DNA damage triggers this dissociation in an otherwise wild-type context.

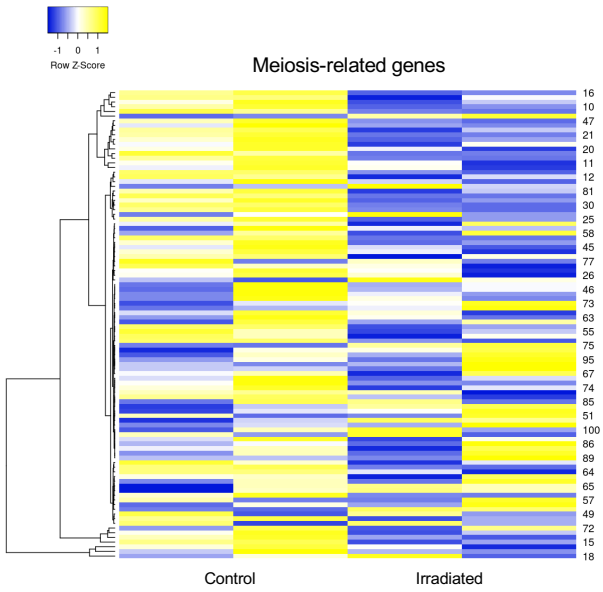

Figure 3.8. Meiosis-related genes are not upregulated in response to IR. (related to Figure 3.7) Expression of meiosis-related genes in control and irradiated E13.5 female germ cells.

Why does IR-induced stimulation of RA signaling not lead to premature meiotic entry in E13.5 female germ cells? One possibility relates to one of the master regulators of meiotic entry, *Stra8* (Koubova et al. 2014). *Stra8* stands for “Stimulated by Retinoic Acid 8” and as the gene name implies, its activity is dependent on RA (Koubova et al. 2006). While RA activates transcription of *Stra8,* expression of *Stra8* leads to the formation of a negative feedback loop and self-repression (Soh et al. 2015). This mechanism ensures that meiotic entry initiates only once. We hypothesized that IR-induced DNA damage

stimulates *Stra8* prematurely, leading to an inappropriate and irreversible repression of meiosis. If this is indeed the case, then we would predict that the irradiated germ cell samples would have a similar gene expression profile to *Stra8*-deficient female germ cells. Using an RNA-sequencing dataset of female *Stra8* mutant germ cells (Soh et al. 2015), we observed that genes highly expressed in *Stra8* mutants are indeed similarly enriched in the irradiated germ cell samples (Figure 3.9).

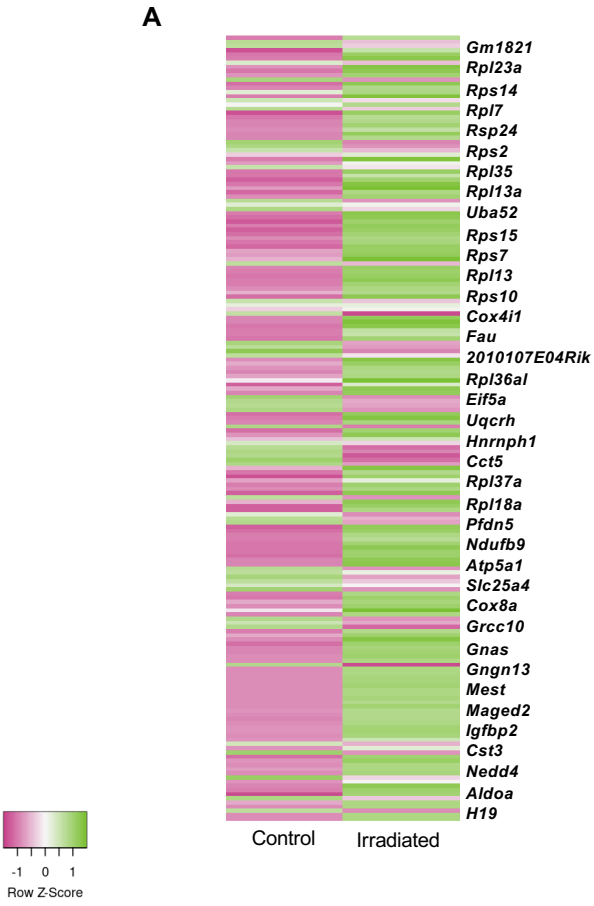

Figure 3.9. Genes highly expressed in *Stra8* mutants are similarly enriched in irradiated female germ cells. (related to Figure 3.7) Heatmap of genes in control and irradiated female germ cells which have high

expression in *Stra8* mutant germ cells (Soh et al. 2015). Genes which have high expression in *Stra8* mutants tend to be more highly expressed in the irradiated condition compared to the control. (Every fifth gene in the heatmap is listed)

Rescue of *Fancm*-deficient Germ Cells by Checkpoint Ablation Leads to an Enrichment of Complex Mutations

To assess how germline mutational burden is impacted when DNA damage checkpoints are abrogated, we sought to examine mutation incidence in a PGC proliferation-defective mouse model. We chose to examine *Fancm*-deficient mice in which male, but not female, germ cell reduction could be partially rescued by deletion of the cyclin-dependent kinase inhibitor, *p21* (Luo et al. 2014). This sexual dimorphism in *p21*-mediated germ cell rescue is consistent with our cell cycle results demonstrating a male-specific establishment of the G1 checkpoint in PGCs after sex determination.

Fancm is the largest subunit of the Fanconi Anemia core complex, which is named after a chromosomal instability syndrome that leads to cancer predisposition, bone marrow failure, congenital abnormalities and infertility (Joenje and Patel 2001). Studies in cell culture systems have shown that *Fancm* facilitates cell cycle checkpoint activation at sites of arrested DNA replication forks, particularly in the contexts of interstrand crosslinks (ICL) (Deans and West 2009). *Fancm* has also been reported to mediate fork reversal when the lagging strand template is partially single-stranded and

bound by the single-stranded DNA binding protein RPA (Gari et al. 2008). Additionally, single molecule studies have indicated that *Fancm* may even be capable of mediating transversal of ICLs by replication forks (Huang et al. 2013).

Using CRISPR/Cas9 genome editing, we simultaneously generated *Fancm* and *p21* null mutations on an isogenic strain background. Characterization of the *Fancm* mutant revealed phenotypic similarities to the previously published mutant including a partial, but significant, rescue of male germ cells in $Fancm^{-/-}$ $p21^{-/-}$ double mutants (Luo et al. 2014) (Figure 3.10). To examine whether rescuing germ cell quantity through checkpoint bypass led to a decrease in germline genome quality, we compared germline mutation incidence between the single- and double-mutants by collecting spermatids from wild-type, $p21^{-/-}$, $Fancm^{-/-}$, and $Fancm^{-/-}$ $p21^{-/-}$ animals and performing whole genome single-cell DNA sequencing on them. An increase in mutation incidence in the double mutants would indicate that removing the *p21*-mediated checkpoint has a negative impact on germline genome integrity. A mutational burden similar to controls would suggest that *p21* loss facilitates germ cell rescue without impacting germ cell quality. Either outcome will lead to important insights regarding the relationship between cell cycle checkpoint response and germline genome maintenance.

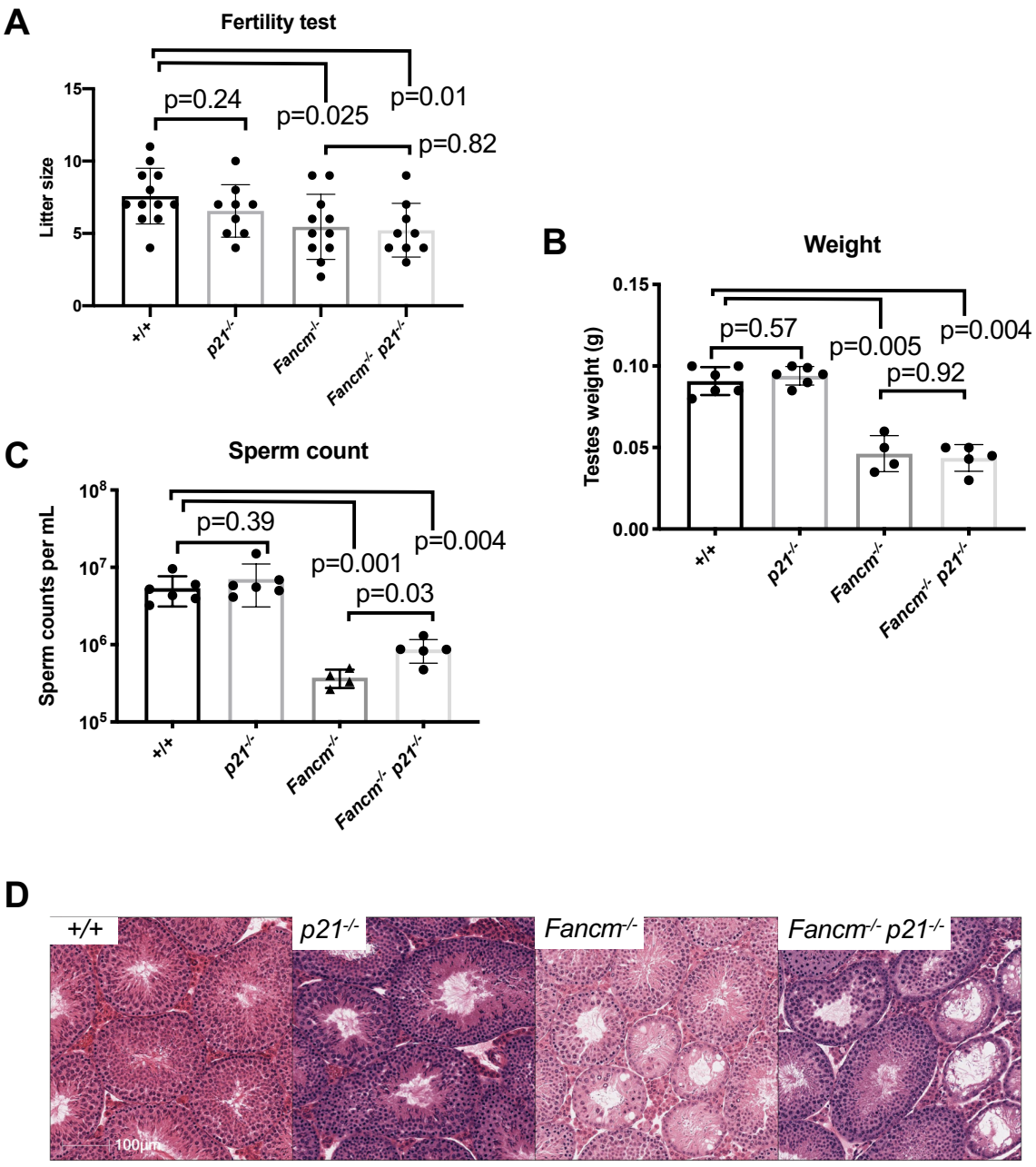

Figure 3.10. Loss of *p21* partially rescues germ cells in *Fancm*-deficient mutants. A. Quantification of litter sizes produced from males of the indicated genotypes mated to wild type females. B. Quantification of testes weights from males of the indicated genotypes. C. Quantification of caudal epididymis sperm from males of the indicated genotypes. D. Hematoxylin and eosin

(H&E) staining of testis cross-sections from 8 week old males. Scale bar=100um

Initial analysis of all detected variants in the cells revealed an over-representation of mutations in double mutant germ cells (Figure 3.11A). Further analysis comparing the types of mutations per genotype indicated that the point mutation frequency, while enriched in *Fancm*$^{-/-}$ *p21*$^{-/-}$ double mutant spermatids did not reach statistical significance when compared to other genotypes (Figure 3.11B). Breakdown of point mutation type (Figure 3.12) also did not show distinctions between any of the genotypes.

Next, we examined insertion/deletion (InDel) frequency and, while depleted in *Fancm*$^{-/-}$ *p21*$^{-/-}$ mutant cells compared to the other genotypes, the differences only reached the threshold for statistical significance when compared to that of *p21*$^{-/-}$ cells (Figure 3.11C). Furthermore, predicted frameshift-causing variants (Figure 3.13) did not differ statistically between double mutant cells and those from wild-type or single mutants. Notably, clusters of mutations in close proximity to one another were enriched in *Fancm*$^{-/-}$ *p21*$^{-/-}$ spermatids compared to wild-type (Figure 3.11D). These complex mutation events were often comprised of InDels along with one or more base substitutions. We defined variants as “complex” if two or more mutations were within 200 nucleotides of one another. Examples of these clustered mutations from individual *Fancm*$^{-/-}$ *p21*$^{-/-}$ germ cells are shown in Figure 3.11E. The enrichment of this mutation cluster signature in

Fancm$^{-/-}$ *p21*$^{-/-}$ germ cells indicates that the p21-dependent cell cycle checkpoint is important for suppressing propagation of germ cells bearing high levels of complex mutations, or which are experiencing a high number of defective replication forks that would lead to such mutational events.

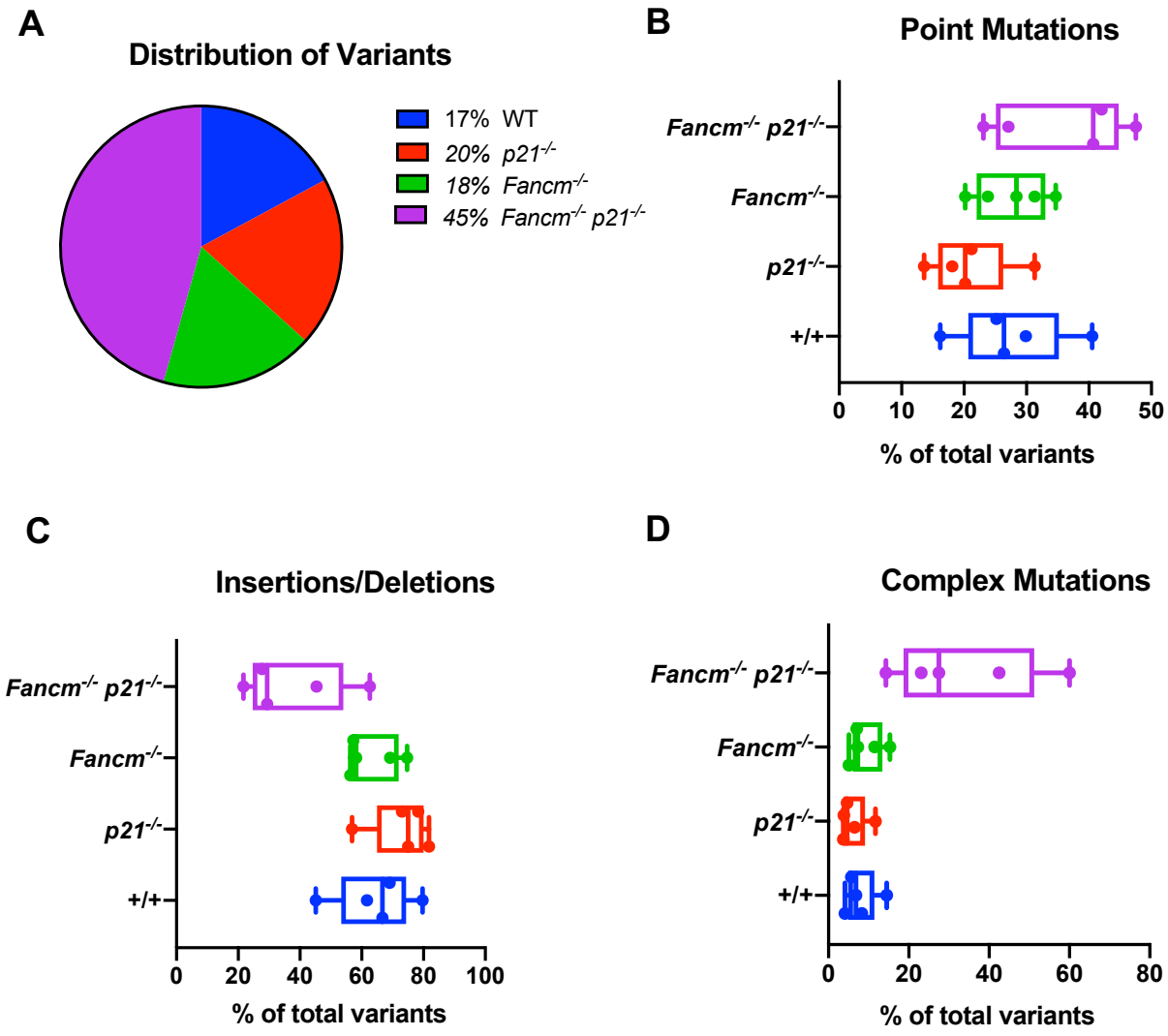

E

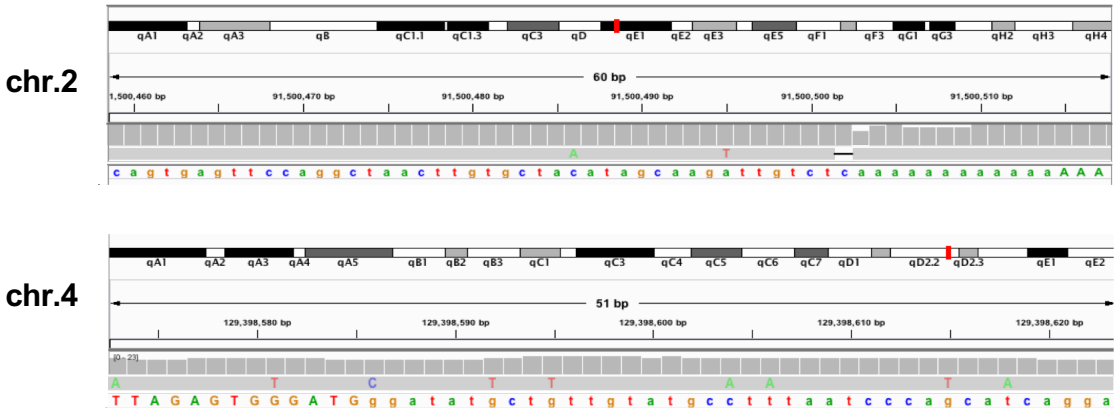

(legend on next page)

Figure 3.11. Variant detection in genetically rescued germ cells reveals an alteration mutational profile compared to controls. A. Distribution of total variants with respect to genotype. B. Point mutation frequency shown as a percentage of the total number of variants identified in each cell. (Kruskal-Wallis test, q=0.09 between *p21*$^{-/-}$ and *Fancm*$^{-/-}$ *p21*$^{-/-}$). C. Insertion and deletion (InDel) mutation frequency shown as a percentage of the total number of variants identified in each cell. (Kruskal-Wallis test, q=0.02 between *p21*$^{-/-}$ and *Fancm*$^{-/-}$ *p21*$^{-/-}$) D. Complex variant frequency shown as a percentage of the total number of variants identified in each cell. (Kruskal-Wallis test, q=0.04 between wild-type and *Fancm*$^{-/-}$ *p21*$^{-/-}$). E. Examples of two complex mutations from *Fancm*$^{-/-}$ *p21*$^{-/-}$ spermatids. Shown are IGV screen shots.

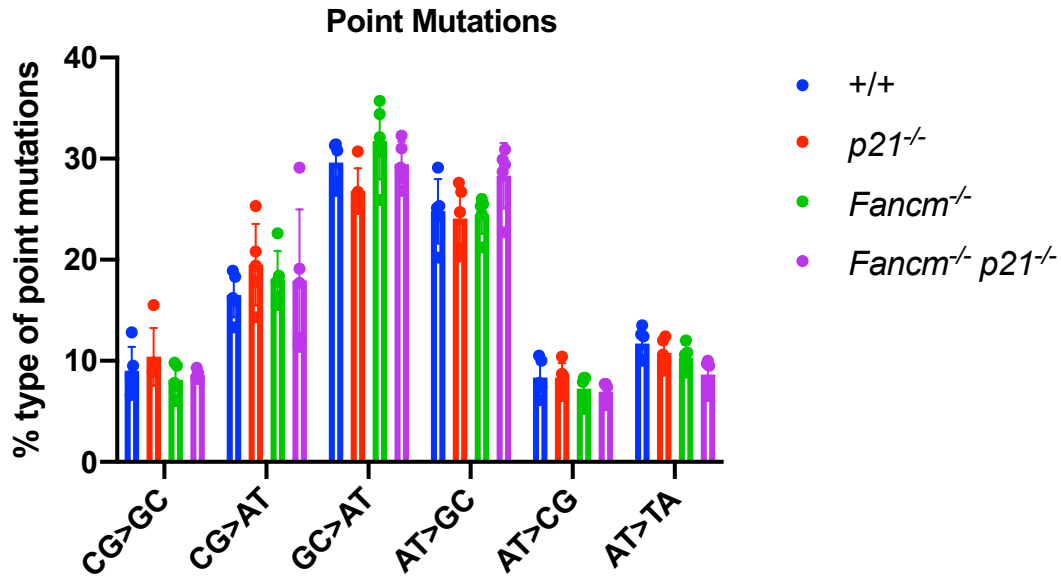

Figure 3.12. Point mutation distribution between genotypes shows no bias towards a specific class of mutations. Point mutation classes per

genotype shown as a percentage of the total number of point mutation variants identified in each cell.

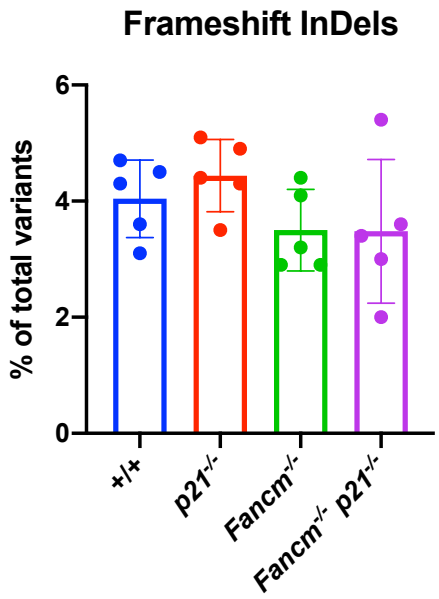

Figure 3.13. Insertions or deletions predicted to cause frameshift mutations are not enriched in double mutant samples. Predicted frameshift causing mutations shown as a percentage of the total number of InDel variants identified in each cell. [Statistical significance was assessed using the Kruskal-Wallis test correcting for multiple comparisons with the Benjamini False Discovery Rate]

4- Discussion

In this study, we examined DNA damage checkpoint activity in mouse PGCs and identified developmental context-dependent responses before and after sex determination in these cells. We found similarities between the DDR

of mESCs (Hong and Stambrook 2004), NSPCs (Roque et al. 2012), HSCs (Brown et al. 2015) and E11.5 PGCs. These similarities have biological and experimental implications. Regarding the former, the results suggest that key features of the DDR are similar amongst distinct stem cell types, from highly pluripotent cells (ESCs) to those dedicated to different lineages (PGCs, NSPCs and HSCs). Experimentally, the data suggest that mESCs, which can be cultured indefinitely and are easily manipulated genetically, could serve as a model for DNA damage responses in PGCs and possibly other cell types that are not easily cultured.

Elucidation of the IR-induced DDR in PGCs following sex determination highlights how perturbations to cell differentiation can be used as a highly sensitive response to preserve the genomic integrity of the final surviving germ cell pool. De-repression of transposons and down-regulation of piRNA signaling in the male germline illustrates the deleterious downstream consequences of DNA damage beyond the direct consequences of the IR itself. Our findings are consistent with a study which showed that in wild-type E13.5 male PGCs, there is a sub-population of cells exhibiting co-occurrence of piRNA pathway down-regulation and up-regulation of apoptotic pathway-associated genes (Nguyen and Laird 2019).

Evidence for RA pathway stimulation in response to DNA damage has also been found in ESCs. In this system, DNA damage induced RA pathway activation promoted cell differentiation through *Stra6. Stra6,* like *Stra8,* is a retinoic acid-responsive gene (Carrera et al. 2013; Serio et al. 2019). We also

observed a DNA damage-induced increase in RA signaling and differentiation in female PGCs, but based on the specifics of RA-induced meiotic entry, cannot exclude the possibility that there is a selective enrichment of more differentiated cells among the surviving irradiated cells. This alternative possibility implies that differentiated female PGCs are more resistant to DNA damage than their less differentiated RA-naïve counterparts. It is possible that our timing of exogenous DNA damage with cells primed to tolerate hundreds of programmed meiotic DSBs may distinguish these cells from their less differentiated counterparts, but, importantly, we show that the irradiated cells exhibit inappropriate expression of meiosis-associated genes. Therefore, these germ cells, regardless of whether they represent RA-exposed cells prior to IR or a population induced to differentiate, are not developmentally competent to establish the germline.

Finally, we assessed the quality of individual haploid germ cells in a replication defective mutant. With whole genome single cell DNA sequencing, we were able to highlight the potential ramifications of manipulating DNA damage checkpoints to facilitate increased germ cell survival. Our results indicate that increasing cell survival in a model of germline DNA repair deficiency leads to germ cells with an increased mutational burden. Repair of *Fancm*-associated DNA lesions in other cell types has been shown to involve exposure of single-stranded DNA and repair by low fidelity translesion synthesis (TLS) DNA polymerases (Grompe and D'Andrea 2001). Specifically in PGCs, *Rev7* (a subunit of the TLS DNA polymerase ζ) has been shown to

be essential for cell survival with complete loss of PGCs by E13.5 in *Rev7*-deficient mutants (Watanabe et al. 2013). Taken together, these findings provide additional independent support for the idea that enriched variants identified in the double mutant spermatids likely arose from TLS events (Harfe and Jinks-Robertson 2000; Stone et al. 2012).

Notably, there are many genes which lead to germ cell depletion, some via apoptosis and some by slowing DNA replication. In this specific genetic context, the absence of *p21* enables the increased survival of cells with complex mutations via checkpoint bypass. It will be important to continue exploring the impact of these various contexts on *de novo* germline variation throughout germ cell development. Overall, our findings provide novel insight into how the germline minimizes mutation transmission to future generations when exposed to DNA damage and replication stress *in utero*.

Supplemental Table Legends

(Supplemental tables are not included in the dissertation due to size limitations. They are available upon request and will be included in the published version of Chapter 3.)

Table S1. Count table and differential expression analysis of E13.5 male germ cells in response to IR from TEtranscripts

Table S2. List of meiosis-related genes (related to Figure S3)

Table S3. Genes associated with spatial development of the fetal ovary listed in the order shown in Figure 5C

Table S4. List of genes used to assess similarity of control and irradiated female germ cells to gene expression in *Stra8* mutants from Soh et al. 2015

Table S5. Count table and differential gene expression analysis of male and female E13.5 fetal germ cells in response to IR

Table S6. Count table and differential gene expression analysis of E11.5 PGCs in response to IR

Table S7. List of piRNAs and their associated Log_2(Fold Change) values corresponding to the order graphed in Figure 3D

Table S8. Oligonucleotides used in this study

Table S9. List of variants called per cell from whole genome single-cell DNA sequencing

5- Materials and Methods

Mouse Models

The use of mice in this study was approved by Cornell's Institutional Animal Care and Use Committee. B6;CBA-Tg(Pou5f1-EGFP)2Mnn/J transgenic mouse strain, commonly referred to as Oct4deltaPE-GFP, (Jackson Laboratory stock # 004654) were used to purify PGCs. For the irradiation

experiments, mice were placed in a ^{137}cesium irradiator with a rotating turntable and exposed to the dose of radiation specified.

Generation of *Fancm*$^{em1/Jcs}$ and *p21*$^{em1/Jcs}$ Mice

p21$^{em1/Jcs}$ was generated using CRISPR/Cas9-mediated genome editing. The sgRNA was *in vitro* transcribed as described previously (Singh et al. 2014) from a DNA template ordered from Integrated DNA Technologies (IDT). See Table S8 for the DNA template primers. Embryo microinjection in C57BL/6J zygotes was performed as described previously using 50ng/uL of sgRNA and 50ng/uL of Cas9 mRNA (TriLink Biotechnologies). The resulting 11bp deletion was identified with Sanger sequencing of genomic DNA. Editing of the allele generated a novel *Bst*UI restriction site which was used to distinguish between wild-type and mutant alleles after PCR amplification (see Table S8 for genotyping primers). Generation and genotyping of *Fancm*$^{em1/Jcs}$ animals was described previously (McNairn et al. 2019).

Cell Lines [related to Figure 3.2]

V6.4 mESCs (You et al. 1998) were maintained under traditional mESC culture conditions (Tremml et al. 2008). Primary C57BL/6J MEFs were isolated from E13.5 embryos in which organs were removed and the remainder of the embryo was trypsinized to make a cell suspension. Cells were cultured in media comprised of DMEM with 10% FBS, 1X nonessential amino acids, and 100 units/mL penicillin-streptomycin.

Cell Cycle Analysis

Fetal gonads from embryos whose mothers were either treated or untreated with radiation were dissected and pooled according to treatment condition and sex. Fetal gonads were disaggregated and dissociated into a single cell suspension using 0.25% trypsin-EDTA and 20μg/mL of DNase I for 15 minutes at 37°C. Trypsin was deactivated with 10% FBS. Suspensions were stained for DNA content with Hoechst 33342 (ThermoFisher 622495) and propidium iodide (PI) (Life Technologies P3566) for dead cell exclusion. Single cell suspensions were labeled for 30 minutes with 100μg Hoechst 33342 in a 33°C water bath shaking at 150rpm. Prior to cell cycle analysis samples were strained through a pre-wetted 40μm filter and labeled with propidium iodide (0.25μg/mL). Cell cycle analysis was performed using FCS Express 6 software. Statistical comparisons of cell cycle graphs were performed using GraphPad Prism8 using unpaired non-parametric Mann-Whitney tests.

RNA-seq Sample Preparation and Gene Expression Analysis

GFP+ PGCs were purified via FACS and total RNA was isolated using Trizol-LS (Thermo Fisher) according to the manufacturer's instructions. RNA quality was assessed by spectrophotometry (Nanodrop) to determine concentration and chemical purity (A260/230 and A260/280 ratios) and with a Fragment Analyzer (Advanced Analytical) to determine RNA integrity. Ribosomal RNA

was subtracted by hybridization from total RNA samples using the RiboZero Magnetic Gold H/M/R Kit (Illumina) and the rRNA-subtracted samples were quantified with a Qubit 2.0 (RNA HS Kit; Thermo Fisher). TruSeq-barcoded RNA-seq libraries were generated with the NEBNext Ultra II RNA Library Prep Kit (New England Biolabs) and each library was quantified via Qubit 2.0 (dsDNA HS kit; Thermo Fisher) prior to pooling. For analysis, reads were trimmed to remove adaptor sequences and low quality reads using Cutadapt v1.8 with parameters: -m 50 –q 20 –a AGATCGGAAGAGCACACGTCTGAACTCCAG –match-readwildcards. Reads were then mapped to the mm10 mouse reference genome/transcriptome using Tophat v2.1. For gene expression analysis, Cufflinks v2.2 (cuffnorm/cuffdiff) was used to generate FPKM values and statistical analysis of differential gene expression (Trapnell et al. 2010)

Gene Ontology analyses were conducted using PANTHER Classification System (Mi et al. 2019) and heatmaps were generated using heatmapper.ca (Babicki et al. 2016)

Transposable Element Expression Analysis

To conduct transposable element differential expression analysis, the software package TEtranscripts (Jin et al. 2015) was used with the default settings and the associated mm10 TE annotation GTF file.

Small RNA-seq Sample Preparation and Analysis

Total RNA was isolated as described above and the presence of small RNAs (smaller than 200 nucleotide fragments) was detected with a Fragment Analyzer (Advanced Analytical). TrueSeq-barcoded RNA-seq libraries were generated with the NEBNext Small RNA Library Prep Kit (New England Biolabs) and size selected for insert sizes ~18-50bp. Each library was quantified with a Qubit 2.0 (dsDNA HS Kit; Thermo Fisher). For piRNA analysis, reads were trimmed using Trim Galore! and then run through piPipes small RNA-seq pipeline with alignment to the mm10 reference genome (Han et al. 2015) and using the default settings.

Fertility Tests, Sperm Counts, and Testis Histology

Methods were conducted as described in (Bloom and Schimenti 2020). Statistical comparisons were performed using GraphPad Prism8 using unpaired non-parametric Mann-Whitney tests.

Single Cell DNA-sequencing and Analysis

Round spermatids were isolated from mice of the following genotypes: wild-type, *p21*$^{-/-}$, *Fancm*$^{-/-}$, *Fancm*$^{-/-}$ *p21*$^{-/-}$ at postnatal day 26 using fluorescence activated cell sorting (FACS). To FACS spermatids, Vybrant DyeCycle Violet Stain was used to label cellular DNA according to the manufacturer's instructions (ThermoFisher Scientific V35003) and PI was used to exclude dead cells as described in the Cell Cycle Analysis methods section.

Spermatids were individually sorted into PCR tubes and flash frozen prior to DNA amplification.

Single cells were subjected to AccuSomatic single-cell multiple displacement amplification (Dong et al. 2017; Milholland et al. 2017) for whole-genome sequencing by Singulomics, New York, NY. Sequencing libraries were also prepared by Singulomics. Amplicons were prepared using the NEBNext® DNA Library Prep Kit following manufacturer's recommendations. The libraries were analyzed for size distribution by an Agilent 2100 Bioanalyzer and quantified using real-time PCR. The libraries were pooled according to their effective concentrations and sequenced on Illumina NovaSeq6000 sequencer with 150 bp paired-end model using the NovaSeq6000 SP Reagent Kit. Approximately 1 Gb of sequencing data was generated per cell. Parental genomic DNA was isolated from spleens and subjected to 100 bp paired-end whole genome sequencing using BGI's DNBseq (BGISEQ-500) platform.

Samples were aligned to the mm10 reference genome using BWA-MEM 0.7.17 (Li 2013) and variants were called from sorted BAM files using Platypus 0.8.1 (Rimmer et al. 2014). The following Platypus settings were applied to all samples: --assemble=1 –assemblyRegionSize=5000 –maxSize=5000. BCFtools 1.9 was used to filter out variants present in both individual germ cell genomes and parental genomes in order to identify germ cell-specific variants. Statistical significance was assessed using the Kruskal-Wallis test controlling for multiple comparisons using a Benjamini False

Discovery Rate (FDR) correction. Genome browser images were generated using the Integrative Genomics Viewer (IGV) (Robinson et al. 2011).

Data Availability

Raw data files from the RNA-seq, small RNA-seq and scDNA-seq experiments have been deposited onto the GEO database with accession number (pending manuscript review; available upon request for reviewers).

6- Acknowledgments

This work was supported by National Institutes of Health grants T32HD057854 to J.C.B. and R01HD082568 to J.C.S. The authors would like to thank J. Grenier and Cornell's Transcriptional Regulation and Expression Facility for assistance with RNA-sequencing and small RNA-sequencing experiments (P50-HD076210) and J. Glaubitz for helpful discussions regarding single cell DNA-sequencing analysis. R. Munroe and C. Abratte of Cornell's Stem Cell and Transgenic Core Facility generated the *Fancm*$^{em1/Jcs}$ and *p21*$^{em1/Jcs}$ mouse lines with partial support from the Empire State Stem Cell Fund (contract # C024174).

Author Contributions

J.C.B. conducted the experiments described and performed data analysis. J.C.S supervised all aspects of the work. J.C.B. and J.C.S wrote the manuscript.

References

Agoulnik AI, Lu B, Zhu Q, Truong C, Ty MT, Arango N, Chada KK, Bishop CE. 2002. A novel gene, Pog, is necessary for primordial germ cell proliferation in the mouse and underlies the germ cell deficient mutation, gcd. *Hum Mol Genet* **11**: 3047–3053.

Anderson EL, Baltus AE, Roepers-Gajadien HL, Hassold TJ, de Rooij DG, van Pelt AMM, Page DC. 2008. Stra8 and its inducer, retinoic acid, regulate meiotic initiation in both spermatogenesis and oogenesis in mice. *Proc Natl Acad Sci USA* **105**: 14976–14980.

Babicki S, Arndt D, Marcu A, Liang Y, Grant JR, Maciejewski A, Wishart DS. 2016. Heatmapper: web-enabled heat mapping for all. *Nucleic Acids Res* **44**: W147-53.

Bloom JC, Schimenti JC. 2020. A reporter mouse for in vivo detection of DNA damage in embryonic germ cells. *Genesis* e23368.

Brown A, Pospiech J, Moehrle B, Martin N, Geiger H. 2015. Assessing the roles of cell cycle checkpoints in HSC. *Exp Hematol* **43**: S54.

Cervantes RB, Stringer JR, Shao C, Tischfield JA, Stambrook PJ. 2002. Embryonic stem cells and somatic cells differ in mutation frequency and

type. *Proc Natl Acad Sci USA* **99**: 3586–3590.

Chuykin IA, Lianguzova MS, Pospelova TV, Pospelov VA. 2008. Activation of DNA damage response signaling in mouse embryonic stem cells. *Cell Cycle* **7**: 2922–2928.

Ciccia A, Elledge SJ. 2010. The DNA damage response: making it safe to play with knives. *Mol Cell* **40**: 179–204.

Deans AJ, West SC. 2009. FANCM connects the genome instability disorders Bloom's Syndrome and Fanconi Anemia. *Mol Cell* **36**: 943–953.

Deniz Ö, Frost JM, Branco MR. 2019. Regulation of transposable elements by DNA modifications. *Nat Rev Genet* **20**: 417–431.

Dokshin GA, Baltus AE, Eppig JJ, Page DC. 2013. Oocyte differentiation is genetically dissociable from meiosis in mice. *Nat Genet* **45**: 877–883.

Dong X, Zhang L, Milholland B, Lee M, Maslov AY, Wang T, Vijg J. 2017. Accurate identification of single-nucleotide variants in whole-genome-amplified single cells. *Nat Methods* **14**: 491–493.

Earnshaw WC, Martins LM, Kaufmann SH. 1999. Mammalian caspases: structure, activation, substrates, and functions during apoptosis. *Annu Rev Biochem* **68**: 383–424.

Endo T, Mikedis MM, Nicholls PK, Page DC, de Rooij DG. 2019. Retinoic acid and germ cell development in the ovary and testis. *Biomolecules* **9**.

Enguita-Marruedo A, Martín-Ruiz M, García E, Gil-Fernández A, Parra MT, Viera A, Rufas JS, Page J. 2019. Transition from a meiotic to a somatic-like DNA damage response during the pachytene stage in

mouse meiosis. *PLoS Genet* **15**: e1007439.

Ernst C, Odom DT, Kutter C. 2017. The emergence of piRNAs against transposon invasion to preserve mammalian genome integrity. *Nat Commun* **8**: 1411.

Ewen KA, Koopman P. 2010. Mouse germ cell development: from specification to sex determination. *Mol Cell Endocrinol* **323**: 76–93.

Favor J. 1999. Mechanisms of mutation induction in germ cells of the mouse as assessed by the specific locus test. *Mutat Res* **428**: 227–236.

Featherstone C, Jackson SP. 1999. DNA double-strand break repair. *Curr Biol* **9**: R759-61.

Fluckiger A-C, Marcy G, Marchand M, Négre D, Cosset F-L, Mitalipov S, Wolf D, Savatier P, Dehay C. 2006. Cell cycle features of primate embryonic stem cells. *Stem Cells* **24**: 547–556.

Gari K, Décaillet C, Delannoy M, Wu L, Constantinou A. 2008. Remodeling of DNA replication structures by the branch point translocase FANCM. *Proc Natl Acad Sci USA* **105**: 16107–16112.

Ginsburg M, Snow MH, McLaren A. 1990. Primordial germ cells in the mouse embryo during gastrulation. *Development* **110**: 521–528.

Gomperts M, Wylie C, Heasman J. 1994. Primordial germ cell migration. *Ciba Found Symp* **182**: 121–34; discussion 134.

Grompe M, D'Andrea A. 2001. Fanconi anemia and DNA repair. *Hum Mol Genet* **10**: 2253–2259.

Grskovic M, Chaivorapol C, Gaspar-Maia A, Li H, Ramalho-Santos M. 2007.

Systematic identification of cis-regulatory sequences active in mouse and human embryonic stem cells. *PLoS Genet* **3**: e145.

Hamer G, de Rooij DG. 2018. Mutations causing specific arrests in the development of mouse primordial germ cells and gonocytes. *Biol Reprod* **99**: 75–86.

Han BW, Wang W, Zamore PD, Weng Z. 2015. piPipes: a set of pipelines for piRNA and transposon analysis via small RNA-seq, RNA-seq, degradome- and CAGE-seq, ChIP-seq and genomic DNA sequencing. *Bioinformatics* **31**: 593–595.

Harfe BD, Jinks-Robertson S. 2000. DNA polymerase zeta introduces multiple mutations when bypassing spontaneous DNA damage in Saccharomyces cerevisiae. *Mol Cell* **6**: 1491–1499.

Hayashi K, Ohta H, Kurimoto K, Aramaki S, Saitou M. 2011. Reconstitution of the mouse germ cell specification pathway in culture by pluripotent stem cells. *Cell* **146**: 519–532.

Heyer BS, MacAuley A, Behrendtsen O, Werb Z. 2000. Hypersensitivity to DNA damage leads to increased apoptosis during early mouse development. *Genes Dev* **14**: 2072–2084.

Hong Y, Cervantes RB, Tichy E, Tischfield JA, Stambrook PJ. 2007. Protecting genomic integrity in somatic cells and embryonic stem cells. *Mutat Res* **614**: 48–55.

Hong Y, Stambrook PJ. 2004. Restoration of an absent G1 arrest and protection from apoptosis in embryonic stem cells after ionizing

radiation. *Proc Natl Acad Sci USA* **101**: 14443–14448.

Huang J, Liu S, Bellani MA, Thazhathveetil AK, Ling C, de Winter JP, Wang Y, Wang W, Seidman MM. 2013. The DNA translocase FANCM/MHF promotes replication traverse of DNA interstrand crosslinks. *Mol Cell* **52**: 434–446.

Jin Y, Tam OH, Paniagua E, Hammell M. 2015. TEtranscripts: a package for including transposable elements in differential expression analysis of RNA-seq datasets. *Bioinformatics* **31**: 3593–3599.

Joenje H, Patel KJ. 2001. The emerging genetic and molecular basis of Fanconi anaemia. *Nat Rev Genet* **2**: 446–457.

Koubova J, Hu Y-C, Bhattacharyya T, Soh YQS, Gill ME, Goodheart ML, Hogarth CA, Griswold MD, Page DC. 2014. Retinoic acid activates two pathways required for meiosis in mice. *PLoS Genet* **10**: e1004541.

Koubova J, Menke DB, Zhou Q, Capel B, Griswold MD, Page DC. 2006. Retinoic acid regulates sex-specific timing of meiotic initiation in mice. *Proc Natl Acad Sci USA* **103**: 2474–2479.

Lesch BJ, Dokshin GA, Young RA, McCarrey JR, Page DC. 2013. A set of genes critical to development is epigenetically poised in mouse germ cells from fetal stages through completion of meiosis. *Proc Natl Acad Sci USA* **110**: 16061–16066.

Li H. 2013. Aligning sequence reads, clone sequences and assembly contigs with BWA-MEM. *ArXiv*.

Luo Y, Hartford SA, Zeng R, Southard TL, Shima N, Schimenti JC. 2014.

Hypersensitivity of primordial germ cells to compromised replication-associated DNA repair involves ATM-p53-p21 signaling. *PLoS Genet* **10**: e1004471.

Luo Y, Schimenti JC. 2015. MCM9 deficiency delays primordial germ cell proliferation independent of the ATM pathway. *Genesis* **53**: 678–684.

McNairn AJ, Chuang C-H, Bloom JC, Wallace MD, Schimenti JC. 2019. Female-biased embryonic death from inflammation induced by genomic instability. *Nature* **567**: 105–108.

Mi H, Muruganujan A, Huang X, Ebert D, Mills C, Guo X, Thomas PD. 2019. Protocol Update for large-scale genome and gene function analysis with the PANTHER classification system (v.14.0). *Nat Protoc* **14**: 703–721.

Miles DC, van den Bergen JA, Sinclair AH, Western PS. 2010. Regulation of the female mouse germ cell cycle during entry into meiosis. *Cell Cycle* **9**: 408–418.

Milholland B, Dong X, Zhang L, Hao X, Suh Y, Vijg J. 2017. Differences between germline and somatic mutation rates in humans and mice. *Nat Commun* **8**: 15183.

Nadler JJ, Braun RE. 2000. Fanconi anemia complementation group C is required for proliferation of murine primordial germ cells. *Genesis* **27**: 117–123.

Nguyen DH, Laird DJ. 2019. Apoptosis in the fetal testis eliminates developmentally defective germ cell clones. *BioRxiv*.

Nikolic A, Volarevic V, Armstrong L, Lako M, Stojkovic M. 2016. Primordial germ cells: current knowledge and perspectives. *Stem Cells Int* **2016**: 1741072.

Rimmer A, Phan H, Mathieson I, Iqbal Z, Twigg SRF, WGS500 Consortium, Wilkie AOM, McVean G, Lunter G. 2014. Integrating mapping-, assembly- and haplotype-based approaches for calling variants in clinical sequencing applications. *Nat Genet* **46**: 912–918.

Rinaldi VD, Hsieh K, Munroe R, Bolcun-Filas E, Schimenti JC. 2017. Pharmacological Inhibition of the DNA Damage Checkpoint Prevents Radiation-Induced Oocyte Death. *Genetics* **206**: 1823–1828.

Robinson JT, Thorvaldsdóttir H, Winckler W, Guttman M, Lander ES, Getz G, Mesirov JP. 2011. Integrative genomics viewer. *Nat Biotechnol* **29**: 24–26.

Rojas-Ríos P, Simonelig M. 2018. piRNAs and PIWI proteins: regulators of gene expression in development and stem cells. *Development* **145**.

Roque T, Haton C, Etienne O, Chicheportiche A, Rousseau L, Martin L, Mouthon M-A, Boussin FD. 2012. Lack of a p21waf1/cip -dependent G1/S checkpoint in neural stem and progenitor cells after DNA damage in vivo. *Stem Cells* **30**: 537–547.

Rucker EB, Dierisseau P, Wagner KU, Garrett L, Wynshaw-Boris A, Flaws JA, Hennighausen L. 2000. Bcl-x and Bax regulate mouse primordial germ cell survival and apoptosis during embryogenesis. *Mol Endocrinol* **14**: 1038–1052.

Russell LB, Selby PB, von Halle E, Sheridan W, Valcovic L. 1981. The mouse specific-locus test with agents other than radiations: interpretation of data and recommendations for future work. *Mutat Res* **86**: 329–354.

Sangrithi MN, Royo H, Mahadevaiah SK, Ojarikre O, Bhaw L, Sesay A, Peters AHFM, Stadler M, Turner JMA. 2017. Non-Canonical and Sexually Dimorphic X Dosage Compensation States in the Mouse and Human Germline. *Dev Cell* **40**: 289–301.e3.

Shaltiel IA, Krenning L, Bruinsma W, Medema RH. 2015. The same, only different - DNA damage checkpoints and their reversal throughout the cell cycle. *J Cell Sci* **128**: 607–620.

Singh P, Aggarwal LM, Parry SA, Raman MJ. 2018. Radiation dosimetry and repair kinetics of DNA damage foci in mouse pachytene spermatocyte and round spermatid stages. *Mutagenesis* **33**: 231–239.

Singh P, Schimenti JC, Bolcun-filas E. 2014. A Mouse Geneticist ' s practical guide to CRISPR applications. *Genetics: Early Online* 1–15.

Soh YQS, Junker JP, Gill ME, Mueller JL, van Oudenaarden A, Page DC. 2015. A gene regulatory program for meiotic prophase in the fetal ovary. *PLoS Genet* **11**: e1005531.

Soh YQS, Mikedis MM, Kojima M, Godfrey AK, de Rooij DG, Page DC. 2017. Meioc maintains an extended meiotic prophase I in mice. *PLoS Genet* **13**: e1006704.

Speed RM. 1982. Meiosis in the foetal mouse ovary. I. An analysis at the light microscope level using surface-spreading. *Chromosoma* **85**: 427–437.

Stallock J, Molyneaux K, Schaible K, Knudson CM, Wylie C. 2003. The pro-apoptotic gene Bax is required for the death of ectopic primordial germ cells during their migration in the mouse embryo. *Development* **130**: 6589–6597.

Stone JE, Lujan SA, Kunkel TA, Kunkel TA. 2012. DNA polymerase zeta generates clustered mutations during bypass of endogenous DNA lesions in Saccharomyces cerevisiae. *Environ Mol Mutagen* **53**: 777–786.

Suvorova II, Grigorash BB, Chuykin IA, Pospelova TV, Pospelov VA. 2016. G1 checkpoint is compromised in mouse ESCs due to functional uncoupling of p53-p21Waf1 signaling. *Cell Cycle* **15**: 52–63.

Szabo PE, Hubner K, Scholer H, Mann JR. 2002. Allele-speci c expression of imprinted genes in mouse migratory primordial germ cells □. *Mech Dev* **115**: 157–160.

Tam PP, Snow MH. 1981. Proliferation and migration of primordial germ cells during compensatory growth in mouse embryos. *J Embryol Exp Morphol* **64**: 133–147.

Tichy ED, Stambrook PJ. 2008. DNA repair in murine embryonic stem cells and differentiated cells. *Exp Cell Res* **314**: 1929–1936.

Trapnell C, Williams BA, Pertea G, Mortazavi A, Kwan G, van Baren MJ, Salzberg SL, Wold BJ, Pachter L. 2010. Transcript assembly and quantification by RNA-Seq reveals unannotated transcripts and isoform switching during cell differentiation. *Nat Biotechnol* **28**: 511–515.

Tremml G, Singer M, Malavarca R. 2008. Culture of mouse embryonic stem cells. *Curr Protoc Stem Cell Biol* **Chapter 1**: Unit 1C.4.

Watanabe N, Mii S, Asai N, Asai M, Niimi K, Ushida K, Kato T, Enomoto A, Ishii H, Takahashi M, et al. 2013. The REV7 subunit of DNA polymerase ζ is essential for primordial germ cell maintenance in the mouse. *J Biol Chem* **288**: 10459–10471.

You Y, Bersgtram R, Klemm M, Nelson H, Jaenisch R, Schimenti J. 1998. Utility of C57BL/6J x 129/SvJae embryonic stem cells for generating chromosomal deletions: tolerance to gamma radiation and microsatellite polymorphism. *Mamm Genome* **9**: 232–234.

CHAPTER 4

OOCYTE ELIMINATION THROUGH DNA DAMAGE SIGNALING FROM CHK1/CHK2 TO p53 AND p63

* This chapter is a reprint with minor reformatting of the manuscript: Rinaldi, V.D.[+], Bloom, J.C.[+], Schimenti, J.C. Oocyte Elimination Through DNA Damage Signaling from CHK1/CHK2 to p53 and p63. *Genetics.* (215),1-6, doi:10.1534/genetics.120.303182 (2020).

[+] These authors contributed equally to this work.

1- Abstract

Eukaryotic organisms have evolved mechanisms to prevent the accumulation of cells bearing genetic aberrations. This is especially crucial for the germline, because fecundity and fitness of progeny would be adversely affected by an excessively high mutational incidence. The process of meiosis poses unique problems for mutation avoidance because of the requirement for SPO11- induced programmed double-strand breaks (DSBs) in recombination-driven pairing and segregation of homologous chromosomes. Mouse meiocytes bearing unrepaired meiotic DSBs or unsynapsed chromosomes are eliminated before completing meiotic prophase I. In previous work, we showed

that checkpoint kinase 2 (CHK2; CHEK2), a canonical DNA damage response protein, is crucial for eliminating not only oocytes defective in meiotic DSB repair (e.g., $Trip13^{Gt}$ mutants), but also $Spo11^{-/-}$ oocytes that are defective in homologous chromosome synapsis and accumulate a threshold level of spontaneous DSBs. However, rescue of such oocytes by Chk2 deficiency was incomplete, raising the possibility that a parallel checkpoint pathway(s) exists. Here, we show that mouse oocytes lacking both p53 (TRP53) and the oocyte-exclusive isoform of p63, TAp63, protects nearly all $Spo11^{-/-}$ and $Trip13^{Gt/Gt}$ oocytes from elimination. We present evidence that checkpoint kinase I (CHK1; CHEK1), which is known to signal to TRP53, also becomes activated by persistent DSBs in oocytes, and to an increased degree when CHK2 is absent. The combined data indicate that nearly all oocytes reaching a threshold level of unrepaired DSBs are eliminated by a semi-redundant pathway of CHK1/CHK2 signaling to TRP53/TAp63.

KEYWORDS: checkpoints; meiosis; mouse; oocytes; transducer kinases

2- Introduction

Oocyte development in females begins in utero, when primordial germ cells enter and complete early stages of meiosis, including recombination, before arresting perinatally in a stage called dictyate. In the first few days after birth, the oocytes undergo folliculogenesis, in which they become surrounded

by flattened granulosa cells (Peters 1969). The resulting “primordial follicles” constitute the finite oocyte pool present in women and female mice of reproductive age (Findlay et al. 2015).

Meiocytes have developed mechanisms for minimizing the production of gametes with genetic anomalies such as unrepaired double-strand breaks (DSBs) and meiotic chromosome asynapsis. Mouse oocytes bearing mutations that prevent repair of programmed SPO11/TOPOVIBL-induced DSBs, which are essential for recombination-mediated pairing and synapsis of homologous chromosomes (Baudat et al. 2000; Romanienko and Camerini-Otero 2000; Mahadevaiah et al. 2001; Robert et al. 2016), are eliminated by a DNA damage checkpoint (Di Giacomo et al. 2005). The molecular nature of this checkpoint was first revealed as involving signaling of CHK2 to TRP53 and the oocyte-specific TransActivation domain of p63, known as TAp63 (Suh et al. 2006; Livera et al. 2008), by studies exploiting a hypomorphic allele of Trip13 (Bolcun-Filas et al. 2014). This allele ($Trip13^{Gt}$) causes sterility in both males and females and is useful because it is defective for DSB repair but not synapsis (Li and Schimenti 2007). Deficiency of Chk2 protected against oocyte loss and restored fertility of $Trip13^{Gt/Gt}$ females. Chk2 also plays a role in the DNA damage checkpoint in spermatocyte meiosis (Pacheco et al. 2015).

Defects in chromosome synapsis during meiotic prophase I also triggers death of most oocytes. There are at least two mechanisms underlying this “synapsis checkpoint.” One is meiotic silencing of unsynapsed chromatin

(MSUC), a process of extensive heterochromatinization and transcriptional downregulation, which appears to function primarily in situations where only about one to three chromosomes are unsynapsed (Kouznetsova et al. 2009; Cloutier et al. 2015). A second mechanism pertains to oocytes that are highly asynaptic, in which the silencing machinery is presumably overwhelmed (Kouznetsova et al. 2009). Surprisingly, this mechanism is also highly dependent on the DNA damage checkpoint. The mechanistic basis for this is the formation of a threshold level (~10) of SPO11-independent, spontaneously arising DSBs (Carofiglio et al. 2013; Rinaldi et al. 2017). Approximately 61% of $Spo11^{-/-}$ oocytes, which do not form programmed meiotic DSBs and consequently are defective for homologous chromosome synapsis (but do exhibit some nonhomologous synapsis), reach this threshold, leading to depletion of the entire ovarian reserve (primordial oocytes) by a few weeks after birth (Baudat et al. 2000; Romanienko and Camerini-Otero 2000). *Chk2* deletion rescued oocyte numbers to ~25% of wild type (WT), indicating that most are either eliminated by an alternative pathway or succumb nonspecifically from a catastrophically high number of DSBs (up to ~100, with an average of ~50/cell) (Rinaldi et al. 2017). Similarly, Chk2 deficiency rescued $Trip13^{Gt/Gt}$ oocytes to around one-third of WT levels (Bolcun-Filas et al. 2014), raising the possibility that the same CHK2-independent pathway may be active in both cases.

Here, we tested the possibility that the incomplete rescue of oocytes mentioned above is due to the existence of another pathway either distinct or complementary to that involving CHK2, but which also involves TRP53 and TAp63. Our results indicate that this is indeed the case, and that most Spo11$^{-/-}$ and TRIP13-deficient oocytes are ultimately eliminated by the combined activation of TRP53 and TAp63.

3- Materials and Methods

Mice

Alleles used in this study and their genetic backgrounds were previously described (Bolcun-Filas et al. 2014). Comparisons of compound mutants and controls utilized littermates when- ever possible, otherwise animals from related parents or different litters from the same parents were used. Animal work was approved by Cornell's Institutional Animal Care and Use Committee, under protocol 2004-0038 to J.C.S.

Histology and follicle quantification

Ovaries were fixed in Bouin's solution, embedded in paraffin, serially sectioned at 6 mm, and stained with hematoxylin and eosin. Follicle identification (Myers et al. 2004) and quantification was as described (Bolcun-Filas et al. 2014). Graphs and statistical analysis were performed with

GraphPad Prism8. Comparisons of follicle numbers across genotypes were performed using an ordinary one-way ANOVA test.

Western blot analysis of protein phosphorylation

Ovaries from postnatal (3–5 day old) mice were collected and divided into control and treatment groups. Treated groups were exposed to 3 Gy of ionizing radiation (IR) as described above and proteins were extracted 3 hr post irradiation. Ovaries from all the females in the litter were dissected and individually frozen while genotyping was performed. Proteins from ovaries of selected genotypes were pooled into groups of four and extracted with lysis buffer containing: 20 mM Tris-HCl (pH 7.4), 150 mM NaCl, 1 mM EDTA, 1 mM EGTA, 1% Triton X-100, protease inhibitors (#11836153001; Complete Mini-Roche), and phosphoprotease inhibitors (#04906845001; PhosSTOP-Roche). Proteins were resolved on 4–20% gradient acrylamide gels (#4561093; Bio-Rad, Hercules, CA), transferred to PVDF transfer membranes (#IPVH00010; Millipore, Bedford, MA) and blocked with 5% BSA or 5% nonfat milk according to the manufacturer datasheet for the corresponding antibody. Membranes were probed with rabbit anti-phospho-Chk1 (Ser345) (1:750, 133D3; Cell Signaling Technology), rabbit anti-p53 (rodent- specific 1:750, D2H90; Cell Signaling Technology), mouse anti-p63 (1:500, CM163A; Biocare Medical), and rabbit anti- DDX4/MVH (1:750, 13840; Abcam).

Data availability statement

Mouse strains that were not obtained from others will be made available upon request. Supplemental Material, Figure S1 is a Western blot that is a biological replicate of Figure 2. Table S1 contains primordial and total follicle counts for the genotypes included in Figure 1. Supplemental material available at figshare: https://doi.org/10.25386/genetics.12092187.

4- Results and Discussion

To address whether a CHK2-independent pathway exists that can eliminate oocytes bearing unrepaired DSBs, we utilized two mutant models, $Trip13^{Gt}$ and a Spo11 null ($Spo11^{-}$). Virtually all $Trip13^{Gt/Gt}$ oocytes are eliminated due to failure to repair SPO11-dependent DSBs (Li and Schimenti 2007) by the end of pachynema (Rinaldi et al. 2017). Chk2 deficiency rescued around one-third of these oocytes, and these rescued oocytes gave rise to viable offspring (Bolcun-Filas et al. 2014). Although disruption of either of CHK2's downstream phosphorylation targets, TRP53 and TAp63, enabled little or no rescue of $Trip13^{Gt/Gt}$ oocytes, $Trip13^{Gt/Gt}$ $TAp63^{-/-}$ $Trp53^{+/-}$ mice exhibited oocyte rescue similar to that of $Trip13^{Gt/Gt}$ $Chk2^{-/-}$ mice (Bolcun-Filas et al. 2014). At the time of that report, double mutants ($TAp63^{-/-}$ $Trp53^{-/-}$; the former allele ablating the TA domain only) were not assayed for the extent to which they could rescue $Trip13^{Gt/Gt}$ oocytes. We hypothesized that the inability to achieve full oocyte rescue in either $Trip13^{Gt/Gt}$ $TAp63^{-/-}$ $Trp53^{+/-}$ or $Trip13^{Gt/Gt}$

Chk2$^{-/-}$ females was due to one of the following: (1) the number of DSBs was so high that elimination of most oocytes occurred in a checkpoint-independent fashion; (2) residual TRP53 activity in the Trip13$^{Gt/Gt}$ TAp63$^{-/-}$ Trp53$^{+/-}$ mice sufficed to trigger apoptosis in many oocytes; and/or (3) a parallel checkpoint pathway is active in Chk2$^{-/-}$ oocytes.

To test these possibilities, we first assessed the ovarian reserve in Trip13$^{Gt/Gt}$ Trp53$^{-/-}$ TAp63$^{-/-}$ mice. Remarkably, the numbers of primordial and later-stage oocytes in the triple mutants were indistinguishable from WT (Figure 4.1, A and B). This result indicates that essentially all Trip13$^{Gt/Gt}$ oocytes are eliminated by checkpoint signaling to TRP53 and TAp63, thereby eliminating hypothesis 1, but supporting hypothesis 2. This result is also consistent with hypothesis 3, implying that another pathway or kinase is signaling to these two effector proteins.

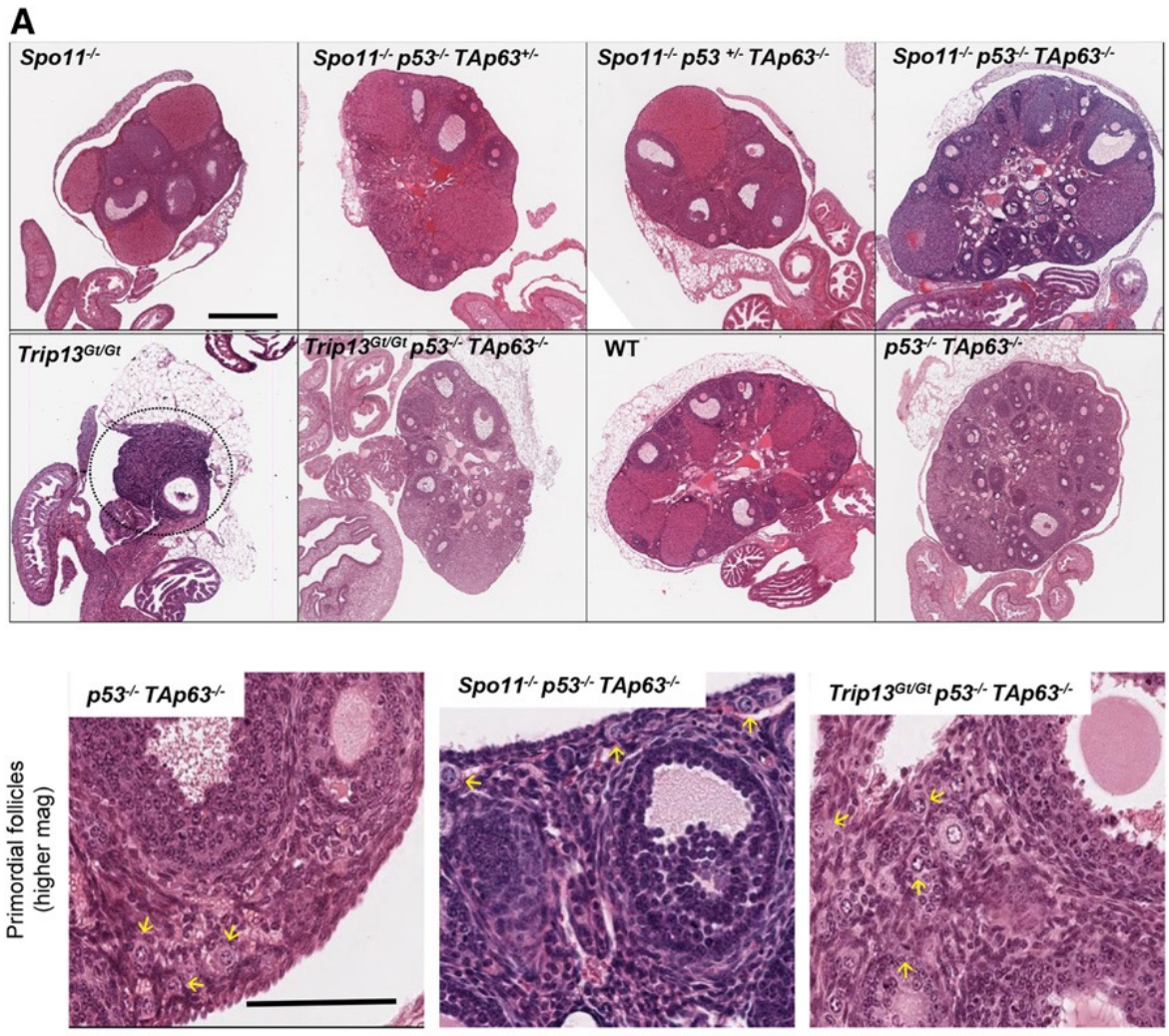

(legend on next page)

Figure 4.1. Rescue of SPO11- and TRIP13-deficient oocytes by compound deletion of p53 and TAp63. (A) Hematoxylin and eosin stained ovaries from 2-month-old mice of the indicated genotypes. The top two rows are images are from histological sections through the approximate center of the ovaries. Bar, 500 μm. The dashed circle indicates the residual $Trip13^{Gt/Gt}$ ovary. The bottom row shows higher magnification images of selected genotypes. Bar, 100 μm. Yellow arrows indicate examples of primordial follicles. (B) Oocyte quantification. To the left is the quantification of primordial follicles [P<0.0001 for all oocyte rescued (in bold) genotypes compared to non-rescued genotypes; P=0.92 for oocyte rescued genotypes vs. WT and $Trp53^{-/-}$ $TAp63^{-/-}$ ovaries]. To the right are total oocytes (from all stages of follicles) from individual ovaries (P<0.0001 for all oocyte rescued genotypes com- pared to non-rescued genotypes; P=0.33 for oocyte rescued genotypes vs. WT and $Trp53^{-/-}$ $TAp63^{-/-}$ ovaries). Genotype abbreviations are as follows: TAp63 is abbreviated as p63; WT, wild type.

Next, we tested whether the incomplete rescue of $Spo11^{-/-}$ oocytes by Chk2 deletion is also potentially a consequence of checkpoint signaling to TAp63 and TRP53 via a different transducer. Accordingly, we bred mice that lacked either or both of these proteins in the context of Spo11 deficiency. Oocyte numbers in $Spo11^{-/-}$ mice that were also homozygous for mutations in either Trp53 or TAp63 and heterozygous for a mutation in the other ($Trp53^{-/-}$ $TAp63^{+/-}$ and $Trp53^{+/-}$ $TAp63^{-/-}$) were indistinguishable from Spo11 nulls; nearly

the entire oocyte reserve was depleted after 2 months of age, as is characteristic for Spo11 deficiency (Di Giacomo et al. 2005). However, homozygosity for both Trp53 and TAp63 dramatically restored oocyte numbers to WT levels (Figure 4.1, A and B). It is unclear why heterozygosity for either Trp53 or TAp63 in the context of nullizygosity for the other gene failed to rescue any $Spo11^{-/-}$ oocytes unlike $Trip13^{Gt/Gt}$ oocytes, but we can speculate that other factors could play a role. These include strain background, enhanced recognition by DNA damage sensors of spontaneous DSBs on asynapsed chromosomes ($Spo11^{-/-}$) vs. meiotically induced DSBs on synapsed chromosomes ($Trip13^{Gt/Gt}$), or greater availability of DNA damage signaling factors in $Spo11^{-/-}$ oocytes stimulated by the MSUC response.

These experiments indicate that unrepaired meiotic DSBs, when present at levels above the threshold to trigger their elimination (Rinaldi et al. 2017), ultimately cause DNA damage signaling to both TRP53 and TAp63. Additionally, we conclude that one or both of these proteins can be activated not only by CHK2, but also another kinase. In our previous studies, we suggested that the apical kinase ATM, which when activated by DSBs typically phosphorylates CHK2, is not essential for the meiotic DNA damage checkpoint (Bolcun-Filas et al. 2014). This conclusion was based on the observation that many $Atm^{-/-}$ oocytes, which have extensive DSBs due to ATM's role in negatively regulating SPO11 (Lange et al. 2011), are eliminated in a CHK2-dependent manner. We proposed (Bolcun-Filas et al. 2014) that the related

kinase ATR (ataxia telangiectasia and Rad3 related) might activate CHK2 in oocytes similar to irradiated mitotic cells (Wang et al. 2006), which in turn would phosphorylate TAp63 and TRP53. Since ATR primarily activates CHK1, albeit most notably in the context of damage at DNA replication forks, we speculated that CHK1 can trigger death of DSB-bearing oocytes by activating TRP53 in the absence of CHK2. TRP53 is a known target of CHK1 (Shieh et al. 2000; Ou et al. 2005), and studies have shown that CHK1 can be activated in response to DSBs either in an ATM- dependent (Flaggs et al. 1997; Maréchal and Zou 2013) or ATM-independent (Flaggs et al. 1997; Balmus et al. 2012) manner. Recombinant CHK1 has also been reported to phosphorylate TRP63 in vitro (Kim et al. 2007).

If this hypothesis is true, CHK1 would be activated in response to DSBs present in oocytes. To test this, we examined levels of CHK1 phosphorylated at Ser345 (pCHK1; indicative of the active form) and TRP53 (which is stabilized by phosphorylation) in various genotypes of neonatal (3–5 days post- partum) ovaries, and also in ovaries exposed to 3 Gy of IR. This level of IR induces ~40 DSBs, as measured by RAD51 foci (a proxy for DSBs) on meiotic chromosomes of oocytes (Rinaldi et al. 2017). By way of comparison, DSB repair- defective Trip13$^{Gt/Gt}$ have ~65 RAD51 foci persisting abnormally on synapsed pachytene cells (Rinaldi et al. 2017). Since ovaries of mutant animals have variable numbers of oocytes, we used the germ-cell-specific

marker MVH as a loading reference for the amount of protein corresponding to oocytes in each sample. Ovaries were harvested at 3 hours post-irradiation.

In unirradiated ovaries, there was no apparent difference between repair-proficient genotypes (WT; $Chk2^{-/-}$; $Spo11^{-/-}$; $Spo11^{-/-}$ $Chk2^{-/-}$) in the levels of pCHK1 or TRP53 (Figure 4.2A). Both unirradiated $Trip13^{Gt/Gt}$ and irradiated WT ovaries had slightly elevated pCHK1, with the former also having a marked increase in TRP53 (note MVH levels for inter-sample comparisons). Interestingly, CHK1 phosphorylation was markedly higher in irradiated $Chk2^{-/-}$ and unirradiated $Trip13^{Gt/Gt}$ $Chk2^{-/-}$ ovaries (Figure 4.2A and Figure 4.4). This implies that the ATM and/or ATR kinases have a higher propensity to activate CHK2 than CHK1 in response to DSBs in meiocytes, but that CHK1 becomes a more prominent target in the absence of CHK2, and is able to trigger a TRP53/TAp63 response that results in apoptosis or eventual DSB repair (Bolcun-Filas et al. 2014).

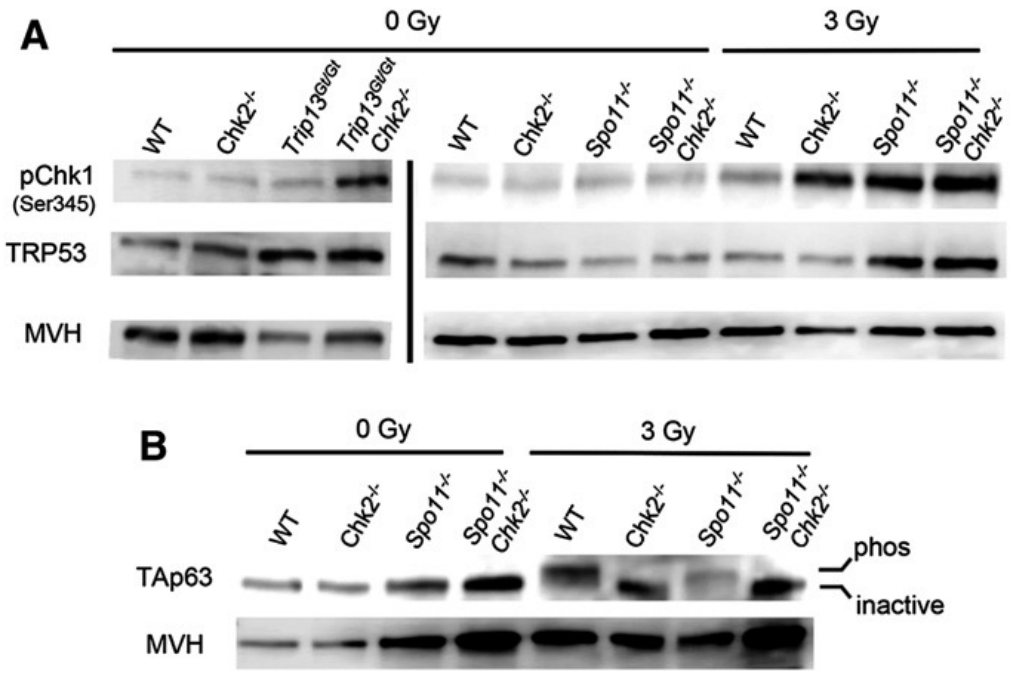

Figure 4.2. Increased CHK1 activation and p53 stabilization, but not TAp63 activation, in CHK2-deficient oocytes. (A) CHK1 phosphorylation in oocytes is stimulated by induced or meiotic DSBs. Shown are Western blots probed with indicated antibodies. Each lane contains total protein extracted from four ovaries (postnatal day 3–5) that were either exposed or not to 3 Gy of ionizing radiation (IR). Ovaries were harvested for protein extraction 3 hr post-IR. The blots on the left, separated by a vertical bar from those on the right, were from a different blot and different protein samples and mice. The same two blots (left and right) were stripped and re-probed sequentially with the three antibodies. A biological replicate is shown in **Figure 4.4**. Note that the decreased MVH levels in Trip13$^{Gt/Gt}$ ovaries is due to reduction in oocytes. (B) Activation of the TAp63 isoform is dependent on DNA damage and CHK2

signaling, not asynapsis. Shown is a Western blot probed sequentially for TAp63 and the germ cell marker MVH. Each lane contains protein extracted from ovaries as described in A. An upward shift in the band indicates the presence of the active (phosphorylated) vs. inactive TAp63. A biological replicate is shown in **Figure 4.4**.

Interestingly, IR also caused a marked increase of pCHK1 in Spo11$^{-/-}$ oocytes compared to WT (Figure 4.2A and Figure 4.4). Levels of TRP53 were also higher in IR-treated Spo11$^{-/-}$ ovaries, but the presence or absence of CHK2 had no consequence (Figure 4.2A). One possible explanation is that repair of IR-induced DSBs by intersister recombination is inhibited in Spo11 mutants, because unsynapsed chromosome axes retain HORMAD1/2 proteins that prevent such repair (Carofiglio et al. 2013; Rinaldi et al. 2017). In contrast, Chk2$^{-/-}$ oocytes would retain intersister repair ability, and thus either delay or minimize signaling to TRP53. A second possible cause of increased pCHK1 in irradiated Spo11$^{-/-}$ oocytes is that asynapsed chromosomes are more susceptible to IR-induced DNA damage than synapsed chromosomes (as in WT and Chk2$^{-/-}$ oocytes). A final possibility is that the presence of ATR on asynapsed chromatin (Turner et al. 2004, 2006) (Perera et al. 2004; Cloutier et al. 2016) facilitates DNA damage signaling to CHK1 under conditions of unrepaired DSBs. This implies that ATR is not only involved in MSUC, but also

retains its function as a key component of the DSB repair machinery (Widger et al. 2018).

As discussed earlier, there is evidence for two processes that can trigger death of oocytes progressing through meiosis: MSUC (which functions when only a few chromosomes are asynapsed) and spontaneous DSBs, when there is extensive asynapsis as in Spo11$^{-/-}$ oocytes. While the experiments above revealed that TRP53 is not activated in unirradiated Spo11$^{-/-}$ oocytes, it remained possible that activation of TAp63 could be induced by MSUC or extensive asynapsis. As we previously showed, CHK2 is required for IR-induced phosphorylation of TAp63 (Figure 4.2B) (Bolcun-Filas et al. 2014), which leads to the conversion of the inactive dimerized to the active tetramer form of TAp63 (Deutsch et al. 2011). However, we found no evidence for activation (phosphorylation) of TAp63 in unirradiated Spo11$^{-/-}$ ovaries (Figure 4.2B).

In summary, we have shown that mouse oocytes with unrepaired DSBs or extensive asynapsis are culled by a DNA damage response funneling through TRP53 and p63. Some, but not all of the damage signaling to these proteins is transduced by CHK2, and we provide evidence that CHK1 can also perform this function (see model in Figure 4.3). The relative contributions of these transducer kinases in meiotic DNA damage responses is unclear. Even though the essential nature of CHK1 in embryonic and premeiotic germ cell development (Abe et al. 2018) complicates analyses, CHK1 conditional

mutagenesis and depletion experiments indicate that this kinase plays a role in modulating cell cycle progression in spermatocytes during meiotic prophase I (Abe et al. 2018), and in oocytes at the G2/M checkpoint (Chen et al. 2012). A key remaining question is whether CHK1 and CHK2 are the sole direct responders for TRP53 and TRP63, or if another transducer kinase(s), such as casein kinases 1 or 2, function in parallel (Figure 4.3).

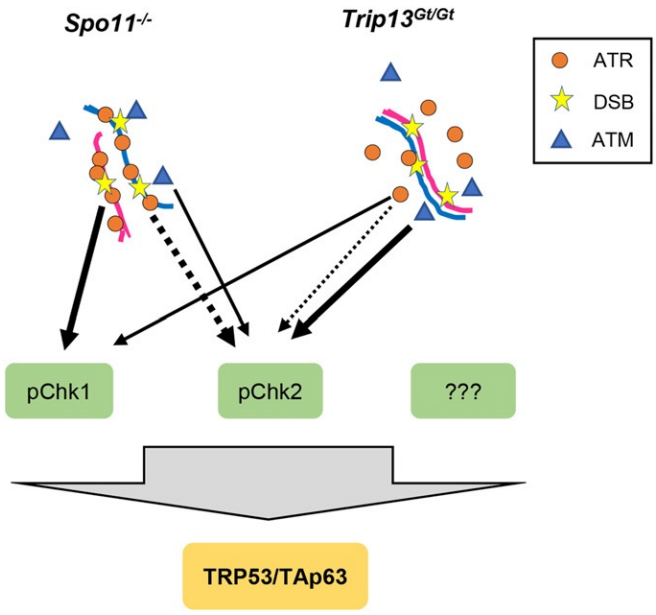

Figure 4.3. Model of checkpoint signaling in mouse oocytes. We propose that all DSB damage signaling in oocytes requires activation of TRP53 and TAp63 for complete oocyte elimination. The dashed lines represent non-canonical phosphorylation of CHK2 by ATR, and the thickness of all lines represents the relative amounts of activation in the two indicated mutant situations. We propose that in highly asynaptic Spo11 mutant oocytes, the "preloading" of ATR as part of the MSUC response leads it to play a larger role

in signaling to CHK1 and CHK2 than under situations in which DSBs occur on synapsed chromosomes.

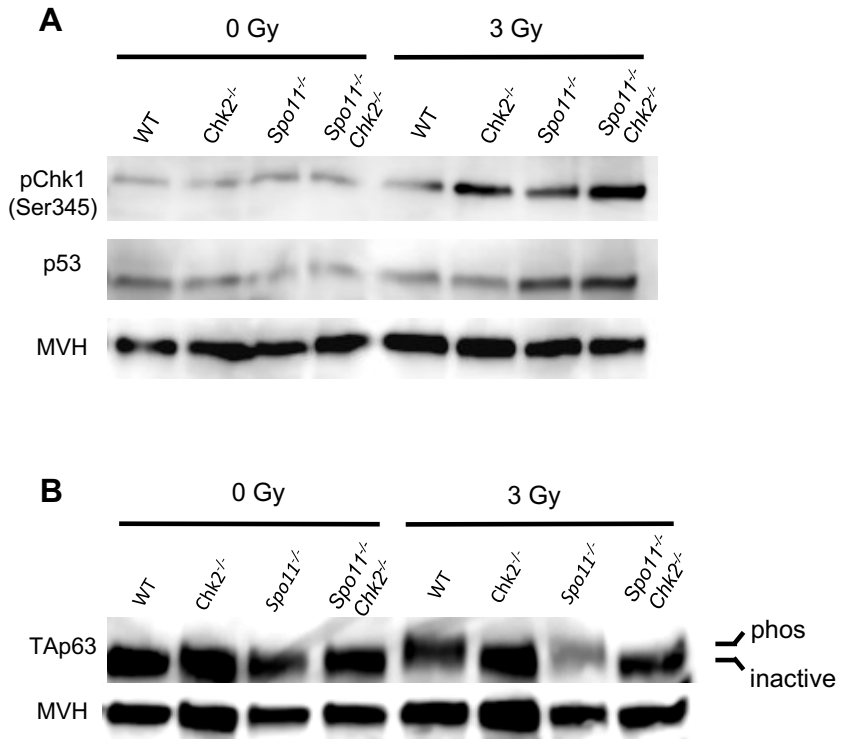

Figure 4.4. Increased CHK1 activation and p53 stabilization, but not TAp63 activation, in CHK2-deficient oocytes. (A) and (B) Western blots probed with indicated antibodies. Each lane contains total protein extracted from four ovaries (postnatal dat 3-5) that were either exposed or not to ionizing radiation (IR). This is a biological replicate of **Figure 4.2**.

5- Acknowledgments

A. Mills originally provided us with TAp63 mutant mice. This work was supported by National Institutes of Health grant GM45415 to J.C.S. and an institutional training grant (T32HD057854) that supported J.C.B.

6- References

Abe, H., K. G. Alavattam, Y. Kato, D. H. Castrillon, Q. Pang et al., 2018 CHEK1 coordinates DNA damage signaling and meiotic progression in the male germline of mice. Hum. Mol. Genet. 27: 1136–1149. https://doi.org/10.1093/hmg/ddy022

Balmus, G., M. Zhu, S. Mukherjee, A. M. Lyndaker, K. R. Hume et al., 2012 Disease severity in a mouse model of ataxia telangiectasia is modulated by the DNA damage checkpoint gene Hus1. Hum. Mol. Genet. 21: 3408–3420. https://doi.org/ 10.1093/hmg/dds173

Baudat, F., K. Manova, J. P. Yuen, M. Jasin, and S. Keeney, 2000 Chromosome synapsis defects and sexually dimorphic meiotic progression in mice lacking. Mol. Cell 6: 989–998. https://doi.org/10.1016/S1097-2765(00)00098-8

Bolcun-Filas, E., V. D. Rinaldi, M. E. White, and J. C. Schimenti, 2014 Reversal of female infertility by Chk2 ablation reveals the oocyte DNA damage

checkpoint pathway. Science 343: 533–536. https://doi.org/10.1126/science.1247671

Carofiglio, F., A. Inagaki, S. de Vries, E. Wassenaar, S. Schoen- makers et al., 2013 SPO11-independent DNA repair foci and their role in meiotic silencing. PLoS Genet. 9: e1003538. https://doi.org/10.1371/journal.pgen.1003538

Chen, L., S.-B. Chao, Z.-B. Wang, S.-T. Qi, X.-L. Zhu et al., 2012 Checkpoint kinase 1 is essential for meiotic cell cycle regulation in mouse oocytes. Cell Cycle 11: 1948–1955. https://doi.org/10.4161/cc.20279

Cloutier, J. M., S. K. Mahadevaiah, E. ElInati, A. Nussenzweig, A. Tóth et al., 2015 Histone H2AFX links meiotic chromosome asynapsis to prophase I oocyte loss in mammals. PLoS Genet. 11: e1005462 (erratum: PLoS Genet. 11: e1005753). https:// doi.org/10.1371/journal.pgen.1005462

Cloutier, J. M., S. K. Mahadevaiah, E. ElInati, A. Tóth, and J. Turner, 2016 Mammalian meiotic silencing exhibits sexually dimorphic features. Chromosoma 125: 215–226. https://doi.org/ 10.1007/s00412-015-0568-z

Deutsch, G. B., E. M. Zielonka, D. Coutandin, T. A. Weber, B. Schäfer et al., 2011 DNA damage in oocytes induces a switch of the quality control factor TAp63a from dimer to tetramer. Cell 144: 566–576. https://doi.org/10.1016/j.cell.2011.01.013

Di Giacomo, M., M. Barchi, F. Baudat, W. Edelmann, S. Keeney et al., 2005 Distinct DNA-damage-dependent and -independent responses drive the loss of oocytes in recombination-defective mouse mutants. Proc. Natl. Acad. Sci. USA 102: 737–742. https://doi.org/10.1073/pnas.0406212102

Findlay, J. K., K. J. Hutt, M. Hickey, and R. A. Anderson, 2015 How is the number of primordial follicles in the ovarian reserve established? Biol. Reprod. 93: 111. https://doi.org/ 10.1095/biolreprod.115.133652

Flaggs, G., A. W. Plug, K. M. Dunks, K. E. Mundt, J. C. Ford et al., 1997 Atm-dependent interactions of a mammalian chk1 homolog with meiotic chromosomes. Curr. Biol. 7: 977–986. https://doi.org/10.1016/S0960-9822(06)00417-9

Kim, M.-A., H.-J. Kim, A. L. Brown, M.-Y. Lee, Y.-S. Bae et al., 2007 Identification of novel substrates for human checkpoint kinase Chk1 and Chk2 through genome-wide screening using a consensus Chk phosphorylation motif. Exp. Mol. Med. 39: 205– 212. https://doi.org/10.1038/emm.2007.23

Kouznetsova, A., H. Wang, M. Bellani, R. D. Camerini-Otero, R. Jessberger et al., 2009 BRCA1-mediated chromatin silencing is limited to oocytes with a small number of asynapsed chromosomes. J. Cell Sci. 122: 2446–2452. https://doi.org/10.1242/ jcs.049353

Lange, J., J. Pan, F. Cole, M. P. Thelen, M. Jasin et al., 2011 ATM controls meiotic double-strand-break formation. Nature 479: 237–240. https://doi.org/10.1038/nature10508

Li, X. C., and J. C. Schimenti, 2007 Mouse pachytene checkpoint 2 (Trip13) is required for completing meiotic recombination but not synapsis. PLoS Genet. 3: e130. https://doi.org/10.1371/ journal.pgen.0030130

Livera, G., B. Petre-Lazar, M.-J. Guerquin, E. Trautmann, H. Coffigny et al., 2008 p63 null mutation protects mouse oocytes from radio-induced apoptosis. Reproduction 135: 3–12. https:// doi.org/10.1530/REP-07-0054

Mahadevaiah, S. K., J. M. Turner, F. Baudat, E. P. Rogakou, P. de Boer et al., 2001 Recombinational DNA double-strand breaks in mice precede synapsis. Nat. Genet. 27: 271–276. https:// doi.org/10.1038/85830

Maréchal, A., and L. Zou, 2013 DNA damage sensing by the ATM and ATR kinases. Cold Spring Harb. Perspect. Biol. 5: a012716. https://doi.org/10.1101/cshperspect.a012716

Myers, M., K. L. Britt, N. G. M. Wreford, F. J. P. Ebling, and J. B. Kerr, 2004 Methods for quantifying follicular numbers within the mouse ovary. Reproduction 127: 569–580. https://doi.org/ 10.1530/rep.1.00095

Ou, Y.-H., P.-H. Chung, T.-P. Sun, and S.-Y. Shieh, 2005 p53 C-terminal phosphorylation by CHK1 and CHK2 participates in the regulation of DNA-

damage-induced C-terminal acetylation. Mol. Biol. Cell 16: 1684–1695. https://doi.org/10.1091/mbc.e04-08-0689

Pacheco, S., M. Marcet-Ortega, J. Lange, M. Jasin, S. Keeney et al., 2015 The ATM signaling cascade promotes recombination- dependent pachytene arrest in mouse spermatocytes. PLoS Genet. 11: e1005017. https://doi.org/10.1371/journal.pgen. 1005017

Perera, D., L. Perez-Hidalgo, P. B. Moens, K. Reini, N. Lakin et al., 2004 TopBP1 and ATR colocalization at meiotic chromosomes: role of TopBP1/Cut5 in the meiotic recombination checkpoint. Mol. Biol. Cell 15: 1568–1579. https://doi.org/10.1091/ mbc.e03-06-0444

Peters, H., 1969 The development of the mouse ovary from birth to maturity. Acta Endocrinol. (Copenh.) 62: 98–116. https:// doi.org/10.1530/acta.0.0620098

Rinaldi, V. D., E. Bolcun-Filas, H. Kogo, H. Kurahashi, and J. C. Schimenti, 2017 The DNA damage checkpoint eliminates mouse oocytes with chromosome synapsis failure. Mol. Cell 67: 1026–1036.e2. https://doi.org/10.1016/j.molcel.2017.07.027

Robert, T., A. Nore, C. Brun, C. Maffre, B. Crimi et al., 2016 The TopoVIB-Like protein family is required for meiotic DNA double- strand break formation. Science 351: 943–949. https://doi.org/ 10.1126/science.aad5309

Romanienko, P. J., and R. D. Camerini-Otero, 2000 The mouse Spo11 gene is required for meiotic chromosome synapsis. Mol. Cell 6: 975–987. https://doi.org/10.1016/S1097-2765(00)00097-6

Shieh, S. Y., J. Ahn, K. Tamai, Y. Taya, and C. Prives, 2000 The human homologs of checkpoint kinases Chk1 and Cds1 (Chk2) phosphorylate p53 at multiple DNA damage-inducible sites. Genes Dev. 14: 289–300.

Suh, E.-K., A. Yang, A. Kettenbach, C. Bamberger, A. H. Michaelis et al., 2006 p63 protects the female germ line during meiotic arrest. Nature 444: 624–628. https://doi.org/10.1038/ nature05337

Turner, J. M. A., O. Aprelikova, X. Xu, R. Wang, S. Kim et al., 2004 BRCA1, histone H2AX phosphorylation, and male meiotic sex chromosome inactivation. Curr. Biol. 14: 2135–2142. https://doi.org/10.1016/j.cub.2004.11.032

Turner, J. M. A., S. K. Mahadevaiah, P. J. I. Ellis, M. J. Mitchell, and P. S. Burgoyne, 2006 Pachytene asynapsis drives meiotic sex chromosome inactivation and leads to substantial postmeiotic repression in spermatids. Dev. Cell 10: 521–529. https:// doi.org/10.1016/j.devcel.2006.02.009

Wang, X. Q., J. L. Redpath, S. T. Fan, and E. J. Stanbridge, 2006 ATR dependent activation of Chk2. J. Cell. Physiol. 208: 613–619. https://doi.org/10.1002/jcp.20700

Widger, A., S. K. Mahadevaiah, J. Lange, E. Ellnati, J. Zohren et al., 2018 ATR is a multifunctional regulator of male mouse meiosis. Nat. Commun. 9: 2621. https://doi.org/10.1038/s41467- 018-04850-0

CHAPTER 5

DISCUSSION AND CONCLUDING REMARKS

1. A Reporter Mouse for *In Vivo* Detection of DNA Damage in Embryonic Germ Cells

Chapter 2 describes the generation and validation of a 53BP1-based transgenic mouse model to detect DNA damage in PGCs. The reporter binds the histone mark H4K20me2 which becomes exposed near sites on DNA where DSBs are induced. With this transgenic reporter, we assessed the impact of exogenous IR-induced DNA damage on PGCs and showed that the reporter responds to IR in both a dose-dependent and time-dependent manner. For the purposes of demonstrating specific expression of the reporter in PGCs, tissue samples were fixed and antibody-labeled with a germ cell-specific antibody, but future work could take advantage of *ex vivo* culture systems for fetal gonads (culture conditions described in Appendix I). *Ex vivo* culture of fetal gonads, including the PGCs contained within them, could be used to assess how the cells respond to DNA damage in a live-cell, dynamic manner to facilitate a better understanding of the DSB repair kinetics in these cells.

Another future experimental direction could be to cross the transgenic reporter into different mutants which have been shown to cause a reduction in PGCs compared to controls. In the context of these different mutant backgrounds (such as those listed in (Hamer and de Rooij 2018)), the field can

begin to stratify mutants based on whether or not they lead to loss of PGCs via an increase in endogenous DNA damage. Of those mutants with increased DNA damage/DSB induction, the reporter can then be utilized in a quantitative manner to assess and compare the number of DSBs, and the persistence of them, in different mutant backgrounds. In addition to examining endogenous sources of DNA damage in PGCs, the response to other exogenous DNA damaging agents can be assessed using the reporter strain in a wild-type background. While the reporter study described in Chapter 2 focused exclusively on IR-induced DNA damage, that was merely because IR is a commonly used experimental DSB-inducing agent and I was trying to demonstrate reporter functionality. In other experimental contexts with genotoxins, whether or not the reporter becomes activated and the extent of activation will likely be an interesting question in itself.

Furthermore, the fluorescent nature of the reporter, which is dimmest in the absence of DSBs and becomes progressively brighter with an increasing number of DSBs, can be used to stratify and purify cells based on the extent of DNA damage/DSBs they are experiencing at a given moment in time. Within a population of PGCs exposed to DNA damage, I always observed some PGCs with foci and others lacking foci. Being able to sort these PGCs into different categories based on the absence or presence of foci/number of foci and then performing downstream molecular analyses (such as RNA-seq) on them would enable an in depth understanding into the variegated cellular responses observed among PGCs exposed to DNA damage. This type of an approach

may lead to a better understanding of the differences between PGCs which survive DNA damage and those which succumb.

Finally, there are at least two major limitations/caveats with respect to the transgenic reporter. One of which is that the reporter expression is significantly dimmer in female PGCs compared to male PGCs. This difference in expression was also observed in a GFP expressing transgenic mouse with the same promoter (Sabour et al. 2011) and indicates that care needs to be taken when making comparisons between reporter dynamics in male and female fetal germ cells using this transgenic line. The second caveat is that the reporter is based upon 53BP1 DSB binding activity. 53BP1 is associated primarily with NHEJ repair pathway and therefore the reporter likely does not localize to DSBs in an unbiased fashion. This idea is discussed more thoroughly in Chapter 2, where 53BP1 activity has been shown to be down-regulated upon entry into meiosis. Overall, even taking these caveats into account, I am confident that the transgenic reporter strain can be used as a tool to aid in the discovery of novel insights related to the PGC hypersensitive DDR.

2. Sexually Dimorphic DNA Damage Responses in PGCs

My original goals when I began studying how PGCs respond to exogenous DNA damage were two-fold. First, I was interested in understanding how the PGC DDR compared to that of better studied cell types, such as ESCs and second, I wanted to identify genes involved in the hypersensitive PGC DDR.

The reason I was interested in identifying genes involved in the DDR was because prior work from the lab revealed that our understanding of the DDR in these cells was incomplete. These studies tried to rescue germ cell loss in different PGC mutants and the most robust rescues achieved were only partial at best (Luo et al. 2014; Luo and Schimenti 2015). This indicated to me that there were other candidate genes involved in the PGC DDR that had yet to be identified. My original RNA-seq experiment (described in Chapter 3) proved not to be as informative as I had hoped in terms of generating a candidate list of DDR-related genes because 8 hours after DNA damage hundreds of genes are differentially expressed in response to IR (which is too many to test *in vivo*). Notably, this dataset was able to provide a developmental-context specific understanding of the PGC DDR which is much of the focus of Chapter 3.

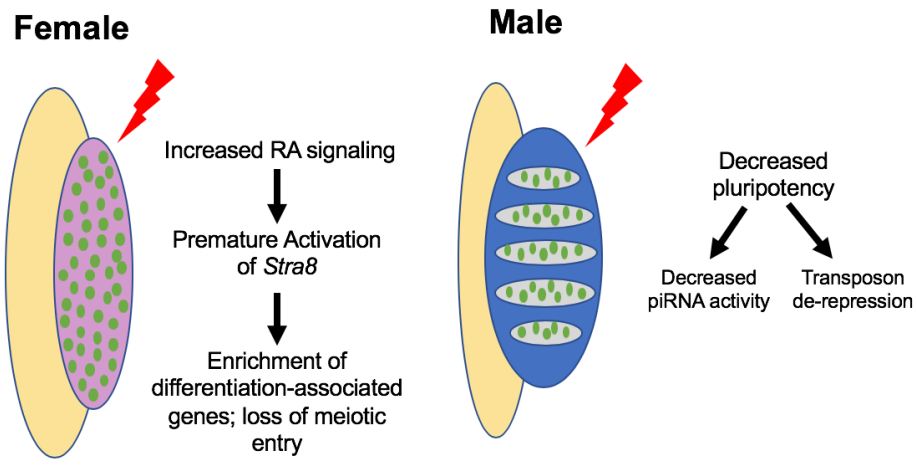

Figure 5.1. Summary models of the irradiation-induced sexually dimorphic PGC DDR described in Chapter 3.

Importantly, I also conducted RNA-seq 4 hours after IR-induced DNA damage to try to better identify candidate genes involved in PGC DDR after I realized that the 8 hour dataset was not going to be instructive for this purpose. In the 4 hour dataset, there were only a few genes differentially up-regulated in response to IR. These genes (included in the tables below) could be promising candidates to explore further in E13.5 female and male germ cells.

(legend on the next page)

Table 5.1. Up-regulated Genes in Response to IR in E13.5 Male PGCs

Gene name	log2(fold change)	Description
Rnu12	10	U12 minor spliceosomal RNA
Btg2*	1.8	BTG Anti-proliferation factor 2; activates mRNA deadenylation
Plk2*	1.8	Serine/threonine protein kinase; plays a role in cells undergoing rapid cell division
*Bbc3**	1.7	Member of the BCL-2 family; part of the BH3-only pro-apoptotic subclass
Ass1	1.6	Argininosuccinate synthase I, part of the arginine biosynthetic pathway
Cst8	1.4	Part of the cystatin superfamily, some family members act as cysteine protease inhibitors; high tissue-specific expression in the reproductive tract
5730408K05Rik	1.2	lncRNA of unknown function
*Phlda3**	1.2	Pleckstrin homology like domain family member A3, p53-mediated repressor of AKT1 signaling leading to apoptosis
*Cdkn1a (p21)**	1.1	Binds to and inhibits G1 associated CDKs
*Rmrp**	1.0	RNA component of mitochondrial RNA processing endoribonuclease

Table 5.1. Genes Significantly Up-regulated in Irradiated E13.5 Male PGCs 4 hours After DNA damage. 10 genes met the criteria for up-regulation in response to DNA damage. Bolded genes are up-regulated in both female and male samples; genes with asterisks are either involved in the cell cycle or apoptosis. (Criteria for up-regulation included those genes with a FPKM of at least 5, a change in expression of at least 2-fold or greater and an adjusted p-value<0.05 calculated by DEseq2; text summarizing gene function was adapted from GeneCards and MGI).

Table 5.2. Up-regulated Genes in Response to IR in E13.5 Female PGCs

Gene name	log2(fold change)	Description
Btg2	1.0	BTG Anti-proliferation factor 2; activates mRNA deadenylation
Plk2	1.2	Serine/threonine protein kinase; plays a role in cells undergoing rapid cell division
C1qa	1.5	Part of the immune system complement cascade which promotes inflammation and helps remove damaged cells

Table 5.2. Genes Significantly Up-regulated in Irradiated E13.5 Female PGCs 4 hours After DNA damage. 3 genes met the criteria for up-regulation in response to DNA damage. Bolded genes are up-regulated in both female and male samples. (Criteria for up-regulation included those genes with a FPKM of at least 5, a change in expression of at least 2-fold or greater and an adjusted p-value<0.05 calculated by DEseq2; text summarizing gene function was adapted from GeneCards and MGI).

Of the two genes shared between female and male E13.5 PGCs that are upregulated 4 hours after DNA damage, transgenic mice which disrupt expression of the each gene have already been generated. The homozygous null mutant *Btg2*^{tm1Wbh} does not exhibit any overt phenotypes (Haubensak et al. 2004) and the null mutant of *Plk2* (available from the Jackson Laboratory) is viable and fertile, but born at lower than expected Mendelian ratios (Inglis et al. 2009). Both genes are associated with cell cycle progression, but research performed with transgenic mouse models thus far has mostly focused on the brain. *Btg2* was found to be expressed in asymmetrically dividing neuroepithelial (NE) cells where it is selectively expressed in the neuron-generating cells rather than the proliferating NE cells (Haubensak et al. 2004). *Plk2* was initially identified as a gene whose expression was associated with serum-starved cells re-challenged with complete media and was later shown to be a transcriptional target of *p53* associated with cell cycle checkpoint function (Simmons et al. 1992; Burns et al. 2003). *Plk2* deletion in mice has been associated with decreases in alpha synuclein phosphorylation in the brain and may be a promising target for the treatment of Parkinson's disease (Inglis et al. 2009).

Both *Btg2* and *Plk2* have been reported to act as tumor suppressors due their down-regulated gene expression in a number of different cancer types (Yuniati et al. 2019; Pellegrino et al. 2010; Coley et al. 2012). Performing follow-up studies to assess if either (or both) of these genes impact PGC

survival in a DNA damage-associated context may bring us closer to an improved understanding of the genes involved in the PGC DDR.

The experimental system used to assess the DDR in PGCs exposed to IR could be easily modified to examine the impact of other genotoxic agents on PGCs. Former studies from the lab using different PGCs mutants have shown that unique genetic contexts can activate distinct and differing sets of DNA damage responsive genes (Luo et al. 2014; Luo and Schimenti 2015). While this is not surprising, it does indicate that the candidate genes listed in the tables above may be more reflective of those contexts similar to the stresses and damage evoked by IR.

3. Preventing Mutation Accumulation in the Germline through G1 Checkpoint Activation

In Chapter 3, we assessed the quality of individual haploid germ cells in the replication defective mutant *Fancm* using whole genome single cell DNA sequencing. Analysis of the variants present in control and mutant cells allowed us to demonstrate the potential ramifications of manipulating the *p21*-mediated DNA damage checkpoint to facilitate increased germ cell survival in *Fancm*$^{-/-}$ germ cells.

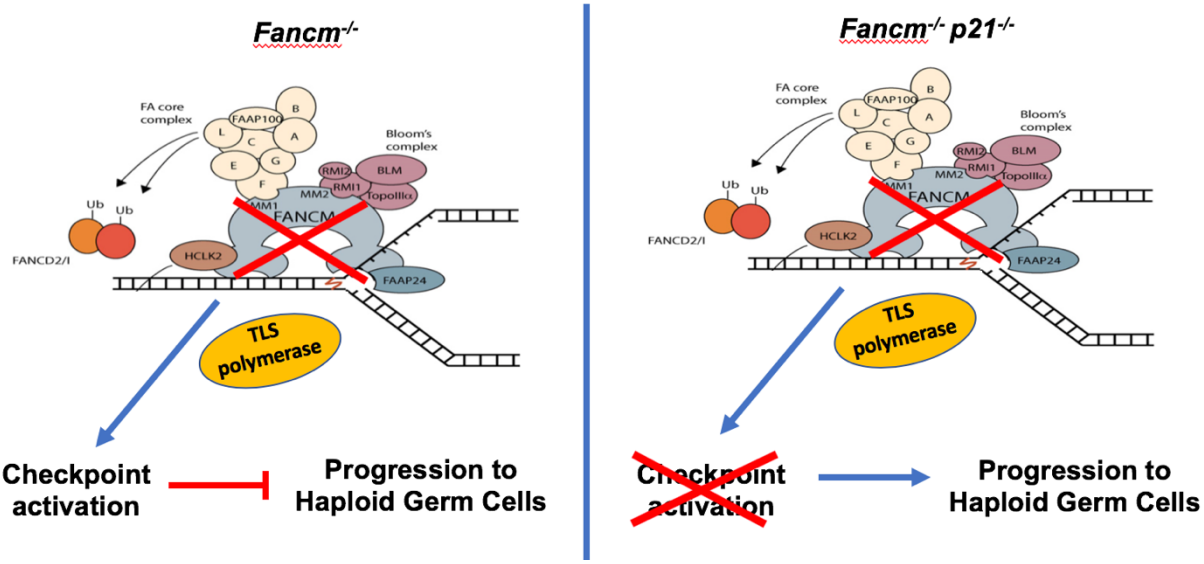

Figure 5.2. Proposed model for the enrichment of complex mutations in *Fancm*$^{-/-}$ *p21*$^{-/-}$ mutant spermatids.

One exciting aspect of this project was our attempt to answer a biological question about germ cell quality control mechanisms using a relatively new technology. On a practical level, we were forced to deviate from our more traditional pedigree-based exome sequencing approach because female *Fancm* mutants on the C57BL/6J strain background are infertile. An unavoidable drawback of our modified approach was that we were no longer able to assess mutation accumulation in the female germline alongside the male germline.

In many ways the sequencing of individual spermatids worked quite well. A technical limitation of the data was that the number of detected “mutations” even in wild-type control cells was about 5-10 times higher than expected

based on the known germline mutation rate in mice. This was most likely due to errors introduced during single cell genome amplification and sequencing. Generally speaking, there are couple approaches taken by the field to overcome these limitations including only considering the overlapping mutations detected in multiple independent variant calling programs and correcting for genome amplification biases by comparing the ratio of heterozygous SNPs at specific loci (Dong et al. 2017; Milholland et al. 2017). In our samples, we could not adjust for amplification biases because the genomes we sequenced were each haploid. In preliminary data analyses, I compared the overlapping point mutations detected in each cell between two different SNP calling programs, GATK HaplotypeCaller and VarScan (McKenna et al. 2010; Koboldt et al. 2012). On average, about half of the individually identified point mutations overlapped between the programs in each cell. Comparison of point mutations from the overlap lists and the individual program output lists did not change the overall distribution/percentage of point mutation types present in the cells.

For subsequent analyses, I used software that was more optimized for detecting InDels and other complex mutations (Rimmer et al. 2014). The results, which are described in more detail in Chapter 3, revealed that mutation clusters are enriched in *Fancm*$^{-/-}$ *p21*$^{-/-}$ germ cells compared to germ cells of the other genotypes. This finding indicates that the p21-dependent cell cycle checkpoint is important for suppressing propagation of germ cells experiencing a high number of defective replication forks that would lead to

specific complex mutational events when *Fancm* is absent. While my analyses focused on identifying whether there were any biases in mutation type present in *Fancm* deficient germ cells, studies have shown that even under normal conditions DNA sequence and epigenomic features can influence local mutation probabilities (Makova and Hardison 2015; Monroe et al. 2020). Follow-up analyses could examine whether the mutations identified in cells of specific genotypes are biased in certain genomic features such as local GC content, histone modifications, and/or chromatic accessibility.

4. Oocyte Elimination through DNA Damage Signaling

In Chapter 4 we showed that nearly all mouse meiocytes with unrepaired DSBs or asynapsis are eliminated before meiotic prophase I via p53 and TAp63 signaling. We also provide evidence that this signaling is mediated through CHK1 in addition to CHK2 (which was previously described in (Bolcun-Filas et al. 2014). A limitation of the CHK1 data is that loss of CHK1 could not be examined in our system due to *Chk1* being an essential gene. Future analyses could take advantage of a *Chk1* conditional allele (Lam et al. 2004) with an appropriate Cre-recombinase line expressed upon entry and throughout meiotic prophase I in female germ cells.

Interestingly, it is unclear why heterozygosity for either *Trp53* or *TAp63* in the context of nullizygosity for the other gene failed to rescue any *Spo11*$^{-/-}$ oocytes, but that loss of *Trp53* alone partially rescued *Trip13*$^{Gt/Gt}$ oocytes (reported in (Bolcun-Filas et al. 2014). We posit some possible explanations in

Chapter 4 including enhanced recognition by DNA damage sensors of spontaneous DSBs on asynapsed chromosomes (*Spo11*$^{-/-}$) vs. meiotically induced DSBs on synapsed chromosomes (*Trip13*$^{Gt/Gt}$) and it would be interesting to test this idea using mutants such as *Dmc1*$^{-/-}$ and *Msh5*$^{-/-}$. These mutants exhibit defects in both synapsis and DSB repair (Di Giacomo et al. 2005) and have an oocyte loss phenotype that resembles *Trip13*$^{Gt/Gt}$. Therefore, it could be informative to assess whether deletion of *Trp53* or *TAp63* leads to a partial rescue of oocytes in these mutants or not. One might expect based on our prediction that loss of either gene (*Trp53* or *TAp63)* would not partially rescue oocytes of either of the mutants due to the presence of asynapsis similar to *Spo11*$^{-/-}$ mutants. In the male germline, it has been reported that co-injection of *Trp53* and *Dmc1* siRNAs into testes (Dai et al. 2017) does not rescue the *Dmc1* single siRNA knock-down phenotype, lending additional support for the idea that a similar phenotype might be observed in the female germline with *Dmc1*$^{-/-}$ *Trp53*$^{-/-}$ double mutants.

Earlier this year, a study showed that the pro-apoptotic BCL-2 pathway eliminates oocytes with persistent DSBs via *Puma, Noxa,* and *Bax* (Ellnati et al. 2020). In this study, the authors examined oocyte rescue in the context of both *Dmc1*$^{-/-}$ and *Msh5*$^{-/-}$ mutants. Loss of *Puma* or *Noxa* alone did not rescue any primordial follicles, but loss of both *Puma* and *Noxa* rescued primordial follicles in both *Dmc1* and *Msh5* mutants to about 40% of wild-type. Double mutants of *Bax* and *Dmc1* or *Msh5* also led to about a 40% rescue in

primordial follicles. While these rescues are significant, they are different than the genetic rescues we performed which led to a complete restoration of oocytes back to wild-type levels. *Puma, Noxa* and *Bax* are all downstream of *Trp53* and *TAp63*, indicating that the field's understanding of the DNA damage signaling downstream of the factors we examined is incomplete and could benefit from additional studies.

5. Final Summation

To conclude, this dissertation describes the research I conducted which sought to contribute novel insights into how genome integrity is maintained in the mammalian germline. The scope of the work encompasses investigations into the DNA damage responses in primordial germ cells as well as in post-natal oocytes. Both germ cell types display highly sensitive responses to irradiation-induced DNA damage underscoring the importance of maintaining genome integrity across numerous stages of germ cell development.

During my time at Cornell, I also contributed to some additional scholarship which I would like to acknowledge below. (asterisks denote equal authorship contributions)

Bloom JC*, Tran TN*, Yamulla RJ*. Mouse Genetics 2016: meeting report. *Mammalian Genome*. 2017 Apr;28(3-4):81-89. PMID: 29782020

Shanahan MT*, Kanke M*, Singh AP*, Villanueva JW, McNairn AJ, Oyesola OO, Bonfini A, Hung Y, Sheahan B, **Bloom JC**, Cubitt RL, Curry EG, Pitman WA, Rinaldi VD, Dekaney CM, Ding S, Peck BCE, Schimenti JC, Dow LE, Buchon N, Tait-Wojno ED, Sethupathy P. miR-375 Regulates Intestinal Crypt Cell Landscape, Proliferation, and Regenerative Capacity.

Guan Y, Leu NA, Ma J, Chmátal L, Ruthel G, **Bloom JC**, Lampson MA, Schimenti JC, Luo M, Wang PJ. SKP1 drives the prophase I to metaphase I transition during male meiosis. *Science Advances.* 2020 Mar;25;6(13) PMID: 32232159

McNairn AJ, Chuang C, **Bloom JC,** Wallace MD, Schimenti JC. Female-biased embryonic death from genomic instability-induced inflammation. *Nature*. 2019 Mar;567(7746):105-108. PMID: 30787433

Fu Y*, Long MJC*, Wisitpitthaya S, Inayat H, Pierpont TM, Elsaid IM, **Bloom JC**, Ortega J, Weiss RS, Aye Y, 2018. Nuclear RNR-alpha Antagonizes Cell Proliferation by Directly Inhibited ZRANB3. *Nature Chemical Biology.* 2018 Oct;14(10):943-954. PMID: 30150681

References

Bolcun-Filas E, Rinaldi VD, White ME, Schimenti JC. 2014. Reversal of female infertility by Chk2 ablation reveals the oocyte DNA damage checkpoint pathway. *Science* **343**: 533–536.

Burns TF, Fei P, Scata KA, Dicker DT, El-Deiry WS. 2003. Silencing of the novel p53 target gene Snk/Plk2 leads to mitotic catastrophe in paclitaxel (taxol)-exposed cells. *Mol Cell Biol* **23**: 5556–5571.

Coley HM, Hatzimichael E, Blagden S, McNeish I, Thompson A, Crook T, Syed N. 2012. Polo Like Kinase 2 Tumour Suppressor and cancer biomarker: new perspectives on drug sensitivity/resistance in ovarian cancer. *Oncotarget* **3**: 78–83.

Dai J, Voloshin O, Potapova S, Camerini-Otero RD. 2017. Meiotic knockdown and complementation reveals essential role of RAD51 in mouse spermatogenesis. *Cell Rep* **18**: 1383–1394.

Di Giacomo M, Barchi M, Baudat F, Edelmann W, Keeney S, Jasin M. 2005. Distinct DNA-damage-dependent and -independent responses drive the loss of oocytes in recombination-defective mouse mutants. *Proc Natl Acad Sci USA* **102**: 737–742.

Dong X, Zhang L, Milholland B, Lee M, Maslov AY, Wang T, Vijg J. 2017. Accurate identification of single-nucleotide variants in whole-genome-amplified single cells. *Nat Methods* **14**: 491–493.

Ellnati E, Zielinska AP, McCarthy A, Kubikova N, Maciulyte V, Mahadevaiah S, Sangrithi MN, Ojarikre O, Wells D, Niakan KK, et al. 2020. The BCL-2

pathway preserves mammalian genome integrity by eliminating recombination-defective oocytes. *Nat Commun* **11**: 2598.

Hamer G, de Rooij DG. 2018. Mutations causing specific arrests in the development of mouse primordial germ cells and gonocytes. *Biol Reprod* **99**: 75–86.

Haubensak W, Attardo A, Denk W, Huttner WB. 2004. Neurons arise in the basal neuroepithelium of the early mammalian telencephalon: a major site of neurogenesis. *Proc Natl Acad Sci USA* **101**: 3196–3201.

Inglis KJ, Chereau D, Brigham EF, Chiou S-S, Schöbel S, Frigon NL, Yu M, Caccavello RJ, Nelson S, Motter R, et al. 2009. Polo-like kinase 2 (PLK2) phosphorylates alpha-synuclein at serine 129 in central nervous system. *J Biol Chem* **284**: 2598–2602.

Koboldt DC, Zhang Q, Larson DE, Shen D, McLellan MD, Lin L, Miller CA, Mardis ER, Ding L, Wilson RK. 2012. VarScan 2: somatic mutation and copy number alteration discovery in cancer by exome sequencing. *Genome Res* **22**: 568–576.

Lam MH, Liu Q, Elledge SJ, Rosen JM. 2004. Chk1 is haploinsufficient for multiple functions critical to tumor suppression. *Cancer Cell* **6**: 45–59.

Luo Y, Hartford SA, Zeng R, Southard TL, Shima N, Schimenti JC. 2014. Hypersensitivity of primordial germ cells to compromised replication-associated DNA repair involves ATM-p53-p21 signaling. *PLoS Genet* **10**: e1004471.

Luo Y, Schimenti JC. 2015. MCM9 deficiency delays primordial germ cell

proliferation independent of the ATM pathway. *Genesis* **53**: 678–684.

Makova KD, Hardison RC. 2015. The effects of chromatin organization on variation in mutation rates in the genome. *Nat Rev Genet* **16**: 213–223.

McKenna A, Hanna M, Banks E, Sivachenko A, Cibulskis K, Kernytsky A, Garimella K, Altshuler D, Gabriel S, Daly M, et al. 2010. The Genome Analysis Toolkit: a MapReduce framework for analyzing next-generation DNA sequencing data. *Genome Res* **20**: 1297–1303.

Milholland B, Dong X, Zhang L, Hao X, Suh Y, Vijg J. 2017. Differences between germline and somatic mutation rates in humans and mice. *Nat Commun* **8**: 15183.

Monroe JG, Srikant T, Carbonell-Bejerano P, Exposito-Alonso M, Weng M-L, Rutter MT, Fenster CB, Weigel D. 2020. Mutation bias shapes gene evolution in *Arabidopsis thaliana*. *BioRxiv*.

Pellegrino R, Calvisi DF, Ladu S, Ehemann V, Staniscia T, Evert M, Dombrowski F, Schirmacher P, Longerich T. 2010. Oncogenic and tumor suppressive roles of polo-like kinases in human hepatocellular carcinoma. *Hepatology* **51**: 857–868.

Rimmer A, Phan H, Mathieson I, Iqbal Z, Twigg SRF, WGS500 Consortium, Wilkie AOM, McVean G, Lunter G. 2014. Integrating mapping-, assembly- and haplotype-based approaches for calling variants in clinical sequencing applications. *Nat Genet* **46**: 912–918.

Sabour D, Araúzo-Bravo MJ, Hübner K, Ko K, Greber B, Gentile L, Stehling M, Schöler HR. 2011. Identification of genes specific to mouse primordial

germ cells through dynamic global gene expression. *Hum Mol Genet* **20**: 115–125.

Simmons DL, Neel BG, Stevens R, Evett G, Erikson RL. 1992. Identification of an early-growth-response gene encoding a novel putative protein kinase. *Mol Cell Biol* **12**: 4164–4169.

Yuniati L, Scheijen B, van der Meer LT, van Leeuwen FN. 2019. Tumor suppressors BTG1 and BTG2: Beyond growth control. *J Cell Physiol* **234**: 5379–5389.

APPENDIX I

WHOLE MOUNT IMMUNOFLUORESCENCE AND FOLLICLE QUANTIFICATION OF CULTURED MOUSE OVARIES

***** This appendix is a reprint with minor reformatting of the manuscript: Rinaldi, V.D., Bloom, J.C., Schimenti, J.C. Whole Mount Immunofluorescence and Follicle Quantification of Cultured Mouse Ovaries. *J. Vis. Exp.* (135),e57593,doi:10.3791/57593 (2018).

1- Abstract

Research in the field of mammalian reproductive biology often involves evaluating the overall health of ovaries and testes. Specifically, in females, ovarian fitness is often assessed by visualizing and quantifying follicles and oocytes. Because the ovary is an opaque three-dimensional tissue, traditional approaches require laboriously slicing the tissue into numerous serial sections in order to visualize cells throughout the entire organ. Furthermore, because quantification by this method typically entails scoring only a subset of the sections separated by the approximate diameter of an oocyte, it is prone to inaccuracy. Here, a protocol is described that instead utilizes whole organ tissue clearing and immunofluorescence staining of mouse ovaries to visualize follicles and oocytes. Compared to more traditional approaches, this protocol is advantageous for visualizing cells within the ovary for numerous reasons: 1) the ovary remains intact throughout sample preparation and

processing; 2) small ovaries, which are difficult to section, can be examined with ease; 3) cellular quantification is more readily and accurately achieved; and 4) the whole organ imaged.

The video component of this article can be found at https://www.jove.com/video/57593/

2- Introduction

In order to study the cellular composition and morphological features of mammalian ovaries, scientists often rely on *in vivo* experiments followed by immunohistological staining of paraffin embedded ovaries. More recently though, whole ovary organ culture has proven to be an effective alternative to study ovarian function[1,2,3,4] because the technique can be coupled with better visualization and quantification tools. Traditionally, analysis of ovarian morphology depends on reconstructing three-dimensional ovarian architecture from paraffin embedded serial sections, but, in addition to being laborious and time consuming, serially sectioning paraffin embedded tissue does not guarantee proper reconstruction of the organ, and sections are often lost or mis-ordered in the process.

In addition to the technical challenges associated with serial sectioning, there are also variations in the methods routinely used to quantify follicle numbers per ovary[5,6]. The methodological variability currently used impairs meta-analysis of ovarian reserve across studies[5,7]. For example, follicle

numbers from different research articles can vary by 10-fold or more between similar developmental ages within a specific strain[6]. These large differences in reported follicle quantification can lead to confusion and have hindered cross-study comparisons. Experimentally, traditional approaches to follicle quantification from serial sections are performed by counting follicles of a pre-defined number of sections (*e.g.,* every fifth, tenth, or other section). Variability in follicle counts using this approach arises not only from the periodicity in which sections are counted but also from variations in section thickness, and technical experience in generating serial sections[5,6]. In addition to its variability, another disadvantage of traditional tissue sectioning is that the sectioning of small ovaries from young animals is especially challenging and highly dependent on tissue orientation[8].

The protocol below describes a routinely used ovary culture technique[1] but greatly improves upon traditional follicle quantification by substituting physical sectioning with tissue clearing and optical sectioning using confocal microscopy[8,9]. Clearing using tissue immersion (without the need for transcranial perfusion or electrophoresis) in a urea- and sorbitol-based solution (*e.g.,* ScaleS(0)[10]) proved compatible with the immunostaining and allowed for the reduction of clearing time without compromising depth of imaging. Other reported methods (*e.g.*, ScaleA2[8,10], SeeDB[11], ClearT[12], and ClearT2[12]) are either more time consuming or do not allow in-depth optical

resolution of the sample. Optical sectioning is advantageous because it is less labor intensive and maintains the organ's three-dimensional architecture[7,8]. Another benefit of this approach is that preparation of the samples does not require costly reagents to clear the tissue and can be conducted with relative ease.

Specifically, the protocol described has been optimized for cultured mouse ovaries at postnatal day five but has been conducted on ovaries ranging from postnatal day 0 - 10. The method makes use of an ovary culture system in which the tissue naturally attaches to the membrane on which it is cultured, facilitating organ handling and manipulation. The culture system described can be used to maintain explanted ovaries for up to 10 days and to assess how different experimental conditions may interfere with oocyte survival[13]. The quantification procedure described is performed using the non-commercial image processing package FIJI-ImageJ[14] and can be conducted on most personal computers. Furthermore, images used for quantification can be made widely available for the scientific community, thus allowing for future meta-analysis.

3- Protocol

Cornell University's Institutional Animal Care and Use Committee (IACUC) has approved all the methods described here, under protocol 2004-0038 to JCS.

1. Preparation of Instruments and Culture Media

1. Wipe the working area clean with 10% bleach and allow the bleach to remain on the work area surface for at least 5 min. After 5 min, remove the excess bleach with clean paper towels and 70% ethanol (EtOH). Clean the dissecting microscope thoroughly with 70% EtOH.

NOTE: It is important that the work area be at least semi-sterile to avoid contamination of organ cultures.

2. Wrap clean forceps and scissors with a paper towel dampened with 70% EtOH until the time of use.

NOTE: The ideal dissection tools may vary according to the age/size of the ovary. Best results are obtained using one sharp micro dissecting scissor, two fine tip forceps (either number 5 or 55) and one micro dissecting iris scissor.

3. In a conical tube, make 50 mL of ovary culture media and warm in a 37 °C water bath.

1. To make ovary culture medium[4], supplement 1x Minimal Essential Media (MEM) with 10% Fetal Bovine Serum (FBS), 25 mM (4-(2-hydroxyethyl)-1-piperazineethanesulfonic acid (HEPES), 100 units/mL penicillin, 100 µg/mL streptomycin, 0.25 µg/mL Amphotericin B (*e.g.,* 45 mL of MEM, 5 mL of heat inactivated FBS, 1.25 mL of HEPES, and 0.5 mL of 100x stock of penicillin, streptomycin, and Amphotericin B).

4. Prepare plates and inserts prior to the ovary culture.

1. In a tissue culture hood, add 1 mL of ovary culture medium to a 35 mm tissue culture plate.

2. Pre-soak insert membrane with the culture medium. Add sufficient media, usually about 0.55 mL per well, to the 24-well carrier tissue culture plate, and place a cell culture insert in the well. Make sure the insert's membrane touches the media.

3. Prepare the number of 35 mm plates and wells with cell culture inserts according to the expected number of ovaries in the experiment. Place the 35 mm plates containing 1 mL of culture media and the 24-well carrier plate containing culture media and inserts in a 37 °C, 5% CO_2, and atmospheric O_2 incubator.

5. Arrange a hot plate next to the dissection scope and set the temperature to 37 °C. Keep a 37 °C, 5% CO_2 and the atmospheric O_2 incubator is close to the dissection room.

2. Ovary Dissection and Organ Culture

NOTE: Ovaries can be dissected at room temperature as long as the exposure to the non-ideal temperature is minimal.

1. Euthanize the female mice at post-natal day 5, by decapitation, one at a

time.

NOTE: Euthanasia must be conducted according to IACUC guidelines present at the facility where the research is being performed.

2. Spray the animal with 70% EtOH. Place the animal on the top of the dry paper towel under the dissection microscope. Place a 35 mm tissue culture dish containing ovary culture media close to the dissection microscope.

3. With forceps or a micro dissection iris scissor, make an incision through the skin of the animal and into the abdominal cavity, using caution not to cut into the intestines. Push the intestines out of the abdominal cavity and locate the ovaries. Extract the ovaries and place them into the 35-mm tissue culture dish containing culture media.

4. Once the ovaries have been dissected from the animal, increase the magnification of the dissection microscope in order to better visualize ovaries and any attached tissue. With clean fine tip forceps, remove all non-ovarian tissue, such as bursa and fatty tissue. Be careful to keep the ovaries intact when removing the attached non-ovarian tissue.

5. Once the ovaries are isolated, place the pair into the pre-soaked cell culture inserts of the carrier 24-well plate (refer to steps 1.4.2 and 1.4.3) and adjust the volume of the medium to ensure that it is sufficient to keep

the organ moist (without completely submerging it). Caution: Be careful not to poke a hole in the membrane of the cell culture insert when transferring the ovaries.

6. Place explanted organs in a 37 °C, 5% CO_2, and atmospheric O_2 incubator.

7. Repeat steps 2.1 - 2.6 until the ovaries of each animal are dissected and placed on the cell culture insert of the 24-well plate containing the ovary culture medium.

8. Change the ovary culture medium every 2 days, using warmed ovary media aliquots from a 37 °C water bath and proceed to Part 3 of the protocol at the desired experimental time point.

3. Tissue Fixation

1. In a 15 mL conical tube, prepare 4% paraformaldehyde (PFA) in 1x phosphate-buffered saline (PBS) (*e.g.,* add 2 mL of 16% PFA electron microscopy grade to 6 mL of 1x PBS).

Caution: PFA is a hazardous substance and should be handled under a chemical hood.

2. Fix the cultured ovaries, without removing the tissue from the culture insert, by covering the tissue with the freshly prepared 4% PFA solution. Seal

the edges of the plate with plastic adhesive (to avoid evaporation) and place the samples at 4 °C overnight.

NOTE: In order to facilitate handling and tissue integrity, avoid displacing ovaries from the cell culture insert throughout the entire procedure. Cultured ovaries attached to the surface of the insert are advantageous for handling without damaging or losing the organ.

3. Rinse the tissue 3x with 70% EtOH and either proceed to step 4.1 or store it in scintillation vials filled with 70% EtOH at 4 °C until further processing.

NOTE: If using tissue endogenously expressing fluorescent proteins, storing the samples with 70% EtOH may greatly reduce the signal. Alternatively, tissue can be rinsed and stored in the PBS with 0.2% sodium azide (NaN_3). NaN_3 is, however, highly toxic and poses a serious inhalation hazard. Make the stock solution in the fume hood and handle wearing appropriate personal protective equipment such as a laboratory coat and nitrile gloves.

4. Whole Mount Immunofluorescence

1. Place the fixed tissue in 1x PBS at RT for a minimum of 4 h prior to the permeabilization step 4.3.

2. Prepare permeabilization solution and blocking solution.

    1. Prepare permeabilization solution as described. To 1x PBS, add

0.2% polyvinyl alcohol (PVA), 0.1% sodium borohydride ($NaBH_4$) solution (from 12 wt.% in 14 M sodium hydroxide (NaOH) solution), and 1.5% polyethylene glycol *tert*-octylphenyl ether (non-ionic surfactant detergent). In a 50 mL conical tube, add 5 mL of 10x PBS, 0.1 g of PVA, 50 µL of $NaBH_4$, and 750 µL of non-ionic surfactant detergent, then add ultrapure water up to 50 mL and agitate well at room temperature until the mixture is entirely in solution.

2. Prepare blocking solution as described. To 1x PBS, add 0.1% non-ionic surfactant detergent, 0.15% of 2.5M glycine pH 7.4, 10% normal goat serum, 3% bovine serum albumin (BSA), 0.2% NaN_3, 100 units/mL penicillin, 100 µg/mL streptomycin, and 0.25 µg/mL Amphotericin B. Prepare a stock solution of 2.5 M glycine by dissolving 93.8 g of glycine in ultrapure water to a 500 mL final volume (pH 7.4) and a stock solution of 10% NaN_3 by dissolving 5 g in 50 mL of ultrapure water; then, in a 50 mL conical tube prepare the blocking solution by adding 5 mL of 10x PBS, 50 µL of non-ionic surfactant detergent, 750 µL of glycine stock solution, 5 mL of goat serum, 1.5 g of BSA, 1 mL of NaN_3 stock solution, and 0.5 mL of 100x stock of penicillin, streptomycin, and Amphotericin B . Add ultrapure water up to a final volume of 50 mL and syringe filter the final solution.

3. Remove and discard the 1x PBS from the vial, and then add enough permeabilization solution to completely submerge the ovaries. Place the sample in permeabilization solution on an orbital shaker (*e.g.,* nutator) at room temperature for 4 h. NOTE: Incubation time may vary

according to the organ thickness.

4. Replace the permeabilization solution with enough blocking solution to completely submerge the ovaries. Seal the vial with the plastic adhesive and leave the tissue incubating for a minimum of 12 h at room temperature on an orbital shaker.

5. Prepare primary antibody dilution in blocking solution as per the manufacturer's datasheet. NOTE: Note that not all antibodies are compatible with the clearing agent. The average volume needed per sample is approximately 750 µL.

1. For oocyte quantification, use TAp63 (nuclear oocyte marker) and MVH (cytoplasmic germ cell marker). NOTE: The antibodies used in the immunofluorescence images are mouse anti-p63 and rabbit anti-MVH). The primary antibody solution can be reused 2x or more if stored at 4 °C between staining protocols and properly handled to avoid bacterial growth.

6. Place the insert containing the tissue in a 24-well plate and add about 750 µL of primary antibody solution. Ensure that ovaries are completely submerged. Seal the plate with plastic adhesive to minimize evaporation and leave the tissue incubating for 4 days at room temperature on an orbital shaker.

7. Prepare washing solution.

1. Prepare washing solution as described. Make 1x PBS, add 0.2% PVA and 0.15% non-ionic surfactant detergent. In a 50 mL conical tube, add 5 mL of 10x PBS, 0.1 g of PVA, 75 µL of non-ionic surfactant detergent and ultrapure water up to a final volume of 50 mL.

8. Remove primary antibody dilution and add a generous amount of washing solution. Always make sure to submerge the ovaries. Allow the ovaries to soak in the solution overnight at room temperature on the orbital shaker.

9. Replace the washing solution and incubate on the orbital shaker for 2 h or more.

10. Repeat the step 4.9 one additional time.

11. Prepare the secondary antibody dilution in blocking solution.

NOTE: The secondary antibodies used are anti-mouse 488 fluorescent dye raised in goat and anti-rabbit 594 fluorescent dye raised in goat. See step 4.5. for the average volume needed per sample.

12. Remove washing solution from the ovaries and add secondary antibody solution. Protect the samples from light (wrap plate with aluminum foil) and seal the plate with plastic adhesive to minimize evaporation. Incubate samples on an orbital shaker at room temperature for 2 days.

NOTE: Continue protecting the samples from light using aluminum foil during all subsequent incubation steps.

13. Remove secondary antibody solution from the samples and add washing solution. Incubate on an orbital shaker for 8 h. NOTE: If 4,6-Diamidino-2-phenylindole (DAPI) staining is desired, add 50 ng/mL of DAPI to the first wash step (~8 h incubation).

14. Replace the washing solution for an overnight wash.

15. While preparing the clearing solution (see section 5), replace the overnight washing solution with fresh solution and keep the samples on the orbital shaker at room temperature.

5. Ovary Clearing and Imaging

1. Prepare ScaleS(0) clearing solution.

1. Prepare ScaleS(0) clearing solution[10] by adding reagents in the given proportion: 40% D-(-) sorbitol (w/v), 10% glycerol, 4.3 M urea, and 20% dimethyl sulfoxide (DMSO), pH 8.1 (*e.g.* in a 50 mL conical tube, add 2.5 mL of glycerol, 10 g of sorbitol, 5 mL of DMSO, and 12 mL of 9 M urea for a total volume of 25 mL. Mix solution by inversion at 50 °C for 30 min and degas prior to use.)

2. Remove the washing solution and submerge the samples in clearing

solution. For better results maintain samples on the orbital shaker.

3. Replace the clearing solution 2x daily until the tissue becomes transparent (approximately 2 days).

4. Once the tissue is cleared, prepare the sample for imaging by carefully removing the insert membrane containing the cultured ovaries with a fine tip scalpel and placing the sample on a glass slide.

5. Proceed to imaging the samples on a microscope capable of optical sectioning.

6. Oocyte Quantification

NOTE: There are many different computer programs that are able to quantify cells. Described below is a protocol for oocyte quantification using the non-commercial image processing package, FIJI-ImageJ[14].

1. Using a flattened maximum intensity projection of the *Z*-stack image series for the specific cellular markers of interest (without the DAPI channel), convert the image into a black and white 8-bit image under **Type** in the **Image** drop-down menu.

2. Under the **Image** drop-down menu, highlight the **Adjust** tab and then select **Threshold**.

3. Manually adjust the threshold to a level that best identifies each individual

oocyte. Once the level is determined, click **Apply** to generate a black and white image. Once completed, quantify the sample by delineating using the **Oval** or **Freehand** icon. NOTE: FIJI-ImageJ has different options to fine tune the image that will be used for the particle quantification. For instance, in **Process | Binary** tab, there are different options that can be used to improve the detection of what will be counted. In **Figure 4**, the options used to better individualize follicles was **Erode**, followed by **Fill holes**, and lastly **Watershed**.

4. Under the **Analyze** drop-down menu, select **Analyze particles**. Set the parameters according to the desired resolution.

4- Representative Results

This protocol includes 6 major steps following dissection of the ovaries, as outlined in **Figure 1**. **Figure 2, Figure 3, Figure 4** highlight the most novel features of this protocol, which include optimization of tissue clearing for ovaries and whole tissue oocyte quantification using FIJI-ImageJ. **Figure 2A** shows images of an uncultured 5-day postnatal fixed ovary before (**left**) and 1 h after (**right**) adding clearing solution to the ovary. The ovary will begin to become translucent within minutes of being submerged in clearing solution. Once cleared, small ovaries like the one imaged in **Figure 2A** become difficult to handle without damaging. Therefore, working with cultured explanted ovaries is advantageous because they become attached to the porous surface

of the insert membrane on which they are cultured. Attachment of the ovary to the insert membrane allows the experimenter to handle the membrane insert rather than the ovary itself (**Figure 2B and Figure 3**). Also, ovaries cultured in close proximity will fuse and **Figure 2B** shows attached fused ovaries before **(left)** and after clearing **(right)** on hematoxylin stained samples.

Performing the optical sectioning of cultured ovaries without clearing is possible; however, cells deep within the tissue have a signal that is difficult to differentiate from the background and this lack of clear signal impedes proper oocyte quantification (**Figure 3A**). In contrast to **Figure 3A**, **Figure 3B** is a representative image of a cleared sample in which oocyte quantification throughout the entire organ is possible. **Figure 3B** demonstrates that whole organ imaging of cleared cultured ovaries can be conducted without significant loss of signal deep within the tissue and images such as the one shown (**Figure 3B**) can be readily quantified. One approach for quantifying oocytes in samples such as these is by converting the Z-stack series of optical sections into a Maximum Intensity Projection and then further processing the file with an image processing package. **Figure 4** highlights the steps used to quantify the number of oocytes in **Figure 3B** using FIJI- ImageJ. **Supplemental Table 1** includes FIJI-ImageJ's particle (oocyte) quantification. Quantification of particles using this method also allows for the analysis of different follicles based on oocyte size, because information on both the number of particles and the corresponding area of each particle is calculated by the software and

provided to the user.

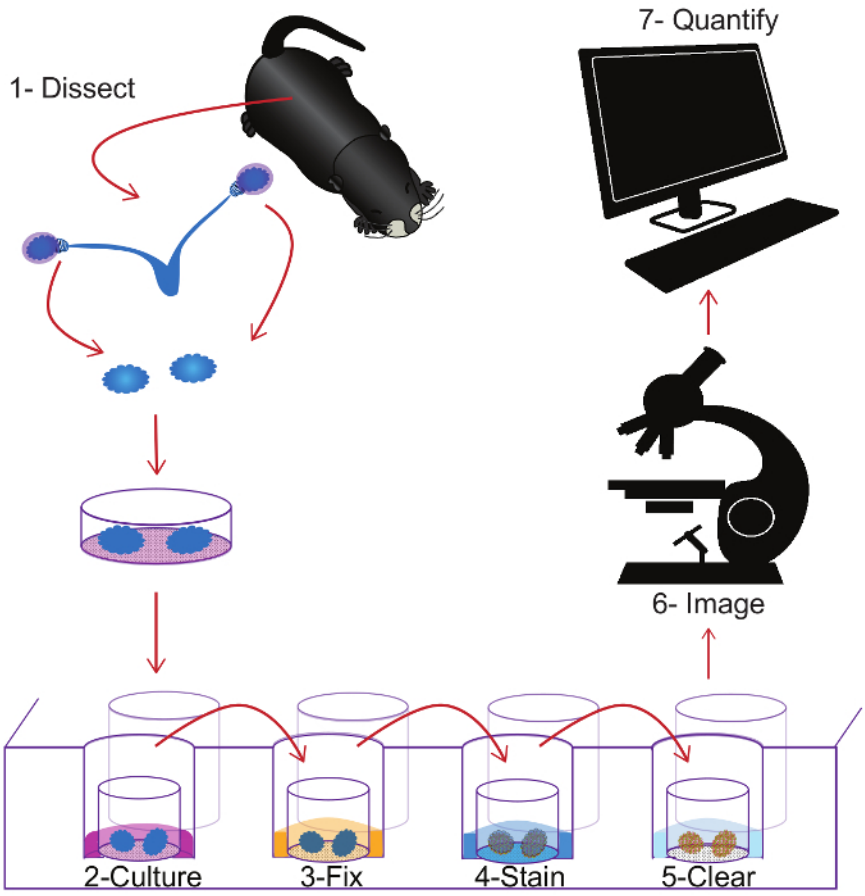

Figure 1: Schematic representation of the entire protocol. Visual summary of the protocol beginning with dissection of the ovary (1), followed by ovary culture (2), tissue fixation with 4%PFA (3), immunostaining using specific antibodies (4), clearing tissue for deep imaging (5), obtaining the optical section using a confocal microscope (6) and ending with oocyte quantification (7).

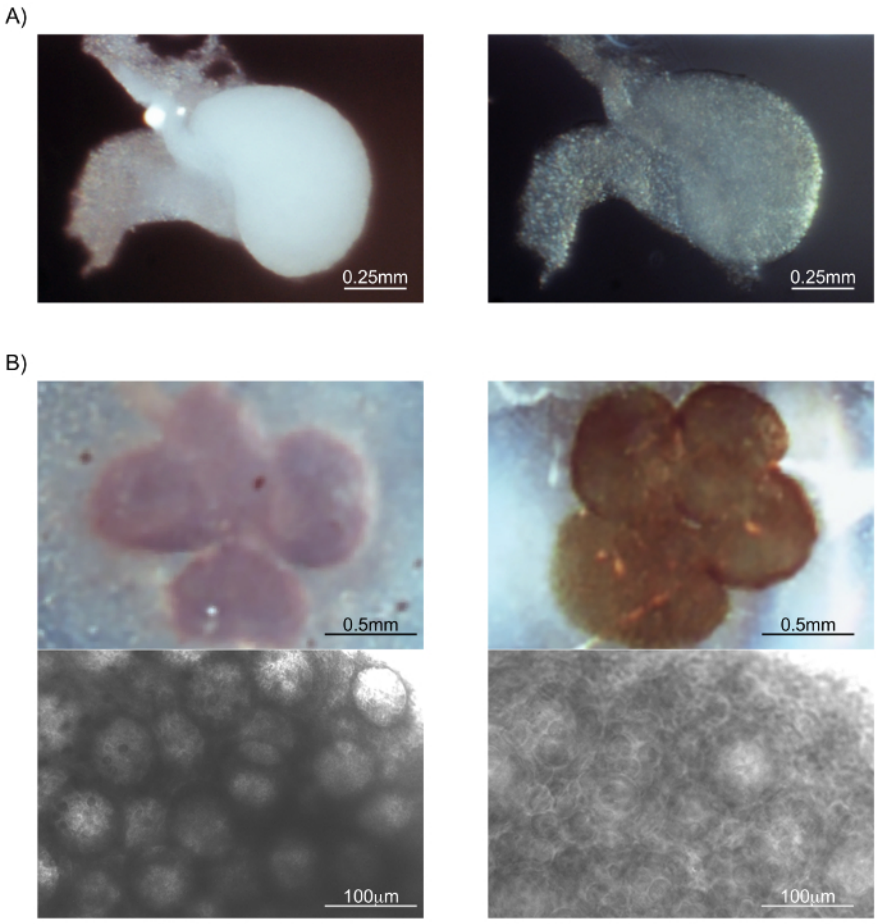

Figure 2: Difference in tissue opacity between un-cleared and cleared ovaries. (A) Ovary from a postnatal day five pup without clearing (left) and after mild clearing of about 1 h (right). **(B)** Multiple ovaries cultured in close proximity to each other for seven days. Two different magnifications of each sample are shown. Leftmost images are without clearing and rightmost images are with clearing. Ovaries will attach to the membrane of the culture insert and can be better handled if kept attached throughout the protocol. In order to improve the contrast of tissue for imaging using white light, ovaries were submerged in hematoxylin for 5 min after fixation.

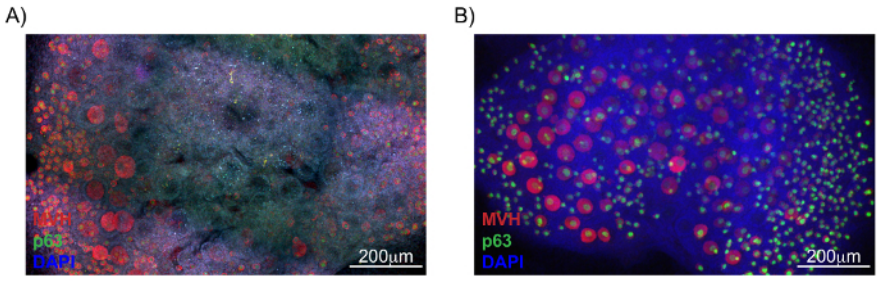

Figure 3: Immunofluorescence imaging of un-cleared and cleared ovaries. Ovaries from postnatal day 5 pups were cultured for 7 days and stained according to the whole mount immunofluorescence staining protocol described. Shown in red are cells labeled with mouse vasa homolog (MVH) to identify germ cells and in green are cells labeled with the nuclear oocyte-specific marker, p63. DAPI, in blue, was used to label all cell nuclei. **(A)** Immunofluorescence image of ovaries without clearing. **(B)** Immunofluorescence image of ovaries with clearing.

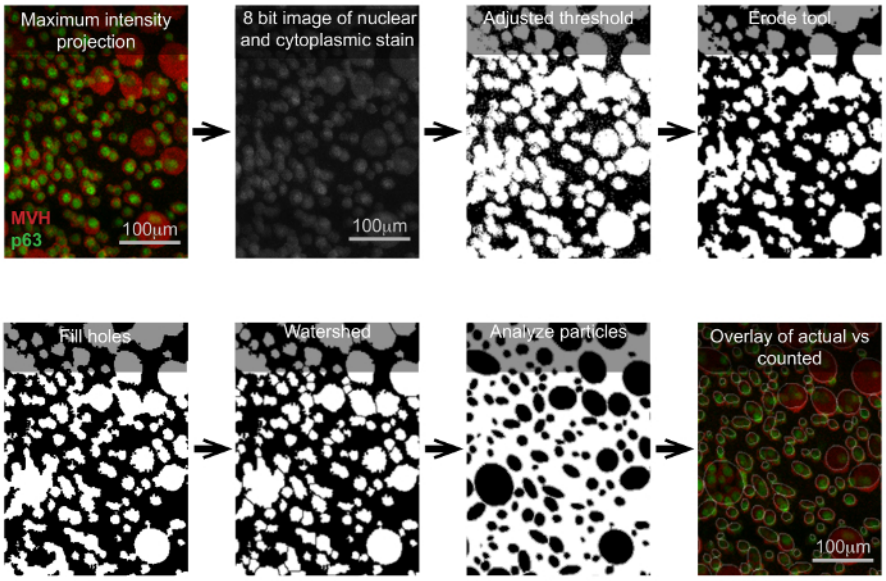

Figure 4: Visual workflow for how to quantify oocytes using FIJI-ImageJ software. In order to facilitate data analysis, images derived from the confocal planes can be reduced to a maximum intensity projection instead of a 3D image. With the maximum intensity projection, the user can define image threshold parameters in such a way that the target particles become evident. Once the simplified image is obtained, the software is used to count the oocytes. Critically examining images while setting the parameters is crucial. This figure shows an example of how the particle/oocyte threshold can be set. The text above each image highlights the parameter used to obtain that image in FIJI-ImageJ. The software also generates a table with the area measurement of the particles.

5- Discussion

The study of mammalian reproduction requires using and quantifying specialized cells that are not routinely amenable to cell culture. However, *ex vivo* culture systems are effective at maintaining ovary and follicle viability[1,15]. During ovary culture, the tissue requires a larger surface area for exchange of nutrients through diffusion. Therefore, 5-day old mouse ovaries are ideal in size and shape for organ culture. This protocol was optimized for ovaries maintained for seven days in culture, but ovary culture length can be adjusted according to the specific scientific question[1,4]. Comparable results have been achieved in ovaries cultured for as little as three days and as long as ten days

(data not shown), but ovaries from animals older than ten days are large and culture may not be as effective, thus highlighting a limitation of the protocol.

If *ex vivo* culturing of the ovary is not needed, it is possible to fix and stain older ovaries with the protocol described, although modifications may be required to adjust to the larger tissue size[9,16]. The staining protocol described depends on passive diffusion of the antibodies into the organ, which indicates that it may be possible to stain larger ovaries with either longer antibody incubation steps or by partitioning the tissue into few smaller pieces that can be reconstructed after imaging. The use of urea and sorbitol in the ScaleS(0) clearing agent proved effective for neonatal cultured ovaries because it required a shorter incubation period than those reported for clearing agents with urea and glycerol (ScaleA2)[8,10]. Furthermore, the use of a low concentration of sodium borohydride ($NaBH_4$) in the permeabilization solution decreased the background noise, and, together with longer incubations of the samples with primary and secondary antibodies, facilitated staining deep within the tissue. Additionally, the use of PVA in the permeabilization and washing solutions prevents spurious particles from sticking to the tissue[17,18].

In this protocol, cultured healthy ovaries will attach to the insert membrane, while unhealthy ovaries may detach from it upon fixation and handling. Handling loose tissue with forceps will damage the ovary and likely compromise imaging. Alternatively, loose tissue can be embedded in 5%

agarose plugs or handled with transfer pipettes as long as the tip opening is wide enough not to damage it. With regard to immunostaining, primary antibodies other than the ones used in this protocol may perform differently and may require optimization in the permeabilization and incubation steps.

Lastly, the protocol describes an alternative approach towards quantifying follicles from young ovaries as compared to traditional paraffin embedded serial sections or other previously described volumetric quantification of follicles from whole mount images[5,9,16]. Depending on the researcher's requirements, the procedure for oocyte quantification described in the protocol can also be used the characterize different stages of follicular development[19]. The particle area generated by the software can be used to determine the cell diameter and thus infer follicular stage.

6- Acknowledgements

We thank Rebecca Williams and Johanna Dela Cruz from the Cornell BRC Imaging and Andrew Recknagel for helpful suggestions and technical assistance. This work was supported to National Institutes of Health grant S10-OD018516 (to Cornell's Imaging Facility), T32HD057854 to J.C.B. and R01-GM45415 to J.C.S.

7- References

1. O'Brien, M.J., Pendola, J.K., Eppig, J.J. A Revised Protocol for In Vitro

Development of Mouse Oocytes from Primordial Follicles Dramatically Improves Their Developmental Competence. *Biology of Reproduction.* **68** (5), 1682-1686 (2003).

2. Morgan, S., Campbell, L., Allison, V., Murray, A., Spears, N. Culture and Co-Culture of Mouse Ovaries and Ovarian Follicles. *Journal of Visualized Experiments.* (97) (2015).

3. Livera, G., Rouiller-Fabre, V., Valla, J., Habert, R. Effects of retinoids on the meiosis in the fetal rat ovary in culture. *Molecular and Cellular Endocrinology.* **165** (1), 225-231 (2000).

4. Livera, G., Petre-Lazar, B., Guerquin, M.-J., Trautmann, E., Coffigny, H., Habert, R. p63 null mutation protects mouse oocytes from radio-induced apoptosis. *Reproduction.* **135** (1), 3-12 (2008).

5. Tilly, J.L. Ovarian follicle counts - not as simple as 1, 2, 3. *Reproductive Biology and Endocrinology.* **1**, 11 (2003).

6. Bucci, T.J., Bolon, B., Warbritton, A.R., Chen, J.J., Heindel, J.J. Influence of sampling on the reproducibility of ovarian follicle counts in mouse toxicity studies. *Reproductive Toxicology.* **11** (5), 689-696 (1997).

7. Skodras, A., Marcelli, G. Computer-Generated Ovaries to Assist Follicle Counting Experiments. *PLOS ONE.* **10** (3), e0120242 (2015).

8. Malki, S., Tharp, M.E., Bortvin, A. A Whole-Mount Approach for Accurate Quantitative and Spatial Assessment of Fetal Oocyte Dynamics in Mice. *Biology of Reproduction.* **93** (5) (2015).

9. Feng, Y. *et al.* CLARITY reveals dynamics of ovarian follicular architecture and vasculature in three-dimensions. *Scientific Reports.* **7** (2017).

10. Hama, H. *et al.* ScaleS: an optical clearing palette for biological imaging. *Nature Neuroscience.* **18** (10), 1518-1529 (2015).

11. Ke, M.-T., Fujimoto, S., Imai, T. SeeDB: a simple and morphology-preserving optical clearing agent for neuronal circuit reconstruction. *Nature Neuroscience.* **16** (8), 1154-1161 (2013).

12. Kuwajima, T., Sitko, A.A., Bhansali, P., Jurgens, C., Guido, W., Mason, C. ClearT: a detergent- and solvent-free clearing method for neuronal and non-neuronal tissue. *Development.* **140** (6), 1364-1368 (2013).

13. Rinaldi, V.D., Hsieh, K., Munroe, R., Bolcun-Filas, E.M., Schimenti, J.C. Pharmacological Inhibition of the DNA Damage Checkpoint Prevents Radiation-Induced Oocyte Death. *Genetics.* genetics.117.203455 (2017).

14. Schindelin, J. *et al.* Fiji: an open-source platform for biological-image analysis. *Nature Methods.* **9** (7), 676-682 (2012).

15. Obata, Y., Kono, T., Hatada, I. Oogenesis: Maturation of mouse fetal germ

cells *in vitro. Nature.* **418** (6897), 497 (2002).

16. Faire, M. *et al.* Follicle dynamics and global organization in the intact mouse ovary. *Developmental Biology.* **403** (1), 69-79 (2015).

17. Byrne, C., Hardman, M.J. Whole-Mount Assays for Gene Induction and Barrier Formation in the Developing Epidermis. *Epidermal Cells.* 127-136 (2005).

18. Lauter, G., Söll, I., Hauptmann, G. Multicolor fluorescent in situ hybridization to define abutting and overlapping gene expression in the embryonic zebrafish brain. *Neural Development.* **6**, 10 (2011).

19. Laronda, M.M. *et al.* A bioprosthetic ovary created using 3D printed microporous scaffolds restores ovarian function in sterilized mice. *Nature Communications.* **8**, ncomms15261 (2017).